

Enzymatic Synthesis of Silicon Dioxide Capsules with Tunable Size, Morphology and Functionality

Von der Fakultät für Mathematik, Informatik und Naturwissenschaften
der RWTH Aachen University zur Erlangung des akademischen Grades
einer Doktorin der Naturwissenschaften genehmigte Dissertation

vorgelegt von

Diplom-Chemikerin

Huihui Wang

aus Sichuan, China

Berichter: Universitätsprofessor Dr. Alexander Böker

Universitätsprofessor Dr. Andrij Pich

Tag der mündlichen Prüfung: 29. April 2015

Diese Dissertation ist auf den Internetseiten der Universitätsbibliothek online
verfügbar.

Die vorliegende Arbeit wurde in der Zeit von April 2010 bis September 2014 am Lehrstuhl für Makromolekulare Materialien und Oberflächen an der RWTH Aachen unter Herrn Prof. Dr. Alexander Böker angefertigt.

To my parents

Contents

1	Introduction	1
1.1	Biom mineralization / Biosilification.....	1
1.1.1	Enzymatic silicification with silicatein.....	2
	<i>Silicatein</i>	2
	<i>Synthesis of inorganic materials or organic /</i> <i>inorganic hybrids with native and recombinant</i> <i>silicatein</i>	6
1.1.2	Biosilicification with other naturally occurring enzymes...	9
	<i>Hydrolases as catalysts for silicification</i>	9
	<i>New material synthesis with native hydrolases</i>	11
1.1.3	Analogues of Enzymes as catalysts for silicification.....	13
	<i>Polypeptides, copolymers or bifunctional small</i> <i>molecules</i>	13
	<i>Poly(N-isopropylacrylamide) microgels</i>	16
1.2	Pickering emulsion as template for capsule formation.....	17
1.2.1	Pickering emulsions.....	17
1.2.2	Interfacial assembly of protein particles.....	20
1.2.3	Microgels at interfaces.....	21
1.3	Outline of this thesis.....	24

2	Experiments	26
2.1	Materials and chemicals.....	26
2.1.1	Catalysts applied for silicification.....	26
2.1.2	Precursors of silica.....	28
2.1.3	Other chemicals.....	30
2.2	Equipment used for the synthesis of silica capsules.....	32
2.3	Characterization.....	33
	<i>Scanning electron microscopy (SEM)</i>	33
	<i>Transmission electron microscopy (TEM)</i>	33
	<i>Energy-dispersive X-ray spectroscopy (EDX)</i>	34
	<i>X-ray diffraction (XRD)</i>	34
	<i>Optical-fluorescence microscopy</i>	34
	<i>Infrared spectroscopy (IR)</i>	35
	<i>Raman spectroscopy</i>	35
	<i>Ultraviolet-visible spectroscopy (UV-Vis)</i>	35
	<i>Pendant drop tensiometry</i>	36
	<i>Thermogravimetric analysis</i>	36
	<i>Zeta potential analysis</i>	37
3	Lysozyme-silica hybrid capsules	38
3.1	Lysozyme as effective biocatalysts and templates for the synthesis of silica capsules.....	38
3.1.1	Interfacial activity of lysozyme.....	38
3.1.2	Enzymatic activity of lysozyme.....	39
3.2	Kinetics of the polycondensation of TEOS in the presence of lysozyme in the o/w Pickering emulsion.....	42
3.3	Influence of emulsification method and mixing sequence on the lysozyme-silica hybrid capsules.....	48
3.4	Inverted and double emulsion lysozyme-silica capsules.....	53
3.4.1	Inverted emulsion (w/o) capsules.....	54

3.4.2	Double emulsion (o/w/o) capsules.....	55
3.5	Influence of buffer on size and morphology of lysozyme-silica capsules.....	56
3.6	Influence of additives on size and morphology of lysozyme-silica capsules.....	60
3.6.1	Sodium salts as additive.....	60
3.6.2	Ionic surfactants as additive.....	63
3.7	Surface functionalization of lysozyme-silica capsules <i>via</i> a one-step approach.....	66
3.8	Double/multilayer structure of capsule shell.....	75
3.8.1	Double layer structure.....	76
3.8.2	Multilayer structure.....	81
4	Silicatein-silica hybrid capsules	84
4.1	Silicatein as effective biocatalysts and templates for the synthesis of silica capsules.....	84
4.2	Silicatein vs. lysozyme.....	89
4.3	Size and morphology control of silicatein-silica capsules <i>via</i> emulsification method and precursor.....	90
5	PNIPAAm-silica hybrid capsules	93
5.1	PNIPAAm microgels as effective catalysts and templates for the synthesis of silica capsules.....	93
5.2	Synthesis of silica capsules with PNIPAAm microgels.....	99
5.3	Thermal treatment of PNIPAAm-silica capsules.....	101
6	Immobilized lysozyme in microgel matrix for the synthesis of silica capsules	103
6.1	Immobilization of lysozyme in PVCL/MEA/AA microgels.....	106

6.2	Immobilized lysozyme as effective catalysts and templates for the synthesis of silica capsules.....	107
6.3	PNIPAAm microgels vs. PVCL/MEA/AA-lysozyme microgels.....	110
7	Enzymatic activity assay of lysozyme and immobilized lysozyme	113
7.1	Hydrolysis of bis(<i>p</i> -aminophenoxy)-dimethylsilane catalyzed by silicatein.....	113
7.2	Enzymatic activity assay of lysozyme by using of bis(<i>p</i> -aminophenoxy)-dimethylsilane.....	115
7.3	Enzymatic activity assay of immobilized lysozyme by using of bis(<i>p</i> -aminophenoxy)-dimethylsilane.....	119
7.4	Enzymatic activity assay of lysozyme by using of bis(<i>p</i> -nitrophenoxy)-dimethylsilane.....	120
8	Summary	125
9	Zusammenfassung	129
10	References	134
11	List of publications	144
12	Acknowledgement	146

List of Abbreviations

°C	Degree Celsius
%	Percent
AA	Acylacid
ACMA	2,2'-azobis[N-(2-carboxyethyl)-2-methylpropionamidine]
APTMS	(3-Aminopropyl)trimethoxysilane
BIS	<i>N,N'</i> -methylenbisacrylamid
cm	Centimeter
CTAB	Cetyltrimethylammonium bromide
Dabsyl chloride	4-Dimetheylaminoazobenzene -4-sulfonyl chloride
DMF	Dimethylformamide
DSC	Differential scanning calorimetry
EDX	Energy-dispersive X-ray spectroscopy
FT	Fourier transformation
h	Hour
IFT	Interfacial tension
IR	Infrared spectroscopy
kV	Kilovolt
m	Meter
mbar	Millibar
MEA	2-methoxyethylacrylat
min	Minute

mg	Mikrogramm
mL	Milliliter
mm	Millimeter
mN	Millinewton
nm	Nanometer
NP	Nanoparticles
PEOS	Polyethoxysilane
PNIPAAm	Poly(<i>N</i> -isopropylacrylamide)
PVCL	Polyvinylcaprolactam
s	Second
SEM	Scanning electron microscopy
t	Time
T	Temperature
TEOS	Tetraethoxysilane
TEM	Transmission electron microscopy
THF	Tetrahydrofuran
TGA	Thermogravimetric analysis
Tris	Tris(hydroxymethyl)aminomethane
UV-Vis	Ultraviolet-visible spectroscopy
μL	Microliter
μm	Micrometer
VCL	<i>N</i> -Vinylcaprolactam
VPTT	volume phase transition temperature
wt%	Weight percent

List of Figures

1.1	Optical micrographs of isolated silicatein spicules from the marine sponge <i>Tethya auranita</i> and the Ribbon model of silicatein α from an energy minimization program.....	3
1.2	SEM images of a native silicatein filament and a cellulose fiber after a 12h reaction with TEO in Tris buffer at 20°C and neutral pH value.....	4
1.3	Proposed mechanism of TEOS hydrolysis catalyzed by the Ser/His active site in silicatein α	5
1.4	Scheme of bioencapsulation of <i>E.coli</i> with silica using silicatein.....	8
1.5	Proposed mechanism of the condensation of Me ₃ SiOEt catalyzed by the Ser/His/Asp triad.....	10
1.6	SEM and TEM images of cage-like silica hollow particles obtained after calcination at 700°C for 2 h.....	11
1.7	Structure of synthetic non-peptide diblock copolymer and the comparison of amino acid chemical structure with the synthetic mimic.....	14
1.8	Small molecules with catalytic activity for silicification <i>via</i> their bifunctionalities.....	15
1.9	Structure of poly-L-lysine.....	15
1.10	Structure of PNIPAAm.....	16
1.11	Scheme of classical emulsion, Pickering emulsion and the wettability of solid particle at interface.....	18

1.12	Synthesis of silica capsules <i>via</i> emulsion-templated method.....	19
1.13	Capsules synthesized from lysozyme, ferritin and hydrophobin stabilized Pickering emulsions.....	21
1.14	Cryo-SEM image and schematic representation of microgels at the water/heptane interface.....	22
1.15	SEM images of Toluene in water emulsion stabilized by PNIPAM microgel particles.....	24
2.1	Structure of PVCL/MEA/AA.....	28
2.2	Reaction scheme of hydrolysis and condensation of TEOS.....	28
2.3	One-pot synthesis of PEOS.....	29
2.4	A pendant drop for the measurement of the interfacial tension of two phases.....	36
3.1	Pendant drop interfacial tensiometry measurements of different enzyme solutions against TEOS.....	39
3.2	SEM images of different samples prepared with TEOS and different hydrolases via sonication after 24 hours.....	40
3.3	EDX analysis, TGA measurements and IR spectra of pure lysozyme-silica hybrid capsules.....	41
3.4	Weight of SiO ₂ in the lysozyme catalyzed polycondensation of TEOS after different reaction times.....	43
3.5	TGA measurements of pure lysozyme and lysozyme-silica capsules after different reaction times.....	43
3.6	SEM images of lysozyme-silica capsules after 1 day, 3 days and 6 days.....	44
3.7	X-ray diffractograms of lysozyme-silica capsules after different reaction time.....	45

3.8	SEM images and IR spectra of 6-day capsules before and after TGA.....	46
3.9	<i>In-situ</i> heating X-ray analysis of lysozyme-silica capsules on a platinum sample holder.....	47
3.10	Overview of the method variation and the corresponding lysozyme-silica hybrid structures.....	48
3.11	SEM images of different hybrid structures prepared by one-step addition of TEOS into lysozyme solution with different emulsification methods.....	50
3.12	SEM image of the template product formed at intermediate stage in the two-step procedure after the first addition of 20 μ L TEOS and 30 min of mild stirring.....	51
3.13	SEM images of different hybrid structures prepared by two-step addition of TEOS into lysozyme solution with different emulsification methods.....	53
3.14	Fluorescence microscopy and SEM images of inverted emulsion capsules.....	54
3.15	Fluorescence microscopy and SEM images of double emulsion capsules.....	55
3.16	SEM images of lysozyme-silica capsules prepared by using glycine buffer and phosphate buffer.....	57
3.17	XRD diffractograms of lysozyme-silica capsules prepared in different buffers.....	59
3.18	EDX spectra of capsules by using glycine buffer and phosphate buffer.....	59
3.19	SEM images of lysozyme-silica capsules <i>via</i> two-step approach with NaCl and NaF as additive.....	60
3.20	Schematic representation of emulsion stability influenced by electrostatic repulsion.....	62

3.21	EDX spectra of lysozyme-silica capsules by using NaCl and NaF.....	63
3.22	SEM image and the corresponding TEM analysis of lysozyme-silica capsules <i>via</i> two-step approach with CTAB.....	65
3.23	Reaction scheme of surface functionalization with APTMS <i>via</i> the one-step approach.....	66
3.24	SEM images of samples with different TEOS/APTMS ratios <i>via</i> the one-step approach.....	68
3.25	SEM and TEM images of silica-lysozyme capsules prepared <i>via</i> mixing TEOS and APTMS (92 wt%/8 wt%).....	69
3.26	Reaction scheme of primary amine with dabsyl chloride.....	69
3.27	UV-Vis spectra of (A) pure dabsyl chloride, (B) dabsyl chloride reacted with silica NP, (C) dabsyl chloride reacted with APTMS functionalized silica NP, (D) dabsyl chloride reacted with lysozyme, (E) dabsyl chloride reacted with normal lysozyme-silica capsules and (F) dabsyl chloride reacted with functionalized lysozyme-silica..	71
3.28	Reaction scheme of calcein and a coupling reagent with primary amine groups.....	72
3.29	Reaction mixture and supernatant collected after each washing step after a reaction of calcein with: column (A) silica NP modified with APTMS; column (B) modified silica capsules with APTMS; column (C) silica capsules without modification.....	73
3.30	UV-Vis spectra of calcein, unmodified lysozyme-silica capsules and modified lysozyme-silica capsules.....	74
3.31	Optical and fluorescent micrographs of unmodified and modified capsules after the treatment with calcein in bright field, green and red channels.....	75
3.32	Mesostructures of abalone shell consisting of inorganic layers separated by protein layers.....	76
3.33	Different samples for the investigation of double layer structure.....	77
3.34	SEM images of the double layer structure prepared in glycine buffer.	79

3.35	SEM images of the double layer structure prepared in phosphate buffer.....	80
3.36	SEM images of two capsules with double layer structure prepared in phosphate buffer.....	80
3.37	Preparation of multilayer structure in phosphate buffer.....	81
3.38	SEM images of sample LT-LT-LT prepared in phosphate buffer.....	82
3.39	SEM images of sample LT-LT-LT-LT prepared in phosphate buffer.	83
4.1	(A) Milli Q H ₂ O, (B) Tris buffer, (C) hydrophobin solution in Tris buffer (D) recombinant silicatein solution in Tris buffer incubated with TEOS after 3 hours at room temperature.....	85
4.2	IR spectra of pure silica and the precipitate isolated from recombinant silicatein after 3 hours incubation with TEOS.....	85
4.3	Dynamic interfacial tension at the interface between Tris buffer and TEOS; refolded silicatein solution and TEOS.....	86
4.4	Change of a pendant drop over time (pendant drop: silicatein solution in Tris buffer, environment: TEOS).....	88
4.5	Dynamic interfacial tensions at the interface between different enzymes solutions and TEOS.....	89
4.6	Change of a lysozyme pendant drop and a recombinant silicatein pendant drop in the TEOS environment.....	90
4.7	SEM images of capsules prepared with recombinant silicatein with different precursors and emulsification methods.....	92
5.1	Chemical structure of PNIPAAm and PVCL.....	94
5.2	Dynamic interfacial tension measurements of interface between PNIPAAm microgels and TEOS, PVCL microgels and TEOS, deionized H ₂ O and TEOS.....	94

5.3	SEM images of PNIPAAm-silica capsules prepared with vortex and sonication.....	96
5.4	EDX analysis of PNIPAAm-silica hybrid capsules.....	96
5.5	TGA measurements of PNIPAAm-silica hybrid prepared with vortex and sonication.....	97
5.6	Hexagonal arrangement of PNIPAAm microgels on the capsule shell.....	98
5.7	IFT between TEOS and PNIPAAm microgel dispersion with different concentration.....	99
5.8	TEOS reacted with dilute PNIPAAm dispersion for 1 day.....	100
5.9	SEM images of PNIPAAm-silica hybrid capsules prepared with PNIPAAm dispersion with different concentrations.....	101
5.10	SEM images of PNIPAAm-silica hybrid structures after heating at 800 °C.....	102
6.1	Schematic representation of the immobilization of lysozyme in a microgel matrix.....	104
6.2	Synthesis of PVCL/MEA/AA microgels <i>via</i> radical polymerization..	105
6.3	Dynamic interfacial tension measurements of PVCL/MEA/AA microgels without and with lysozyme at the interface between H ₂ O and TEOS.....	108
6.4	IR spectra of pure silica, precipitate isolated from the reaction of pure lysozyme with TEOS and immobilized lysozyme with TEOS...	109
6.5	SEM images of immobilized lysozyme in PVCL/MEA/AA-silica hybrid structure at different pH	110
6.6	Comparison between capsules synthesized with PVCL/MEA/AA-lysozyme and PNIPAAm microgels.....	111

7.1	Proposed hydrolysis mechanism of bis(<i>p</i> -aminophenoxy)-dimethylsilane catalyzed by Ser/His active site of silicatein.....	114
7.2	Change of absorption spectra during incubation of silicatein in the presence of bis(<i>p</i> -aminophenoxy)-dimethylsilane.....	115
7.3	UV-Vis measurements during incubation of lysozyme (in glycine buffer, pH 9) in the presence of bis(<i>p</i> -aminophenoxy)-dimethylsilane in the two-phase system and in an emulsion system...	117
7.4	Change of absorption at 300 nm during the incubation of lysozyme with bis(<i>p</i> -aminophenoxy)-dimethylsilane in a two-phase system and an emulsion.....	118
7.5	UV-Vis spectra of the hydrolysis of bis(<i>p</i> -aminophenoxy)-dimethylsilane in the presence of lysozyme by using phosphate buffer at pH 9 and the Change of absorption at 300 nm during the reaction.....	118
7.6	UV-Vis spectra of hydrolysis of bis(<i>p</i> -aminophenoxy)-dimethylsilane in the presence of immobilized lysozyme in a two-phase system.....	119
7.7	Proposed hydrolysis of bis(<i>p</i> -nitrophenoxy)-dimethylsilane catalyzed by lysozyme.....	120
7.8	Determination of the molar absorption coefficient ϵ of <i>p</i> -aminophenol at 300 nm and <i>p</i> -nitrophenol at 400 nm in glycine buffer.....	121
7.9	Synthesis of bis(<i>p</i> -nitrophenoxy)-dimethylsilane.....	122
7.10	UV-Vis spectra of NO ₂ -silane at different concentrations in glycine buffer at pH 9 (left) and the determination of the molar absorption coefficient at 400 nm.....	123
7.11	UV-Vis measurements of the control sample without lysozyme in the presence of bis(<i>p</i> -nitrophenoxy)-dimethylsilane in the two-phase system.....	124

List of Tables

2.1	Chemicals used for the synthesis of silica capsule.....	30
2.2	Equipment applied for the synthesis of silica capsules.....	32
3.1	Enzymatic activity of different enzymes for silicification.....	40
3.2	Buffers used for the synthesis of lysozyme-silica hybrid capsules.....	57
3.3	Changes in size and morphology by using different buffers.....	58
3.4	Changes in size and morphology by using different additives.....	65
3.5	Samples with different TEOS/APTMS ratios.....	67
3.6	Zeta-potential measurements for double layer structure.....	77
4.1	Silica capsules prepared with silicatein solution after a reaction of 24 hours at room temperature.....	91
5.1	Samples prepared with PNIPAAm and PVCL.....	95
5.2	Composition of PNIPAAm-Silica hybrid structures.....	98
6.1	Pure carriers and immobilized lysozyme in the carrier materials at three different pH.....	106
6.2	Zeta potential before and after immobilization of lysozyme.....	107
6.3	Results of pure carriers and immobilized lysozyme after incubation with TEOS.....	109

1 Introduction

1.1 Biomineralization/biosilicification*

The outstanding properties of natural materials are often based on the hybrid character of these structures in which proteins fulfill a key role.^[1] Particularly interesting is the fact that proteins with specific size, catalytic activity, coordinating ability and behavior similar to colloidal particles can introduce highly useful properties in the process of biomineralization.^[2] Silica is the most frequently used minerals in these hybrid structures because of the convenient semi-organic precursors.^[3] While synthetic organosilicon chemistry requires high temperatures, pressures or extreme pH, nature is able to produce silica with specific fine structures in the micro- and nano-regime at ambient temperatures and pressures and at near neutral pH.^{[4] [5]} Organisms, including diatoms, radiolaria, choanoflagellates, sponges and higher plants, build up their skeleton with silica with the help of specialized proteins. It is possible to isolate specific proteins from these organisms that are involved in the biosilicification process, producing the hard exoskeleton.^[6] Such proteins inspire the material scientist to fabricate novel materials with various shapes and compositions in non-natural but still environmental friendly and economic conditions.^[4] A well-known example is silicatein (silica proteins) isolated from marine sponges.^{[5] [6] [7]}

(* Parts of this section have been published in reference ^{[4].})

1.1.1 Enzymatic silicification with silicatein

Silicatein

Silicatein was at first discovered by Morse and coworkers from the silica spicules, which constitute 75% of the dry weight of marine sponge *Tethya auranita*. Each spicule contains a central axial filament of protein named silicatein (Fig.1.1A/B). There are three similar subunits under silicateins: silicatein α , β , γ and about 70% of the mass of the proteinaceous filament is composed of silicatein α .^[5] Fig. 1.1C shows the stimulated ribbon model of silicatein α with active site (in green) and the disulfide bonds (in blue).

The silicateins control the biosilicification process in siliceous sponges enzymatically and meanwhile serve as the organic matrix for the silica product.^[8] It was reported that the native silicatein filaments can catalyze the polycondensation of tetraethyl orthosilicate (TEOS) to form silica *in vitro* at neutral pH 6.8 and 20 °C. The absence of silicatein or the use of denatured silicatein under the same conditions yielded little silica product, indicating the enzymatic activity of the silicateins and the importance of the three-dimensional conformation of the proteins (Fig. 1.2).^[5]

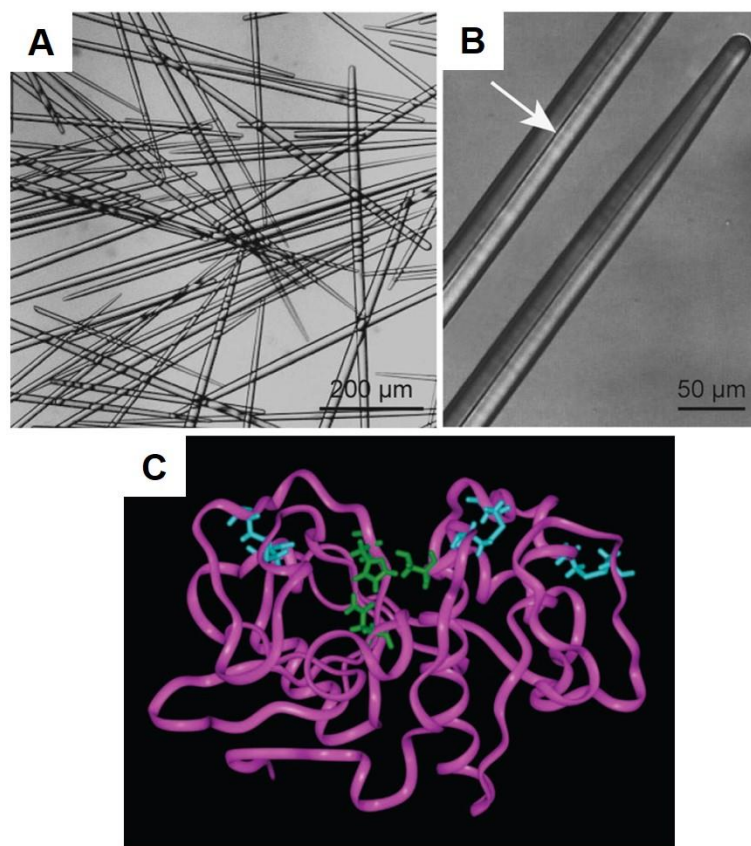


Fig. 1.1: (A) Optical micrographs of isolated spicules from the marine sponge *Tethya auranita*. (B) The higher magnification image reveals the axial protein filaments (indicated by white arrow). Reprinted with permission from reference ^[9]. Copyright 2003 Wiley-Liss. (C) Ribbon model of silicatein α from an energy minimization program. Reprinted with permission from reference ^[10]. Copyright 2006 National Academy of Sciences.

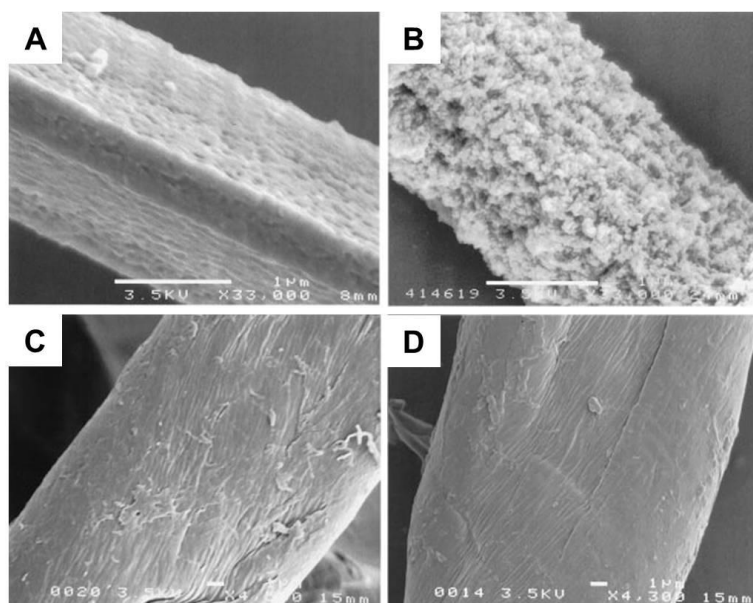


Fig. 1.2: SEM images of (A) native silicatein filament, (B) silicatein filaments after a 12h reaction with TEOS in Tris buffer, (C) cellulose fiber, (D) cellulose fiber after a 12h reaction with TEOS under the same condition of (B). The change of the filament surface after a 12 hours reaction with TEOS at 20°C and neutral pH value confirms the enzymatic activity of silicatein. Cellulose fiber was used for the same reaction but no condensation of precursor was observed. Reprinted with permission from reference [5]. Copyright 1999 National Academy of Science.

The key step in the silica synthesis is the Si-O-Si bond formation from the condensation of two Si-OH groups either in silica-forming organisms or in *in vitro* silicification.^[11] The hydrolysis of alkoxy silanes is the rate-limiting step in the silica condensation and needs typically acids or bases as catalysts, therefore it is proposed that silicateins catalyze this hydrolytic reaction at neutral pH. Silicateins exhibit high similarities, with respect to the hydrolytic enzyme cathepsin L, which belongs to the group of papain-like protease with the characterizing active triad histidine (His), asparagine (Asp) and cysteine (Cys). The similarities include amino acid sequences and three-dimensional structures. In the silicateins, cysteine is replaced by serine (Ser). A possible mechanism of hydrolysis catalyzed by the Ser/His active site of silicatein α is shown in Fig. 1.3.^[12]

1 Introduction

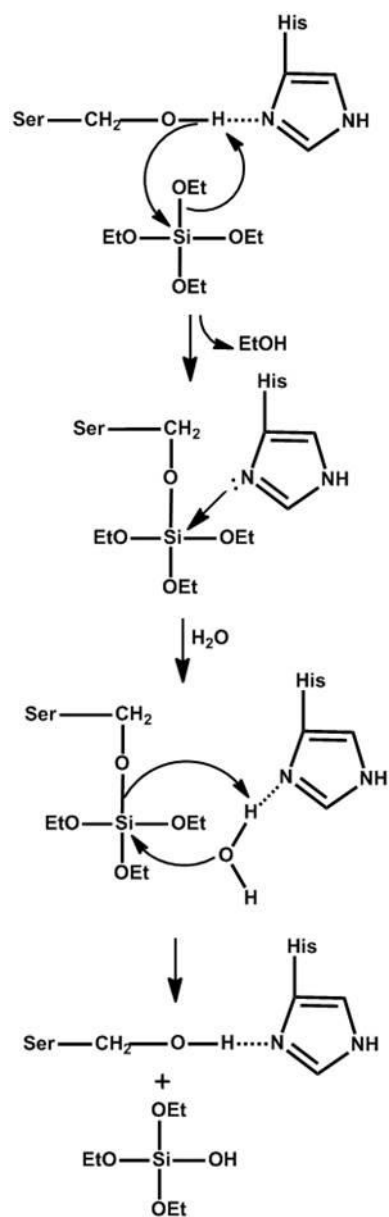


Fig. 1.3: Proposed mechanism of TEOS hydrolysis catalyzed by the Ser/His active site in silicatein α . Reprinted with permission from reference ^[12]. Copyright 1999 John Wiley & Sons, Inc.

Besides the native silicateins isolated from sponges, recombinant silicatein α was also successfully expressed from a recombinant DNA template in *Escherichia coli*. Müller, Tremel and coworkers have determined the enzymatic activity of recombinant

1 Introduction

silicatein α in the condensation of Dimethylsilane (DMS) to form oligomer PDMS at ambient conditions. The mass spectrum of the silicon product formed in the presence of silicatein showed the signal of the chain length up to twelve repeating monomer units, while without silicatein only a weak signal up to seven repeat units was present. In the ^{29}Si NMR analysis, intensive signals of hydrolysis intermediates and dimers of DMS were detected after 5 hours of incubation with silicatein, suggesting the catalytic activity in the hydrolysis of DMS. No signals for higher oligomers because of the concentration limit of the NMR technique. UV/Vis spectroscopy was applied to analyze the reaction *in situ*. The methoxy group was substituted with *p*-aminophenoxy group and the increasing absorption at 290 nm of the byproduct *p*-aminophenol in the presence of silicatein also revealed that recombinant silicatein is active towards silica condensation.^{[13] [14]}

Synthesis of inorganic materials or organic/inorganic hybrids with native and recombinant silicatein

The enzymatic activities of native or recombinant silicateins provide significant potential in developing an environmentally friendly approach to create new materials, especially hybrids of organic/inorganic substances.

The biocompatible biosilica, mediated by either native silicatein or recombinant silicatein under near physiological conditions, could be very advantageous in biomedical application like bone regeneration and tissue engineering. Schröder *et al.* demonstrated that collagen-coated surfaces modified by biosilicification from TEOS with recombinant silicatein could increase calcium phosphate deposition *in vitro*.^[15] A new implant material for bone reconstitution based on the osteoinduction of biosilica and the enzymatic activity of recombinant silicatein was developed by Wiens *et al.*. In this work the silicatein and its substrate sodium metasilicate were encapsulated into biodegradable and biocompatible poly(D,L-lactide)/poly(vinyl pyrrolidone) microspheres. These silicatein/silica containing microspheres were integrated in a

1 Introduction

plastic-like matrix to form a functional implant material.^[16] It was also possible to generate silica layers on teeth by biosilicification with silicatein to protect teeth from bacterial attack.^[8] The research of Müller *et al.* indicated that biosilica nanoparticle isolated from marine sponge *S. domuncula* strongly increase the expression levels of enamelin and amelogenin *in vitro*, which contribute to hydroxyapatite crystallite formation, therefore the biosilicification by silicatein may be a novel approach for tooth reconstruction.^[17]

Silicateins are not only able to produce silica enzymatically with controlled structure but are also capable of catalyzing and templating the formation of other metal oxides such as titanium dioxide and gallium oxide.^[7] Sumerel *et al.* have reported the biocatalytically templated synthesis of titanium dioxide TiO₂ from titanium bis-(ammonium-lactato)-dihydroxide (Ti[BALDH]) at neutral pH and mild temperature with native silicatein filaments isolated from Sponge *Tethya aurantia*. The further thermal annealing led to different crystallite diameters and phases of TiO₂, compared to the materials obtained from the same precursor *via* traditional alkali or thermal catalysis.^[18]

O'Leary *et al.* have tested the use of silicatein filaments to silicify trialkoxysilanes bearing an organometallic species e.g. functionalized Pt and Pd complexes. This benign method provides a new possibility for the future immobilization of the catalysts which are sensitive to specific environmental conditions.^[19]

Curnow *et al.* have applied bacterial *E.coli* cells, whose cell-surface displayed recombinant silicatein after the transformation with a silicatein gene, as a whole-cell biocatalyst to fabricate ordered titanium phosphate on the cell surfaces at low temperature and neutral pH from Ti[BALDH].^[20] Müller *et al.* have also demonstrated that silicatein was deposited on the surface of *E. coli* surface after the transformation and the bacterial cells could be encapsulated with silica after further incubation with silicic acid under physiological conditions (Fig. 1.4). However, the growth kinetics of the bacteria remained unaffected, suggesting that the bacteria was still active after the

1 Introduction

encapsulation. Therefore this method can improve the technique of immobilization and application of bacteria or yeast cells without affecting their activities.^[21]

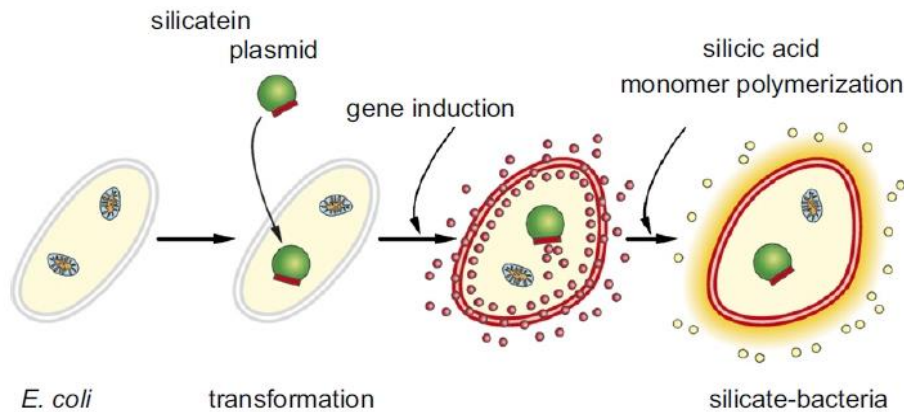


Fig. 1.4: Scheme of bioencapsulation of *E.coli* with silica using silicatein. Reprinted with permission from reference ^[21]. Copyright 2008 Elsevier.

It is also quite meaningful to coat other materials, especially materials which are sensitive to heat, alkaline or acidic conditions with silica or other metal oxides assisted by silicatein under mild conditions. Rai and Perry have achieved to fabricate uniform silica films with a thickness of about 20-100 nm on gold surfaces bound with silicatein and by varying the amount of absorbed silicatein and the reaction times with precursor tetramethyl orthosilicate (TMOS), the physical properties of the silica films such as thickness, roughness and hydrophilicity were tunable.^[22] Shukoor *et al.* have applied silicatein to form magnetic $\gamma\text{-Fe}_2\text{O}_3$ nanoparticles with silica coating, which could offer protection to the magnetic nanoparticles from the environment and increase their biocompatibility for biomedical applications.^[23]

1.1.2 Biosilicification with other naturally occurring enzymes

Hydrolases as catalysts for silicification

While natural organisms rely on specific proteins for certain processes, other more accessible proteins show similar capabilities even though it is not their native function. As mentioned in the last section the hydrolysis of alkoxy silanes is the rate-limiting step in the silica condensation and needs to be catalyzed. A series of commercially available hydrolases, including proteases, lipases and phosphatases, which are not naturally associated with silica production, show their potential as biocatalysts for silicification.

Bassindale *et al.* have studied *in vitro* siloxane bond formation from Ethoxytrimethylsilane (Me_3SiOEt) at neutral pH and room temperature with different hydrolases.^[11] ^[24] Several enzymes, including *bovin pancreatic* trypsin (TPCK treated), α -chymotrypsin, *Aspergillus ficuum* phytase, *Aspergillus. niger* phytase, chicken egg white lysozyme, *porcine gastric mucosa* pepsin and *phizopus oryzae* lipase, were found to catalyze the condensation of Me_3SiOEt to form Hexamethyldisiloxane (HMDSO) in aqueous solution. The enzymes Trypsin was found to be the most effective for the Si-O-Si bond formation and the Me_3SiOEt condensation in the presence of Trypsin was nearly complete after 3 hours.^[24] Trypsin and α -chymotrypsin could also act as catalysts for the polycondensation of TEOS.^[25] It was also revealed that papain was able to mediate the formation of silica from TMOS.^[26]

All of these hydrolytic enzymes exhibit one or more serine, aspartate or histidine residues or a combination of these three residues, which resembles the catalytic triad of the Silicatein and therefore are able to perform similar reactions like silicification, though with reduced activity. The proposed mechanism for a Ser/His/Asp triad involved silanol condensation (Fig. 1.5) extends the comprehension of the interaction between enzymes and silica precursors.^[11]

1 Introduction

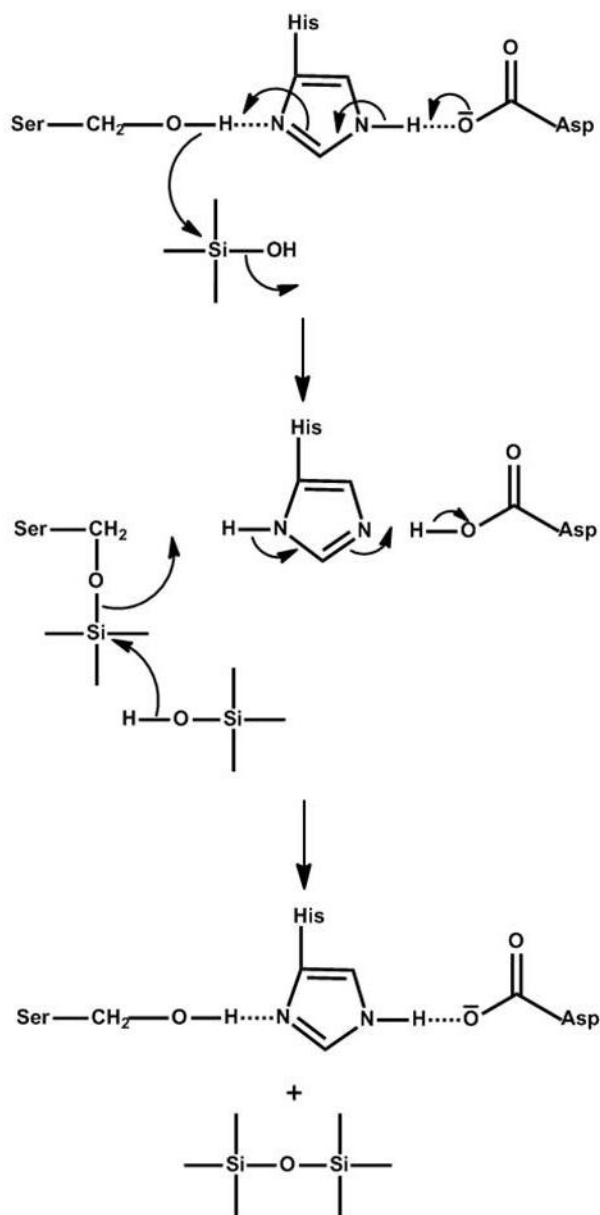


Fig. 1.5: Proposed mechanism of the condensation of Me₃SiOEt catalyzed by the Ser/His/Asp triad. Reprinted with permission from reference ^[11]. Copyright 2011 Elsevier.

New material synthesis with native hydrolases

The hydrolases, particularly lysozyme, which are capable of catalyzing the silicification process are also of great interest for the design of new materials based on silica. Schiomi *et al.* reported the synthesis of lysozyme-silica hybrid hollow spherical particles at ambient conditions, using the catalytic activity of lysozyme for silica formation from TEOS and the foaming effect of lysozyme.^[27] In the hybrid shell, lysozyme structures disperse uniformly within the silica matrix and by the removal of the lysozyme under calcination, cage-like spherical silica capsules were formed, with a silica shell thickness of ~100 nm containing pores of 50-250 nm in diameter. (Fig. 1.6) This has potential applications in controlled release systems for biomacromolecules like proteins and DNAs.^{[28] [29]}

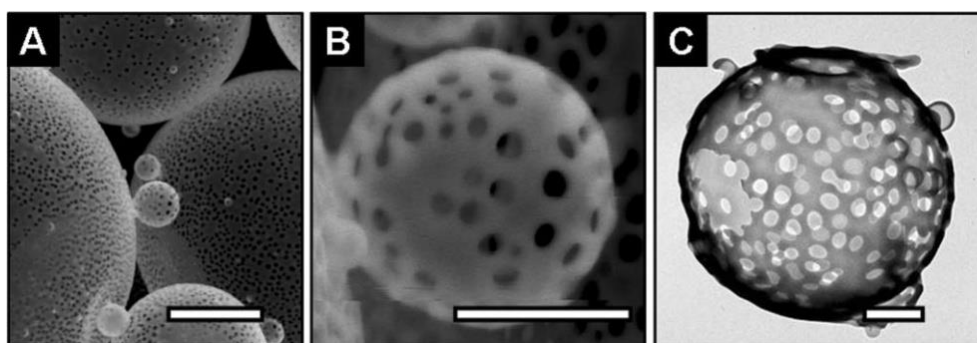


Fig. 1.6: SEM (A, B) and TEM (C) images of cage-like silica hollow particles obtained after calcination at 700°C for 2 h. Scale bars: (A) 3 μm, (B) and (C) 500 nm. Reprinted with permission from reference ^[28]. Copyright 2007 Royal Society of Chemistry.

It has been suggested that lysozyme catalyzes not only the precipitation of silica from TEOS but also the formation of titania from potassium hexafluorotitanate (PHF-Ti) or Ti[BALDH]. A mild one-pot method was reported to generate lysozyme-silica or lysozyme-titania bionanocomposites with the antibacterial properties of lysozyme. It was also possible to add additional enzyme during the lysozyme-mediated

1 Introduction

mineralization so that the enzyme could be encapsulated in the silica or titania matrix. The benefit of this approach is that the silica or titania prevents the enzyme from physical denaturation and protects the lysozyme from microbial degradation.^[30]

A simple preparation of another silica-enzyme composite with trypsin instead of lysozyme was reported by Bassindale *et al.* and in this composite at least 40 % of the activity of trypsin could be retained after one week at ambient temperature.^[31] These findings suggest that the silica matrix allows for the encapsulated enzyme to retain its activity.

Another example for the entrapment of an enzyme in a biologically synthesized silica matrix by lysozyme was the co-immobilization of carbon nanotubes and glucose oxidase for direct electron transfer. The glucose oxidase is a stable redox enzyme with high catalytic activity and the direct bio-electrocatalysis of glucose oxidation could be of great interest for the development of bioelectrodes for biosensors and biofuel cells. However, the redox center was not accessible after the traditional immobilization of glucose oxidase so the electron transfer between the enzyme and the electrode surface was limited. The lysozyme catalyzed the silica formation from TMOS on conductive carbon paper with the addition of carbon nanotubes and glucose oxidase. During the silicification the carbon nanotubes and the glucose oxidase were incorporated in the silica matrix. With the help of this co-immobilization technique, the carbon nanotubes could provide an electrical connection between the enzyme and the carbon paper surface and the electron-transfer rate was increased compared to that of an unmodified electrode and the immobilized enzyme retained its catalytic activity for a period of one month.^[32]

1.1.3 Analogues of enzymes as catalysts for silicification

Polypeptides, copolymers or bifunctional small molecules

Inspired by silicatein, other analogue molecules for the catalysis of biomineralization have been designed. For example, synthetic cysteine-lysine diblock copolypeptides are applied to catalyze the condensation of TEOS with controlled dimensions. In this block-copolypeptide the poly-lysine is the cationic polyelectrolyte with amine groups, which is water soluble at pH 7, and the poly-cysteine is the water insoluble domain with hydrolytic activity. The amphiphilic block-copolypeptide self-assembled into aggregates in water and the reduced (under N₂) or oxidized (under air) forms of the block-copolymer initiated different aggregate morphologies due to the formation of disulfide bonds in oxidative environment, leading to different silica shapes.^[33] Another example is a non-peptide diblock copolymer containing both nucleophilic side groups with –OH group and nitrogen containing side chains with pyridine group (Fig. 1.7A) to mimic the enzymatic active site of silicatein, The hydroxyl functionality acts as the serine-26 and the pyridine functionality acts as the histine-165 (Fig. 1.7B).^[34]

1 Introduction

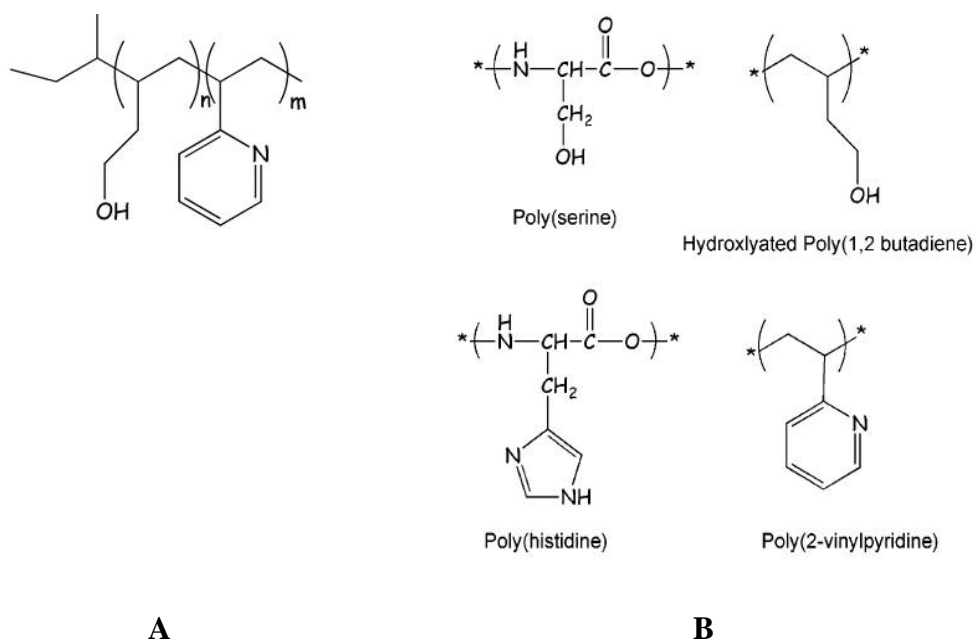


Fig. 1.7: (A) Structure of synthetic non-peptide diblock copolymer; (B) Comparison of amino acid chemical structure with the synthetic mimic. Reprinted with permission from reference ^[34]. Copyright 2004 American Chemical of Society.

Besides copolypeptides or copolymers, an array of small molecules with bifunctionalities also show catalytic capability for silicification (Fig. 1.8). These small molecules exhibit a nucleophilic group, such as $-\text{SH}$, $-\text{OH}$, $-\text{SC}_2\text{H}_5$, and a hydrogen-bonding acceptor group, such as $-\text{NH}_2$, $-\text{NHR}$, $-\text{NR}_2$. The distance between the two functional groups is 2.9 \AA , which is close to the distance 3.2 \AA between sulfur and nitrogen in the active site in cathepsin L or in other hydrolases with serine, histidine and asparagine as catalytic triad. Among those candidates cysteamine was the most successful biomimetic catalyst and the reaction with TEOS led to amorphous silica spheres with a diameter of 40-100 nm. Furthermore silicification of TMOS catalyzed by cysteamine was applied for encapsulation of biomaterials such as Luciferase, GFP and *E.coli* cells, and the biomaterials retained their activities after the encapsulation.^[35]

1 Introduction

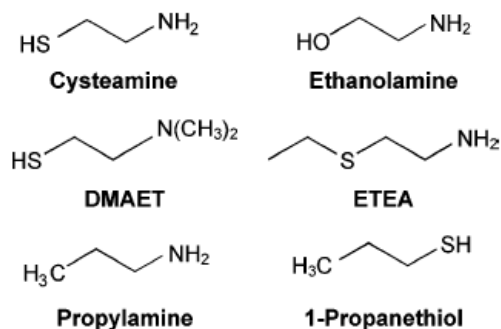


Fig. 1.8: Small molecules with catalytic activity for silicification *via* their bifunctionalities. Reprinted with permission from reference ^[35]. Copyright 2005 American Chemical of Society.

Pogula *et al.* have fabricated continuous thick silica coatings with TMOS under benign conditions on glass fibers with the help of poly-L-lysine (Fig. 1.9), which also showed the activity to catalyze silicic acid deposition. By varying the mixing sequence of a poly-L-lysine solution, phosphate buffer and silicic acid precursor, different silica structures were formed.^[36] Goldberg *et al.* have applied poly-L-lysine with pre-hydrolyzed TMOS to form a silica coating on dentin surfaces, suggesting that also biosilicification with synthetic polypeptide catalysts is a potential dental treatment strategy.^[37]

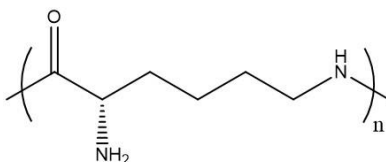


Fig. 1.9: Structure of poly-L-lysine.

PNIPAAm microgels

Since (co)polypeptides can catalyze silica formation, other polymers with sufficient amide groups presumably also exhibit similar catalytic ability. Poly(*N*-isopropylacrylamide) (PNIPAAm) is a potential candidate with plenty of amide groups in the side chains (Fig. 1.10). When treated with cross linkers PNIPAAm forms a three dimensional structure, namely microgel. PNIPAAm microgels are interfacial active particles and could be very useful for the silica synthesis from both water-soluble (silicic acids) and water-insoluble precursors (alkoxysilanes). Furthermore, PNIPAAm microgels are well known for their thermo-sensitivity. When heated in water above the volume phase transition temperature (VPTT) 33 °C they shrink to a dehydrated state.^[38] This thermo-responsive behavior together with a probable catalytic activity for silicification enables PNIPAAm microgels promising application in biocatalysis or biomedicine like tissue engineering or drug delivery.^[39]

The further advantages of PNIPAAm microgels include: 1) compared with isolation of native proteins or synthesis of proteins, they are easy to be prepared and accessible in large amount; 2) they can be synthesized with controlled size, which could influence the structure of silica; 3) it is simple to introduce new functionalities, adding interesting complexity to PNIPAAm-based silica.

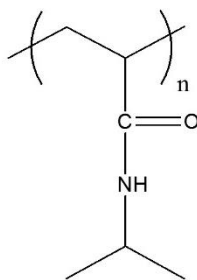


Fig. 1.10: Structure of PNIPAAm.

1.2 Pickering emulsion as template for capsule formation

Interface and colloidal chemistry is an interdisciplinary science, studying the physical and chemical processes at surfaces/interfaces in multiphase systems, multiphase colloidal dispersions, polymer solutions and various forms of molecular aggregates. In many industrial fields such as chemical industry, pharmaceutical, cosmetic, biotechnology, agriculture production, nanotechnology, interface and colloidal science plays an extremely important role.^[40]

1.2.1 Pickering emulsions

An emulsion is a mixture of two immiscible liquids. A liquid (disperse phase) forms small droplets, dispersing throughout the other liquid (continuous phase). There are two types of emulsions of water and oil: water-in-oil emulsion (w/o) and oil-in-water emulsion (o/w). Besides the two liquids, another important component in an emulsion is a surfactant, which assembles at the interface between the droplets and continuous phase, preventing a phase separation. Emulsions are formed either spontaneously or by mechanical means such as agitation and sonication.^[41]

A Pickering emulsion is a class of emulsions stabilized by the self-assembly of small colloidal particles (e.g. inorganic nanoparticles, polymers or proteins) instead of conventional surfactants at the interface.^[42] The difference between conventional emulsion and Pickering emulsion is shown in Fig. 1.11A. Since amphiphilicity is not necessary, the adsorption of colloidal particles at the interface is different from that of surfactants.^[43] The self-assembly of particles is *via* partial wetting of the surface of the particle by water and oil, leading to a decrease of the total free energy. The contact angle θ is used to describe the wettability of the solid particle in two different phases (Fig. 1.11B). The less wetting phase is normally the dispersed phase. If $0^\circ \leq \theta \leq 90^\circ$, the particles are hydrophilic and prefer to be wetted by water. The oil in water emulsion is more stable. If $90^\circ \leq \theta \leq 180^\circ$, the particles are hydrophobic and preferentially wetted by oil. In this case the water in oil emulsion is preferred.^{[42] [43]}

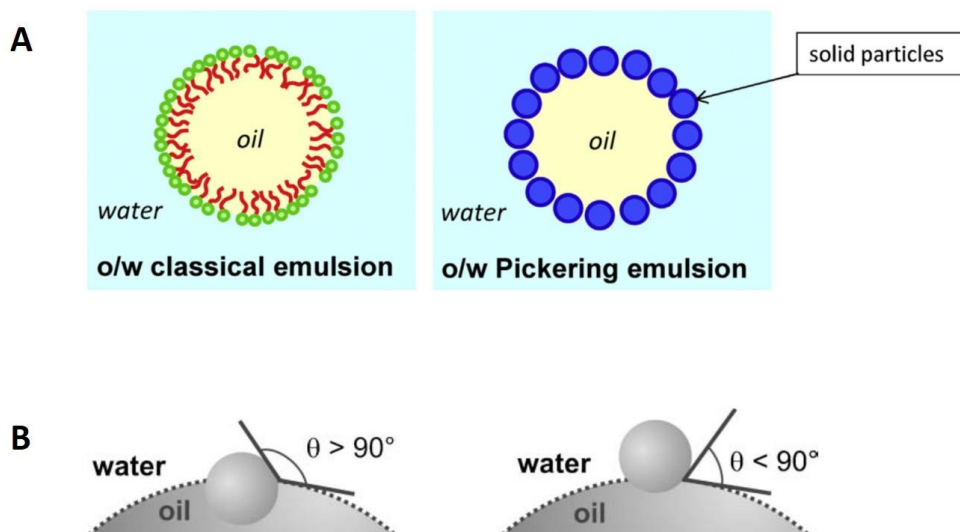


Fig. 1.11: (A) Classical emulsion and Pickering emulsion. Reprinted with permission from reference ^[43]. Copyright 2013 Elsevier. (B) Wettability of solid particle at interface. Reprinted with permission from reference ^[42]. Copyright 2007 Royal Society of Chemistry.

Many inorganic or organic particles can be used to stabilize Pickering emulsions. Silica particles are the most popular stabilizers. Besides silica, latex particles, carbon nanotubes, and block copolymer micelles are also widely reported. To add more complex properties to the Pickering emulsions, functional particles such as magnetic particles (iron oxide) or thermo/pH sensitive microgels are chosen as stabilizing particles. Furthermore, biological particles such as proteins and viruses are also able to assemble at interfaces.^{[42] [43] [44] [45]}

Comparing with conventional emulsions, Pickering emulsions often show high resistance to coalescence, and their surfactant-free character makes their application in many fields such as wastewater treatment, cosmetic formulations and food production very beneficial.^[43] By varying organic core matrices, colloidal particles, or emulsification methods, Pickering emulsions can serve as excellent templates for

the fabrication of different materials like organic/inorganic core-shell structures, hollow microspheres, and Janus particles with different size and property.^{[46] [47] [48]}

Fig. 1.12 shows the process of the formation of silica capsules in a Pickering emulsion. The silica precursor e.g. TEOS is the oil phase and the surface active agent solution is the aqueous phase. The precursor condenses at the o/w interface to form hollow structures. The capsules are hybrid, consisting of silica and the surface active agent. Normally the polycondensation of the silica precursor is quite slow and requires strong acid or base catalysis, high temperature and pressure. A very novel solution for this challenge is the use of enzymes which can accelerate the silicification and meanwhile are also surface/interface active, providing a stable emulsion as templates for capsules.^{[27] [49]} This method can avoid the use of other synthetic surfactants as a template for silica formation, and furthermore, it is not necessary to remove the template, compared to other templated synthesis of hollow silica spheres.^{[49] [50] [51] [52]}

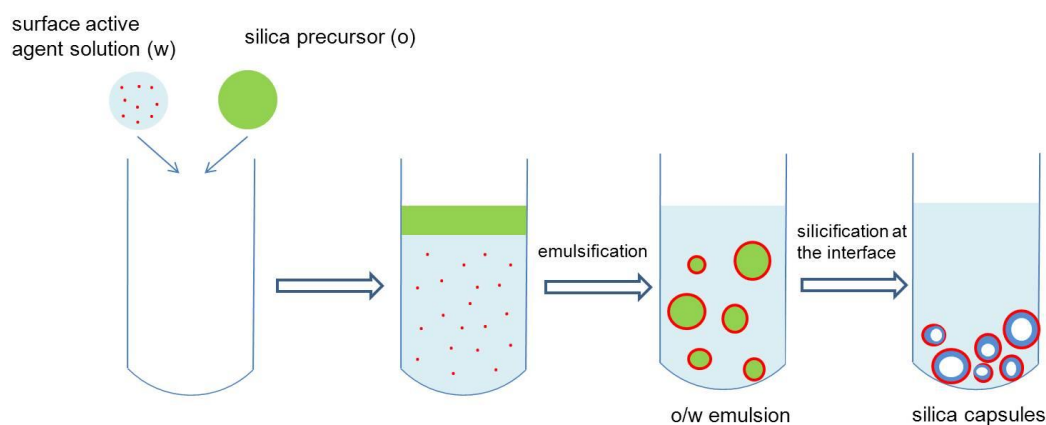


Fig. 1.12: Synthesis of silica capsules *via* emulsion-templated method.

1.2.2 Interfacial assembly of protein particles

Proteins are the most widely used stabilizers in the food industry and they assemble at air/liquid, liquid/liquid and air/solid interfaces.^{[53] [54]} However, the absorption of proteins at various interfaces is not only important in the food science but also in material science.^{[55] [56]} Due to their relatively fixed three-dimensional conformation, protein particles with uniform sizes show advantages at interfacial assembly among all the Pickering emulsion stabilizing particles. Furthermore, the convenient possibility to modify protein molecules makes them promising building blocks for novel capsules.^{[42] [57]}

For the protein assembly at air/liquid or liquid/liquid interfaces, the solution conditions *e.g.* concentration, pH value and ionic strength have significant influence on the interfacial behavior of proteins particles.^[54] It was also reported that some protein molecules form intermolecular disulfide bonds at the interfaces, which enhances the stability and the elasticity of the protein layer.^[58]

In section 1.1.2 it was mentioned that using the interfacial activity of lysozyme, lysozyme-silica hybrid capsules can be easily synthesized.^[27] Other proteins such as bovine serum albumin (BSA), ferritin and hydrophobin are also successfully applied to stabilize Pickering emulsions and provide a scaffold for capsules (Fig.1.13).^{[49] [57]} Especially the amphiphilic proteins hydrophobin, which occur naturally in filamentous fungi, are one of the most surface active proteins.^[59] In most proteins, the hydrophobic and hydrophilic residues are unsymmetrically distributed and (partially) buried in their three-dimensional structures.^[54] On the contrary, the hydrophobin molecule has a hydrophobic patch on the one side and a hydrophilic patch on the other side of the three-dimensional structure (similar with conventional surfactants), which makes hydrophobins macromolecular amphiphiles.^[59] Therefore hydrophobins are highly surface active and form very stable monolayers at interfaces.^[49]

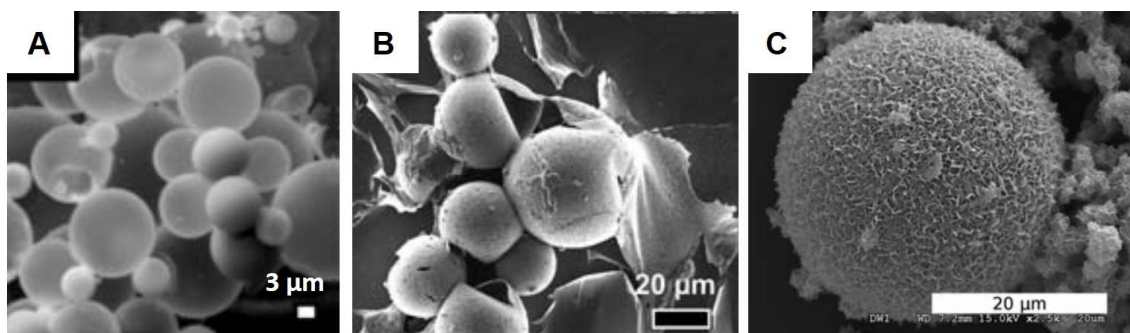


Fig. 1.13: Capsules synthesized from (A) lysozyme (reprinted with permission from reference ^[27]. Copyright 2005 Royal Society of Chemistry), (B) ferritin (reprinted with permission from reference ^[57]. Copyright 2010 Royal Society of Chemistry), (C) hydrophobin stabilized Pickering emulsions (reprinted with permission from reference ^[49]. Copyright 2011 Royal Society of Chemistry).

1.2.3 Microgels at interfaces

Microgels are intramolecular cross-linked polymer networks and can assemble at oil/water interface to stabilize emulsions. With a soft and porous structure, microgels behave differently at the interface compared to conventional surfactants and rigid Pickering particles. In solution microgel particles are spherical, while at the oil/water interface they are deformed.^[61] Aqueous microgels are found mainly in the water phase in both oil-in-water and water-in-oil emulsions. Fig. 1.14 presents the interfacial behavior of microgel particles, which is different from that of rigid solid particles exhibited in Fig. 1.11. Due to the porous structure, the oil/water interface could penetrate through the particles.

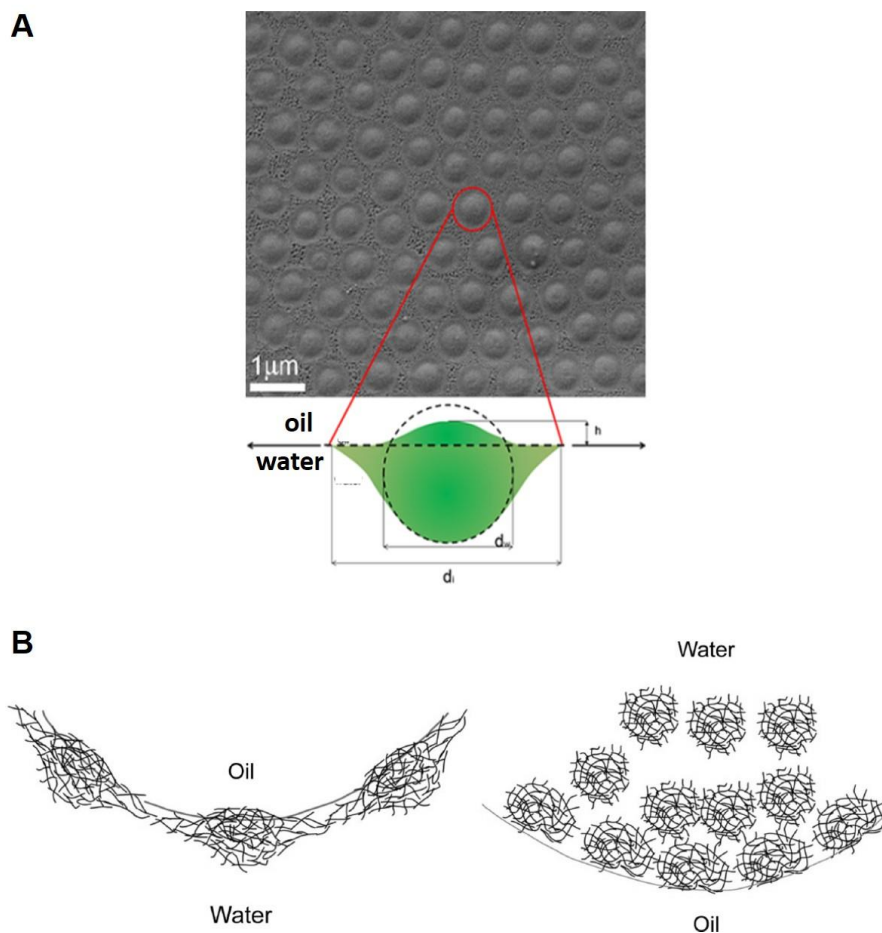


Fig. 1.14: (A) Cryo-SEM image and schematic representation of microgels at the water/heptane interface. Reprinted with permission from reference ^[61]. Copyright 2012 American Chemical Society. (B) Schematic representation of microgels at the interface of o/w and w/o emulsions. Reprinted with permission from reference ^[62]. Copyright 2012 American Chemical Society.

Furthermore, many microgels are stimuli (pH, thermo, solvent composition or magnetic and electrical fields)-responsive and hence microgel-stabilized emulsions or microgel-based capsules have advantages to be applied in controlled release or biocatalysis in a two-phase reaction. For the drug delivery the microgels can effectively shield the encapsulated drugs before they reach the target sites. With external stimuli they can shrink and release a certain amount of drugs. For a two-phase enzymatic reactions the microgels can increase the interface area by forming an

1 Introduction

emulsion hence increase the contact of the substrates to enzyme. Meanwhile they protect the immobilized enzymes from denaturation at the interface. After the reaction the emulsion can be broken into two separated phases by external stimuli, the organic phase contains the reaction product and the enzyme as well as the shrunken microgels are now in the aqueous phase, which makes the separation of product and the recycling much easier.^{[39] [63]}

PNIPAAm microgels are well known Pickering emulsifiers and prefer to form O/W emulsions with various oils such as heptane, hexadecane, trichloroethylene, and toluene.^[44] As mentioned in the last section, PNIPAAm microgels are temperature sensitive and have a volume phase transition temperature (VPTT) of 33°C. They are swollen in water when $T < \text{VPTT}$ and shrunken when $T > \text{VPTT}$. Pickering emulsions stabilized by PNIPAAm microgels are stable if $T < \text{VPTT}$. By increasing the temperature over VPTT emulsions are destabilized.^{[38] [64]} Therefore PNIPAAm is an ideal candidate for the catalytic silicification at mild temperatures.

PNIPAAm microgel particles pack densely with a hexagonal array at the interface in toluene/water emulsions, which was reported by Tsuji and Kawaguchi (Fig. 1.15).^[44] Destribats *et al.* and Schmidt *et al.* also confirmed the hexagonal arrangement of PNIPAAm microgels or other NIPAAm based microgels at the interface with other oil droplets such as n-heptane, 1-octanol or hexadecane.^{[60] [64]}

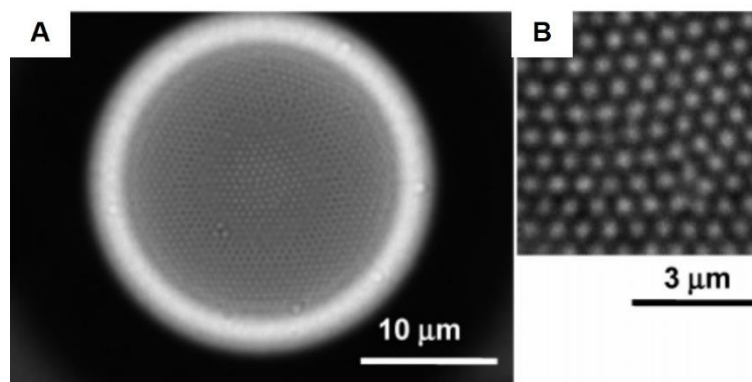


Fig. 1.15: (A) SEM images of toluene in water emulsion stabilized by PNIPAM microgel particles, (B) close-up view of emulsion interface. Reprinted with permission from reference ^[44]. Copyright 2008 American Chemical Society.

1.3 Outline of this thesis

This thesis deals with a bioinspired approach, combined with stabilisation of interfaces using particles (Pickering emulsion as templates), to synthesize protein-silica hybrid materials with controlled size, structure and morphology. It is structured as follows:

Chapter 2 presents information and details about the materials and equipment applied for the synthesis of protein-silica hybrid structures. Additionally, characterization methods and the analytic devices are described.

Chapter 3-7 discuss all experiments and results. **Chapter 3** describes how the native hydrolase lysozyme catalyses silicification to form various lysozyme-silica hybrid capsules with tunable size, morphology, thickness and functionality. **Chapter 4** is about the recombinant silicatein-silica hybrid capsules. Inspired by naturally

occurring enzymes for silicification, the adaption of an analogue of enzyme (PNIPAAm microgels) for silica capsule synthesis is described **in chapter 5**. The **chapter 6** presents the immobilized lysozyme in microgel matrix and its application for silica capsules synthesis. **Chapter 7** discusses the enzymatic assay of lysozyme for the hydrolysis of alkoxy silane measured by UV-Vis spectroscopy.

Chapter 8 summarizes the research and a short outlook will be given at the end of this chapter. A summary in German will also be presented here in **chapter 9**.

2 Experiments

2.1 Materials and chemicals

2.1.1 Catalysts applied for silicification

Lysozyme

The lysozyme was purchased from Sigma Aldrich (L6876, lyophilized powder, protein \geq 90 %, activity \geq 40.000 units/mg protein, mol. Wt. 14.3 kDa).

Papain

The papain from *carica papaya* was provided by Appli Chem (A3824, lyophilized powder, activity $>$ 30.000units/mg, mol. Wt. 23.0 kDa).

Trypsin

The trypsin from *bovine pancreas* was supplied by Appli Chem (A3964, salt-free, lyophilized powder, activity \geq 2.500 units/mg, mol. Wt. 23.8 kDa).

α -Chymotrypsin

The α -chymotrypsin from *bovine pancreas* (Grade I) was purchased from Appli Chem (A4531, salt-free, lyophilized powder, activity ≥ 1.500 units/mg, mol. Wt. ~ 25.0 kDa).

Recombinant silicatein

Recombinant silicatein was obtained from cooperation partner Prof. Schwaneberg and his coworkers. The recombination of silicatein was expressed in *E.coli* and received in Tris buffer (0.15 mg/mL, pH 7).

PNIPAAm microgels

The PNIPAAm microgels (Fig.1.10) were received as dispersion in deionized water from cooperation partner Prof. Pich and his coworker Dr. Andreea Balaceanu. The average hydrodynamic radius is 125 nm and the VPTT is around 33 °C.^[38]

Immobilized lysozyme in poly(*N*-vinylcaprolactam-*co*-2-methoxyethylacrylat-*co*-acrylid) microgels (PVCL/MEA/AA)

The synthesis of PVCL/MEA/AA microgels (Fig. 2.1) and the immobilization of lysozyme in the microgels were performed by Andrea Götz from research group of Prof. Pich. The samples were received as dispersion in Na₃PO₄ buffer. The average hydrodynamic radius is about 130 nm and the VPTT is around 35 °C. The concentration of the immobilized lysozyme is about 3 mg/mL.

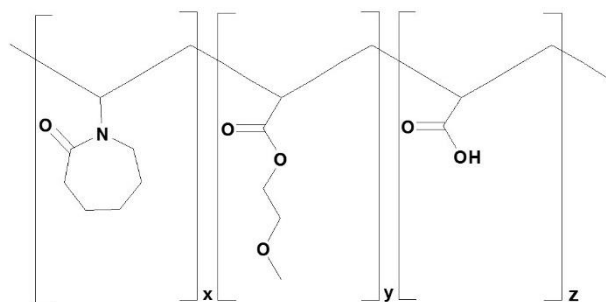


Fig. 2.1: Structure of PVCL/MEA/AA.

2.1.2 Silica precursors

Tetraethyl orthosilicate (TEOS)

TEOS (333859, from Sigma Aldrich) is liquid at room temperature and often used as silica precursor. Fig. 2.2 shows the general reaction scheme of the silica formation from TEOS, consisting of the hydrolysis of ethoxy groups and condensation of hydrolyzed intermediates.

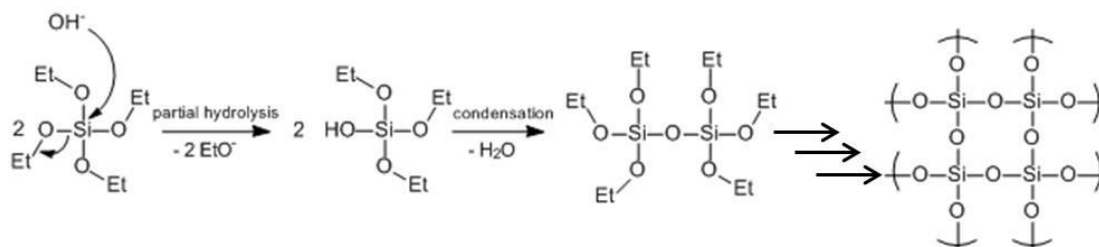


Fig. 2.2: Reaction scheme of hydrolysis and condensation of TEOS.

Polyethoxysilane (PEOS)

PEOS is an oil-like polymeric silica precursor with a hyperbranched structure and was provided by Dr. Xiaoming Zhu. It was prepared *via* a catalytic condensation of TEOS with acetic anhydride (Fig.2.3).^[65] Since PEOS has different structure and viscosity than TEOS, it could affect the natures of emulsion. Furthermore, PEOS is a product from a partial condensation of TEOS, the silicification from PEOS to silica could probably be more efficient since fewer condensation steps are needed.

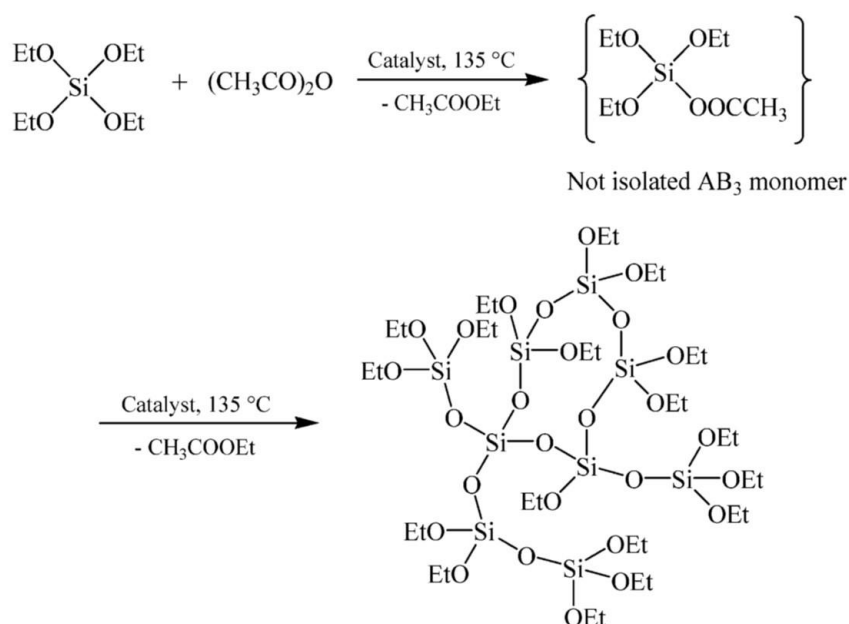


Fig. 2.3: One-pot synthesis of PEOS. Reprinted with permission from reference ^[65]. Copyright 2006 American Chemical Society.

2 Experiments

2.1.3 Other chemicals

Tab. 2.1: Chemicals used for the synthesis of silica capsules.

Chemical		Company
Glycine	≥99 %	Alfa Aesar
Sodium dihydrogenphosphate (Na ₂ H ₂ PO ₄)	99 %	Sigma Aldrich
Sodium chloride (NaCl)	≥99 %	Sigma Aldrich
Sodium fluoride (NaF)	≥99 %	Sigma Aldrich
Hexadecyltrimethylammonium bromide (CTAB)		Sigma Aldrich
Sodium dodecyl sulfate (SDS)	≥99.5 %	Roth
(3-Aminopropyl)trimethoxysilane (APTMS)	97 %	Sigma Aldrich
Nile Red	standard	Sigma Aldrich
4- <i>N,N</i> -dimethylaminoazobenzene-4'-sulfonyl chloride (Dabsyl chloride)		Sigma Aldrich
Bis[<i>N,N</i> -bis(carboxymethyl)aminomethyl] fluorescein (Calcein)		Sigma Aldrich
<i>N</i> -(3-Dimethylaminopropyl) <i>N</i> -ethylcarbodiimide hydrochloride		Sigma Aldrich
Bis(<i>p</i> -aminophenoxy)-dimethylsilane		Fluorochem
<i>p</i> -Nitrophenol	standard	Sigma-Aldrich
Triethylamine	≥99.5 %	Sigma Aldrich

2 Experiments

Chemical		Company
Dichlorodimethylsilane	≥99.5 %	Sigma Aldrich
Ethanol	99.8 %	VWR
Dimethylformamide (DMF)	99.5 %	Fluka
Tetrahydrofuran (THF)	99.9 %	VWR
Hydrochlorid acid (HCl)	conc. 0.37	Sigma Aldrich
Sodium hydroxide solution (NaOH)	conc. 0.2	Sigma Aldrich
Amorphous SiO ₂ powder	≥99.8 %	Evonik

*All chemicals were used without any further purification.

2.2 Equipment used for the synthesis of silica capsules

Tab. 2.2: Equipment applied for the synthesis of silica capsules.

Equipment	Conditions	Model	Manufacture
Vortex mixer	50~60 Hz	VV3 S40	VWR
Ultrasonic bath	50~60 Hz	USC 200T	VWR
pH meter		inoLab® pH/Cond 720	WTW
Platform shaker	5 oscil/min	PMR-30	Grant
Centrifuge	1000 rpm/min, 10 min	5415R	eppendorf
Milli-Q	18.2 MΩ.cm	arium® 611DI	sartorius
Lyophilizer	-40 °C, 0.12 mbar	ALPHA 1-4 LD plus	VWR

*Without further indication of temperature in column ‘conditions’, the operation of the equipment is at room temperature.

2.3 Characterization

Scanning electron microscopy (SEM)

Scanning electron microscopy (SEM) is applied for the investigation of the size of capsules and their surface morphology. The SEM scans the sample surface with a focused beam of high energy electrons, with an acceleration voltage in the range of 0.1~15 kV. A SEM image is produced with the beam position and the detected signals from the interaction between the electrons and the atoms in the sample.^{[66] [67]}

SEM images of capsules with a size $> 2 \mu\text{m}$ were taken with a scanning electron microscope HITACHI S-3000N. For the characterization of nanoparticles and small capsules HITACHI S-4800 with higher resolution was applied.

Transmission electron microscopy (TEM)

Transmission electron microscopy (TEM) is a technique also working with a beam of high energy electrons. Unlike SEM in which the beam scans the sample surface, the electron beam in TEM is transmitted through the sample with a high acceleration voltage ($>100 \text{ kV}$). The sample for the TEM analysis should be ultra-thin so that the electrons can pass through the whole sample and provide a TEM image with ideal contrast.^[68]

For an exact investigation of the hollow structure of small particles and capsules, TEM analysis was performed on a ZEISS LIBRA120 PLUS transmission electron microscope, operating at 120 kV. For all samples carbon-coated copper grids (S160, Plano) were used as substrates.

Energy-dispersive x-ray spectroscopy (EDX)

EDX is an analytical method used for the elemental analysis or chemical characterization of a sample. A high-energy beam of charged electrons or a beam of X-rays scans the sample. The atoms in the sample are stimulated and emit characteristic X-rays subsequently, as each element has its unique atomic structure and allows unique set of peaks on its X-ray spectrum.^[69]

The elemental analysis of the silica capsules was done on the scanning electron microscope HITACHI S-3000N (15 kV) with an EDX detecting unit (EDAX).

X-ray diffraction (XRD)

The crystallinity of the silica capsules was investigated by X-ray diffraction and was performed with a Philips X'Pert PRO diffractometer (source of electrons: copper, 40 kV, 40 mA). For the measurements at room temperature, a single crystal Silicon cut at special orientation was used as sample holder, which has zero background noise from 2 to 120 ° (angle range 5 ~ 90 °, step size 0.008 °, time per step 50 s, scan speed 0.02 °/s). For the in-situ heating measurements, a Platinum sample holder was applied, which is stable at high temperature but shows strong diffractions (room temperature ~ 800 °C, angle range 5 ~ 90 °, step size 0.016 °, time per step 100 s).

Optical-fluorescence microscopy

Fluorescence and optical microscopy images were done with a Keyence microscope (Biozero BZ-8100E). The excitation-mode of green fluorescent proteins GFP (480 nm) and Texas Red (560 nm) allow the visualization of calcein and Nile red separately.

Infrared spectroscopy (IR)

IR spectroscopy uses the absorption of infrared light, which cause vibrations and rotations in molecules to determine chemical bonds and functional groups.^[70] The qualitative chemical composition analysis of silica capsules was performed on a FT-IR spectrometer (Nexus 470, Thermo, software Omnic 6.1a).

Raman spectroscopy

Raman spectroscopy is also a technique to identify molecules, using specific vibrational and rotational information of chemical bonds. However, Raman is based on the scattering of light while IR relies on the absorption of light. The vibration is Raman active if it changes polarisability, while IR active vibration requires a change in dipole moment. Therefore Raman can provide complementary information to IR spectroscopy.^[71]

Here Raman was used to analyze the amide bands as well as the secondary structure of the proteins in the protein-silica hybrid capsules.^{[72] [73]} The measurements were done with a FT-Raman spectrometer (RFS 100/S, Bruker, Laser Nd:YAG, wavelength 1064 nm, 200 mW, resolution 4 cm⁻¹, software Opus 4.0).

Ultraviolet-visible spectroscopy (UV-Vis)

The UV-Vis spectroscopy is a common qualitative as well as quantitative analytic technique, which using the specific absorption of UV light by molecules. The intensity of the absorbed light is proportional to the sample concentration.^[70]

The enzyme assays as well as the qualitative analysis of functionalized silica capsules treated with dabsyl chloride and calcein were carried out with an UV-Vis spectrophotometer (EVOLUTION 300, Thermo) from 200 nm to 800 nm.

Pendant drop tensiometry

The dynamic interfacial tension between the different aqueous protein solutions and the oil phase or between the microgel suspensions and the oil phase were determined at room temperature with the pendant drop method (Fig.2.4). The measurements were performed on a tensiometer (DSA100, Krüss) with a CCD-camera for drop-image processing, which allows rapid drop-image acquisition, edge detection and fitting of the Laplace equation. For the generation of a pendant drop a cannula with 1.83 mm in diameter (NE45 Krüss) was used.

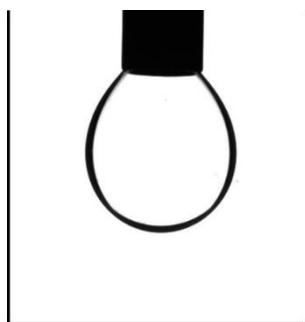


Fig. 2.4.: A pendant drop for the measurement of the interfacial tension of two phases (drop and the environment).

Thermogravimetric analysis (TGA)

TGA is a very precise thermal analysis to measure mass change of materials caused by physical phenomena *e.g.* absorption, sublimation or chemical reaction *e.g.* decomposition, oxidation as a function of temperature change. This technique is commonly applied in material science to evaluate thermal stability or to determine organic or inorganic content of a sample.^[74] A thermal analyzer (STA 6000, Perkin Elmer) was used for the quantitative determination of the composition of the hybrid materials, operating at 10 °C/min with a gas flow of 20 mL/min (25 ~ 900 °C, artificial air: 20 % oxygen, 80 % nitrogen).

Zeta potential analysis

The particles in a colloidal suspension or emulsion usually carry an electrical charge to stabilize the system (section 3.6). The potential difference between the dispersion medium and the stationary layer of fluid attached to the disperse particle is called zeta potential, which is a very important property of suspension or emulsion. The zeta potential determination bases on the electrophoresis process, in which an electric field is applied to the sample and the movement of charged particles towards electrode is measured. The more charge they possess, the faster are their movement.^[40]

For the analysis of multilayer structure of silica capsules as well as the immobilization of enzyme in microgel particles, zeta potential of different solutions and dispersions was measured with a zeta sizer (Nano-ZS, Malvern). All the measurements were performed at 25 °C after an equilibration for 2 min in a capillary cell including electrodes.

3 Lysozyme-silica hybrid capsules*

3.1 Lysozyme as effective biocatalyst and templates for the synthesis of silica capsules

For a successful enzymatic synthesis of silica capsules with the Pickering emulsion template method, the applied protein should meet two requirements: 1) it possesses enzymatic activity towards silicification; 2) it is interfacially active and can stabilize emulsion droplets.

3.1.1 Interfacial activity of lysozyme

The interfacial activities of different enzymes can be measured by a pendant drop method with a tensiometer. Fig. 3.1 shows the change of IFT between different enzymes solutions in buffer (5 mg/mL) and TEOS with time. Among the four enzymes the lysozyme (green curve) reduced the IFT most rapidly and after one hour the IFT reached approximately 10 mN/m, while the decreases of IFT of other enzymes were much slower. This demonstrates that lysozyme solution is most interfacially active when compared to trypsin, α -chymotrypsin and papain.

*Parts of this section have been published in references [75] [3].

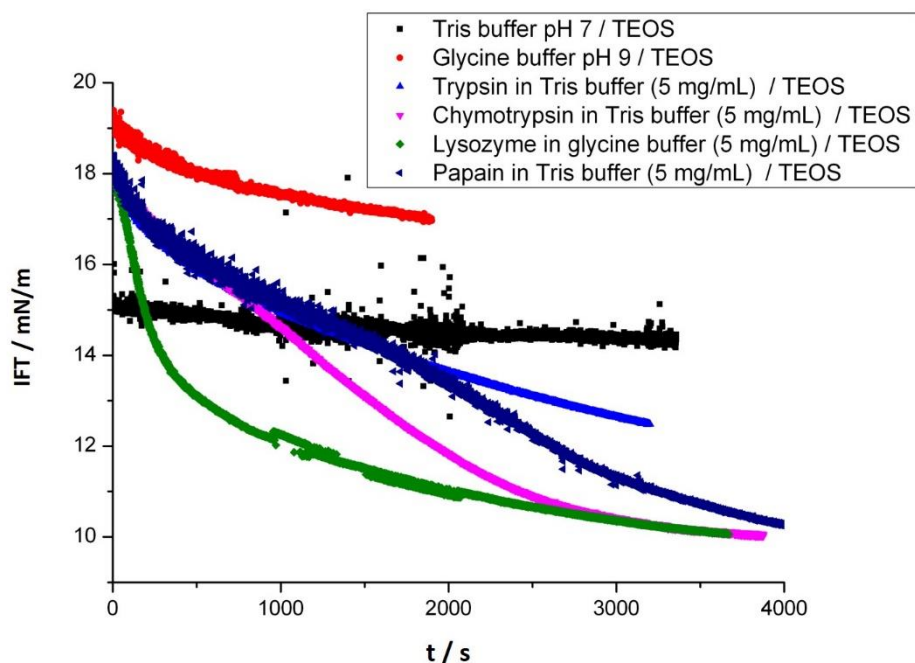


Fig. 3.1: Pendant drop interfacial tensiometry measurements of different enzyme solutions against TEOS.

3.1.2 Enzymatic activity of lysozyme

To check the enzymatic activity of these enzymes, 900 μL enzyme solution (5 mg/mL) and 100 μL TEOS were added into a 2 mL Eppendorf tube. The mixture was treated by sonication for 15 min and reacted at room temperature for 24 hours. As mentioned in section 1.1.2, each of the studied enzyme has a similar active site as silicatein, therefore all of them should be able to catalyse the silicification, which was then studied by SEM, EDX and IR analysis. However, only in the presence of lysozyme, silica in the form of capsules was isolated in a large amount. In the sample with α -chymotrypsin a few capsules were also observed besides bulk cluster silica, but the amount is far less than that in the lysozyme sample (Tab. 3.1, Fig. 3.2).

3 Lysozyme-silica hybrid capsules

Tab. 3.1: Enzymatic activity of different enzymes for silicification.

Sample	Result after a 24 h reaction
900 μ L Trypsin* + 100 μ L TEOS	Silica cluster, no capsules
900 μ L α -Chymotrypsin* + 100 μ L TEOS	Silica cluster, a few capsules
900 μ L Papain* + 100 μ L TEOS	Silica cluster, no capsules
900 μ L Lysozyme* + 100 μ L TEOS	Silica capsules in high yield

*Trypsin, α -chymotrypsin and papain were in 0.05 M Tris buffer (5 mg/mL, pH 7) and lysozyme was in 0.05 M glycine buffer (5 mg/mL, pH 9). The choice of different buffer and pH value is based on the enzymatic activity of each protein.

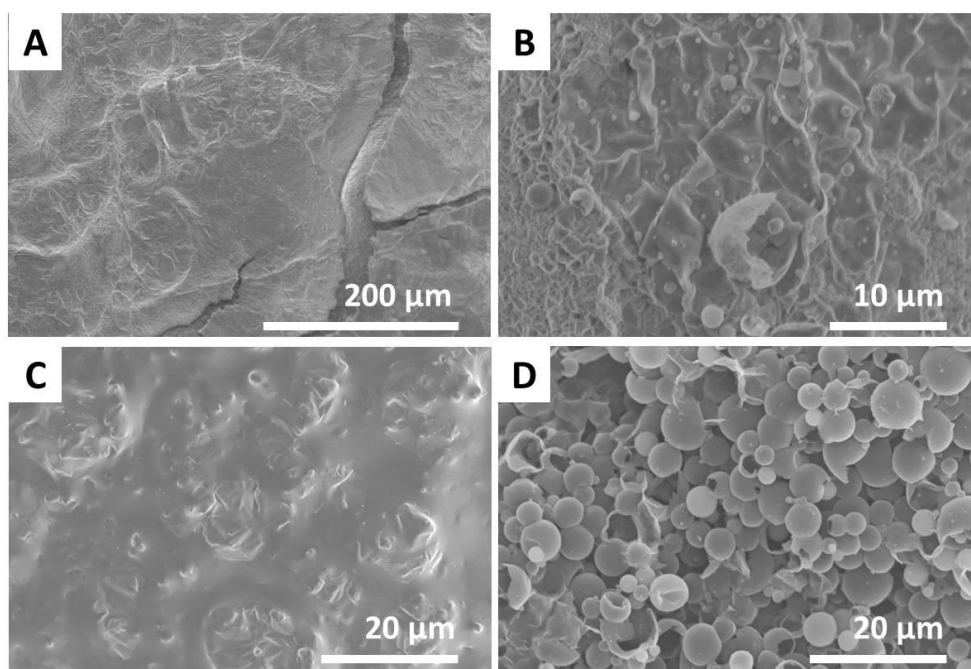


Fig. 3.2: SEM images of different samples prepared with TEOS and (A) trypsin (B) α -chymotrypsin (C) papain (D) lysozyme *via* sonication after 24 hours.

3 Lysozyme-silica hybrid capsules

Compared with other enzymes, lysozyme shows the capability for the emulsion template synthesis of capsules due to its excellent interfacial activity as well as the enzymatic activity for silicification.

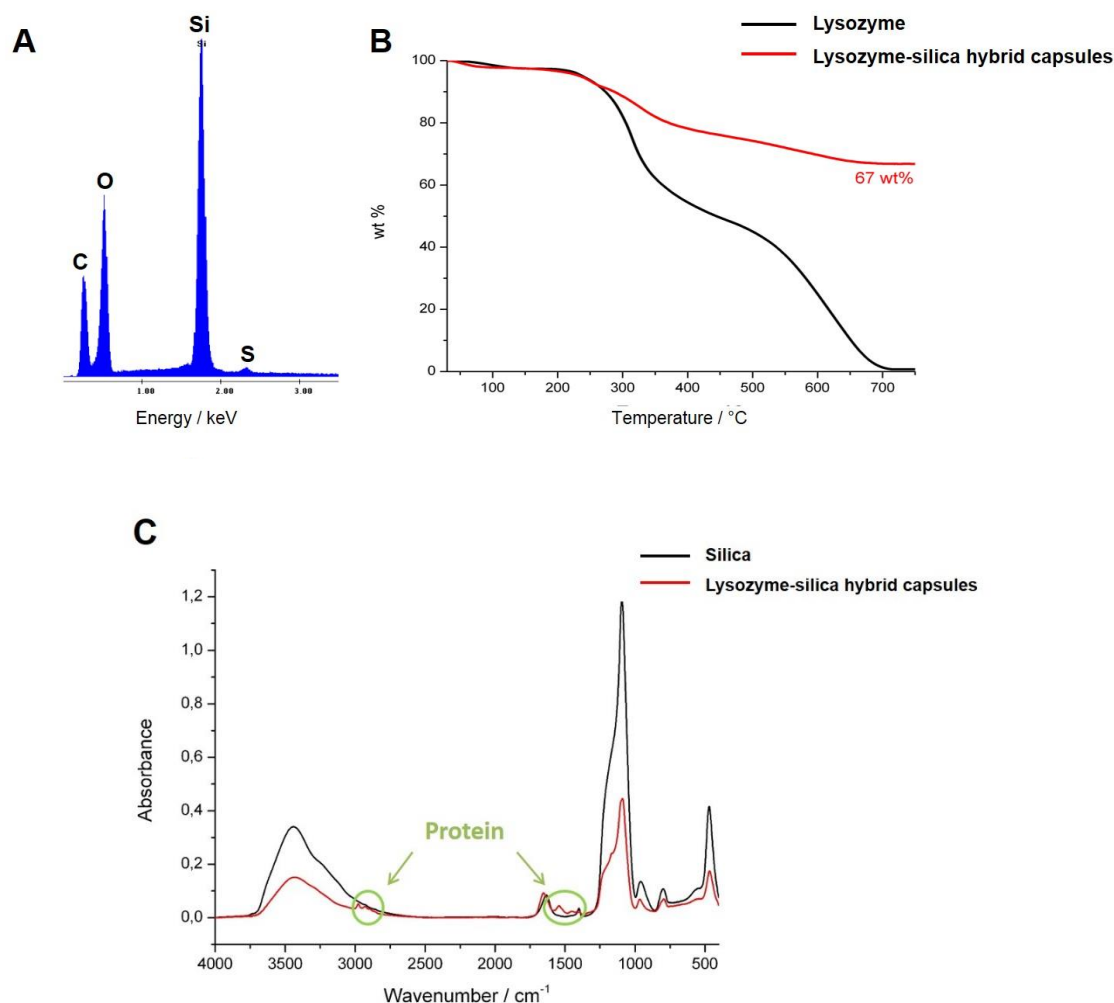


Fig. 3.3: (A) EDX analysis (B) TGA measurements (C) IR spectra of pure lysozyme-silica hybrid capsules.

IR spectra of pure silica and the capsules formed with lysozyme prove that the capsules consist of silica and protein. The peaks at 3440 cm⁻¹ and 967 cm⁻¹ correspond to Si-OH stretching vibrations. The peak at 1639 cm⁻¹ represents to Si-H₂O flexion.

Si-O-Si, Si-O and O-Si-O vibration bands appear at 1089 cm^{-1} , 800 cm^{-1} and 471 cm^{-1} respectively.^[76] The weak peaks near 2900 cm^{-1} represent organic groups and the ones at about 1650 cm^{-1} and 1540 cm^{-1} belong to amide I and II respectively (Fig. 3.3C). The presence of Si and O elements is also confirmed by EDX analysis (Fig. 3.3A). Furthermore, TGA measurements showed the composition of the capsules. The mass loss of pure lysozyme above $700\text{ }^{\circ}\text{C}$ is nearly 100 % while in the capsule sample 67 wt% remains at the end of a measurement, which means that the capsules are hybrid consisting of both lysozyme ~33 wt% and silica ~67 wt% (Fig. 3.3B).

3.2 Kinetics of the polycondensation of TEOS in the presence of lysozyme in the o/w Pickering emulsion

For the quantitative evaluation of the enzymatic activity of lysozyme for the polycondensation of TEOS, the mass of SiO_2 was determined after distinct reaction times. For this analysis the standard one-step preparation (900 μL 5 mg/mL lysozyme solution in glycine buffer, 100 μL TEOS, 15 min ultrasonic treatment before the reaction) was applied. If the 100 μL TEOS completely convert to SiO_2 , 27 mg SiO_2 should be obtained. The diagram (Fig. 3.4) shows the weight increase of SiO_2 (only the SiO_2 part of lysozyme-silica hybrid was taken into account and the lysozyme part was excluded) with time. It is difficult to determine the kinetics of this reaction. However, it is obvious that the reaction is finished after 72 hours, which can be also proven by TGA measurements. Fig. 3.5 shows the TGA curves of capsules purified after different reaction times. The SiO_2 part in the hybrid capsules increased with time and after 3 days no increase was observed. Both curves after 3 and 6 days end by ~67 wt% at $900\text{ }^{\circ}\text{C}$. In a blank sample without lysozyme no solid white precipitate was isolated after 3 days.

For a better understanding of the kinetics of enzyme activity another enzymatic activity assay should be applied.

3 Lysozyme-silica hybrid capsules

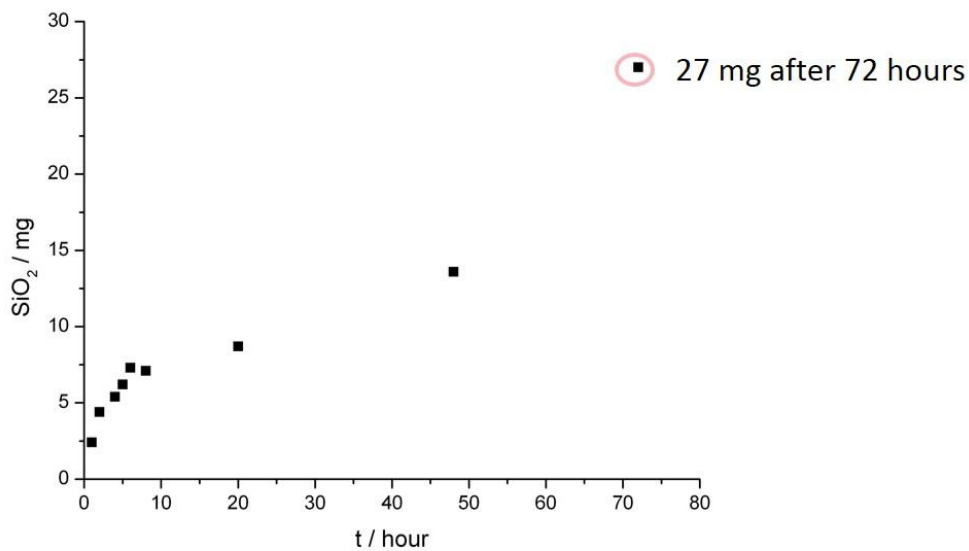


Fig. 3.4: Weight of SiO₂ in the lysozyme catalyzed polycondensation of TEOS after different reaction times.

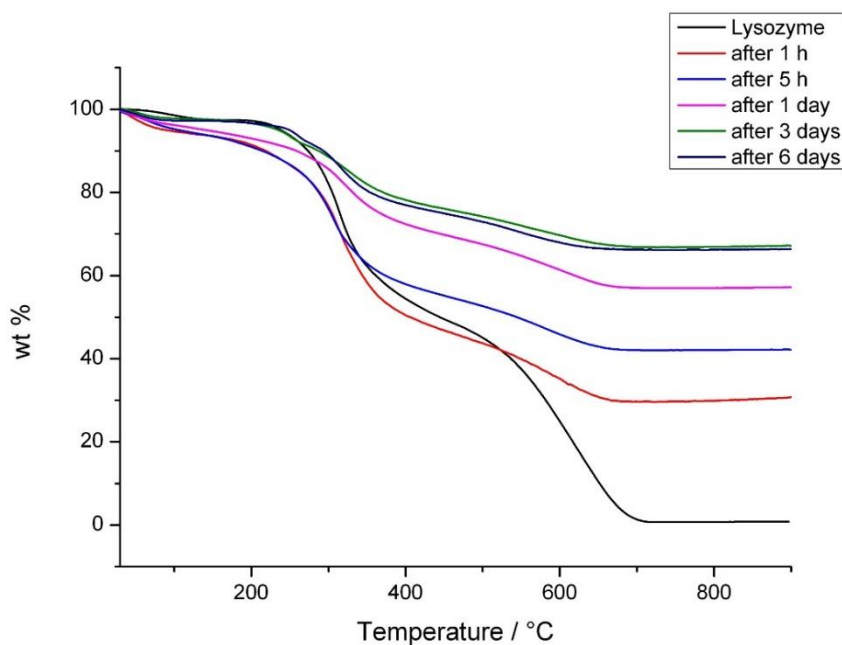


Fig. 3.5: TGA measurements of pure lysozyme and lysozyme-silica capsules after different reaction times.

3 Lysozyme-silica hybrid capsules

Additionally, it was also observed that the morphology of capsules changed over time. After one day capsules with a smooth surface were formed (Fig. 3.6A) and after 3 days the shell was still very smooth (Fig. 3.6B). However, after 6 days the surface became rough (Fig. 3.6C). Actually the condensation of TEOS was done after 3 days and TGA measurements also show no difference in the composition between 3-day capsules and 6-day capsules. To find out the reason for the change of morphology, XRD was applied to determine the crystallinity of the lysozyme-silica hybrid capsules.

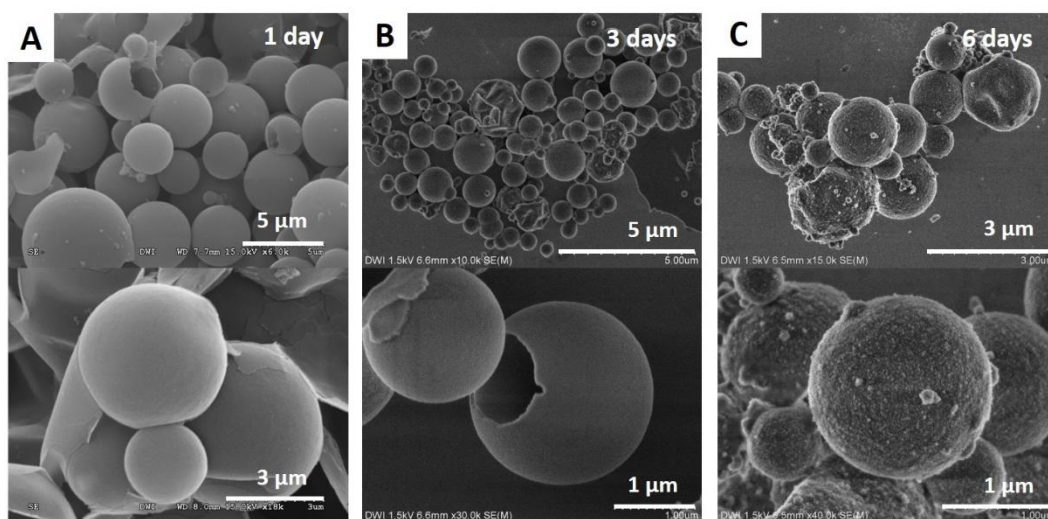


Fig. 3.6: FESEM images of lysozyme-silica capsules after (A) 1 day, (B) 3 days and (C) 6 days.

The XRD analysis of lysozyme-silica capsules after different reaction times was presented in Fig. 3.7. The characteristic peak at $\sim 22.5^\circ$ for non-crystalline silica^[44] can be observed in every sample, which means the capsules were amorphous and the reaction time has no influence on the crystallinity of SiO_2 . Pure lysozyme has two separate peaks at $\sim 10^\circ$ and 20° separately. Due to the smaller amount of lysozyme in the hybrid (~ 33 wt %), these two peaks are not visible in the diffractograms of hybrid capsules.

3 Lysozyme-silica hybrid capsules

The SiO₂ found in sponges, diatoms or radiolarians as an essential component is non-crystalline, therefore it makes sense that the silica capsules *via* biosilicification with lysozyme are also amorphous. Furthermore, the substances like organisms as well as opal, lechatelierite and obsidian with amorphous SiO₂ have different composition, while the crystalline forms such as quartz, cristoballite have low tolerance of impurities and differ only in their structure. Since the capsules are hybrid materials consisting SiO₂ and protein, their amorphousness can also be explained.

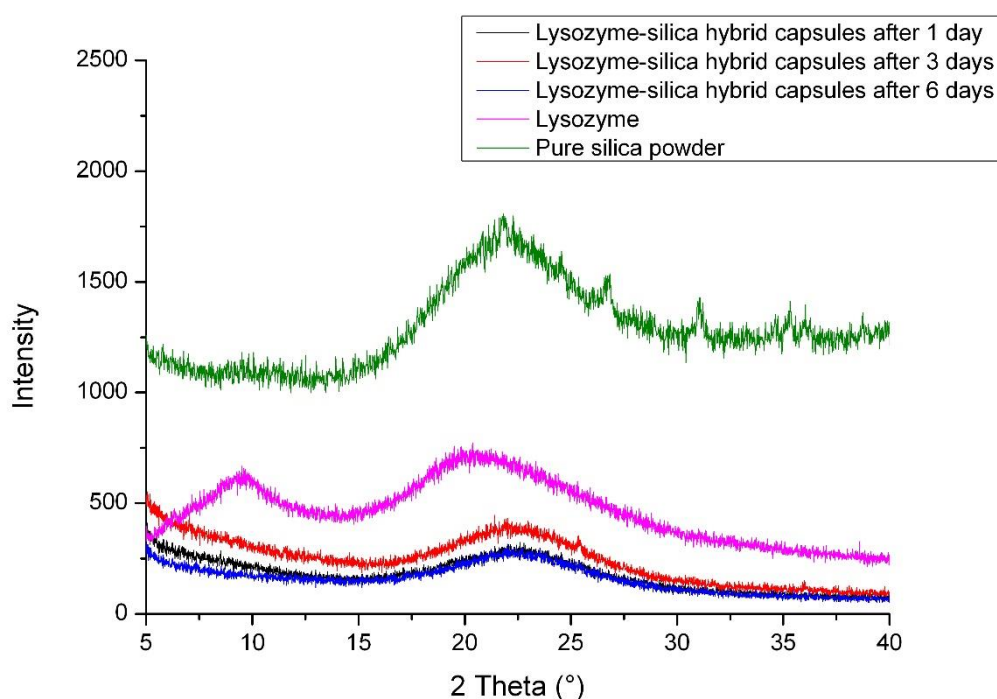


Fig. 3.7: X-ray diffractograms of lysozyme-silica capsules after different reaction time. (The amorphous silica powder was kindly provided by Evonik.)

According to TGA curves, 3-day capsules and after 6-day capsules have same composition (Fig. 3.5). However, after TGA measurement the rough surface of 6-day capsules turned smooth again (Fig. 3.8). The disappearance of protein signals in IR

3 Lysozyme-silica hybrid capsules

spectrum after TGA indicates that the presence of protein has influence on the morphology of the hybrid capsules.

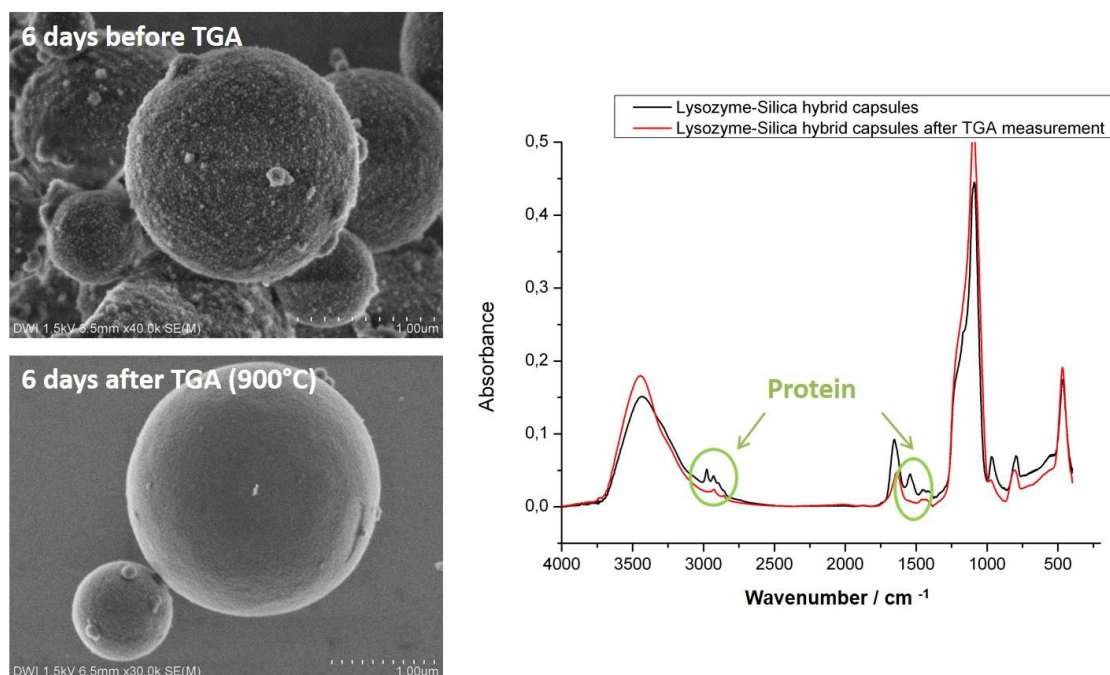


Fig. 3.8: SEM images (left) and IR spectra (right) of 6-day capsules before and after TGA.

For a further investigation on how temperature influences the crystallinity of SiO₂, in-situ heating XRD analysis was performed. Another 6-day capsule sample without thermal treatment was measured between 30 °C and 800 °C (850 °C is the limit of the heating unit). The results are presented in Fig. 3.9. The angle range was from 5 to 90 °, however, only the part of 5 ~ 40 ° is shown here because the platinum sample holder has very strong diffractions in the 40 ~ 90 ° range. The two weak peaks between 25 ° and 30 ° are part of platinum spectrum (black line in Fig. 3.9). The characteristic diffraction at ~22.5 ° for non-crystalline silica was observed in every measurement and a phase transition did not occur during the heating process. It was reported that

3 Lysozyme-silica hybrid capsules

the glass temperature of fused quartz is about 1200 °C,^[77] which can explain the retained amorphousness at 800 °C.

The XRD measurements for the sample after different reaction times (Fig. 3.7) and at different temperatures (Fig. 3.9) indicate that the change of morphology is not due to crystallinity, since no change in amorphousness of silica capsules was observed. IR and SEM analysis of the 6-day capsules reveals the presence of protein possibly has influence on morphology. However, the 3-day and 6-day capsules possess the same composition and the reason for the difference in morphology is unknown.

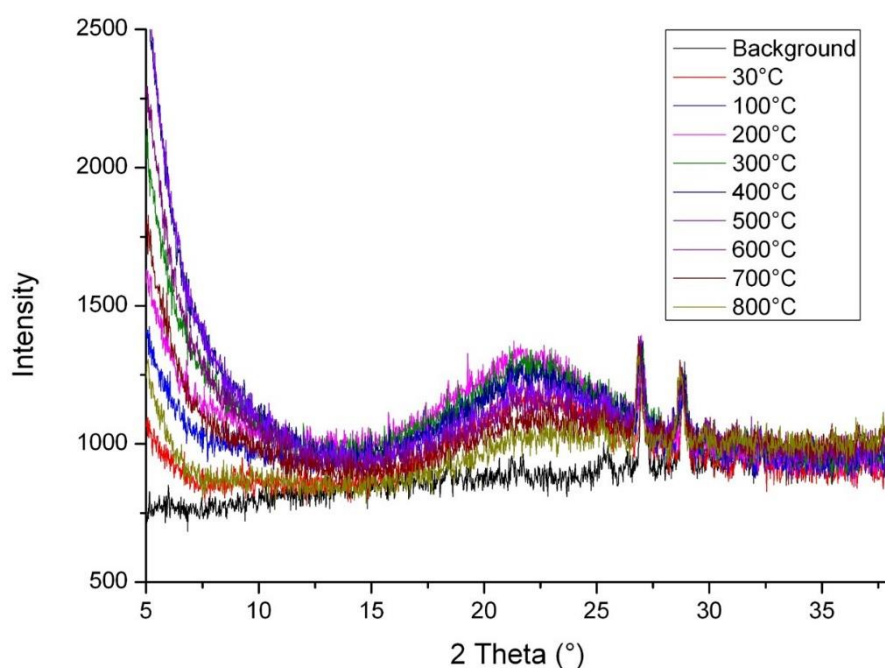


Fig. 3.9: *In-situ* heating X-ray analysis of lysozyme-silica capsules on a platinum sample holder. The two peaks between 25 ° and 30 ° are part of platinum spectrum (background). The characteristic diffraction at ~22.5 ° is from non-crystalline silica.

3.3 Influence of emulsification method and synthetic procedure on lysozyme-silica hybrid capsules

The size and morphology is essential to the applications of silica capsules in coating technology, catalysis, controlled release studies, micro-reactors and composite materials. [22] [2] It is possible to synthesize a wide variety of stable silica hybrid capsules/particles without changing the specific chemical component.

By altering the sequence of addition as well as the emulsification method, silica nanoparticles or capsules with controlled size exhibiting various surface morphologies were formed. The standard composition of the reaction mixture was lysozyme (5 or 2.5 mg/mL) in 0.05 M glycine buffer pH 9.0 (900 μ L) and TEOS (100 μ L). The mixture and preparation conditions were varied with lysozyme concentration, single or sequential addition of TEOS, and emulsification method (mechanical mixing or sonication). A schematic overview of the different synthetic procedures and resulting hybrid structures (**HS**) is shown in Fig. 3.10.

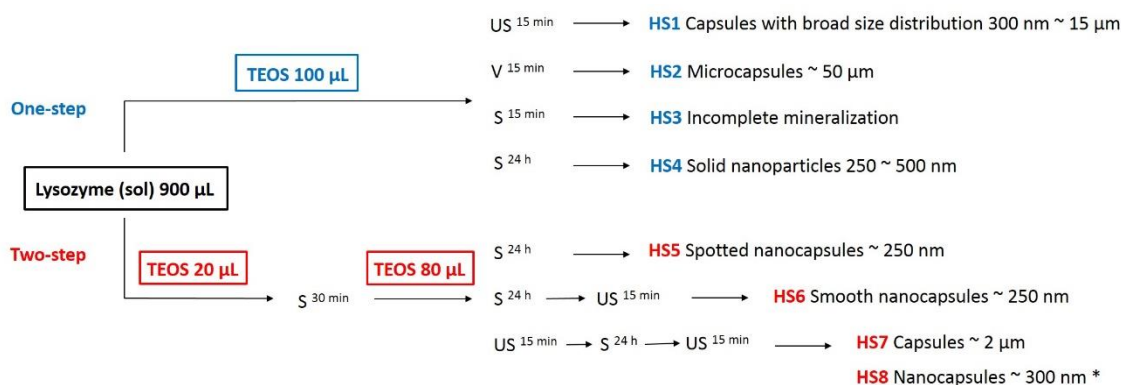


Fig. 3.10: Overview of the method variation and the corresponding lysozyme-silica hybrid structures. (US=ultrasound, V=vortex, S=stirring, * lysozyme 2.5 mg/mL)

3 Lysozyme-silica hybrid capsules

With the conventional one-step approach, namely 900 μL lysozyme solution and 100 μL TEOS and mixing *via* sonication (15 min), small capsules were formed due to efficient emulsification (**HS1**, Fig. 3.11A). These capsules have a broad size distribution (300 nm to 15 μm). Varying the emulsification method provides very different structures. 15 min vortex instead of sonication resulted in large capsules in the range of 50~100 μm with a much thinner shell (**HS2**, Fig. 3.11B) while slow stirring (15 min) provided irregularly shaped particles with much smaller size (50~300 nm) (**HS3**, Fig. 3.11C). The particles were mineralized together into a large cluster which is probably due to the mild stirring. The formed particles are not well separated and have enough time to grow together. The surface of the particles HS3 seems to be very rough in contrast to the particles **HS4** shown in Fig. 3.11D (TEM inset displays homogeneously solid structures) where the sample was stirred for the entire reaction (24 h). This indicates when continuous mild stirring was applied, a smoother particle surface was obtained and they were well separated.

Precipitation of silica particles comprises four steps: 1) hydrolysis of the alkoxy-silane precursor, 2) nucleation, 3) oligomer agglomeration forming primary particles and 4) the further agglomeration. Based on this mechanism, by increasing the time of stirring at constant strength, the number of monodisperse particles increases and they become more spherical due to sufficient nucleation time (**HS4**, Fig. 3.11D).

3 Lysozyme-silica hybrid capsules

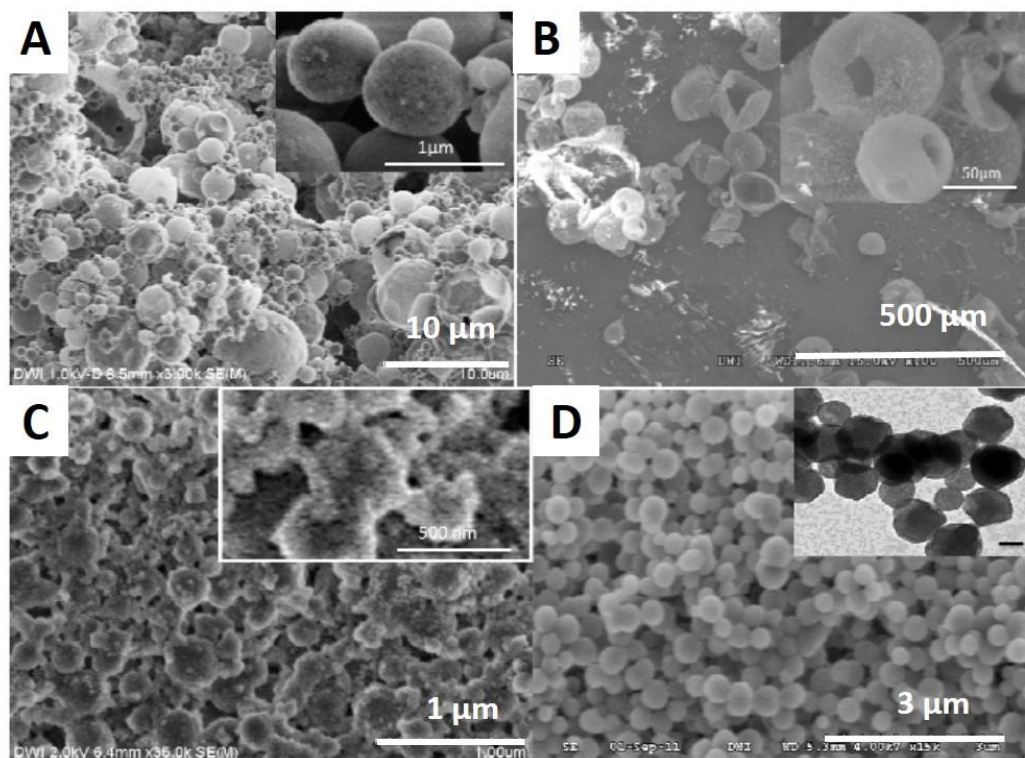


Fig. 3.11: SEM images of hybrid structures (A) HS1 (B) HS2 (C) HS3 (D) HS4 prepared by one-step addition of 100 μL TEOS into 900 μL lysozyme solution (5 mg/mL) with different emulsification methods. Insets are higher magnifications showing the surface structures in more detail (insert in D is a TEM image with a scale bar 300 nm). Reprinted with permission from reference ^[75]. Copyright 2012 the Royal Society of Chemistry.

Previously, it was found that precursor hydrolysis and formation of primary particles are important for particle growth.^{[78] [79]} It is noteworthy to mention that aggregation of oligomers leads to formation of primary particles which mainly control further emulsion templating due to their colloidal properties.^[80] Using the knowledge that these reaction intermediates (primary particles) exist during the process and affect the emulsion templating properties, the synthetic method was adjusted from the one-step addition of TEOS to a two-step addition.

3 Lysozyme-silica hybrid capsules

Firstly only 20 μL of TEOS was added to 900 μL lysozyme solution followed by 30 min mild stirring. Finally the remaining 80 μL of TEOS was added leading to the same overall composition of 100 μL . The obtained emulsion was then stirred for 24 h. By addition of a first part of TEOS followed by stirring, formation of oligomers and nucleation proceed throughout the other precipitation steps, ensuring a homogenous distribution of nuclei over the sample.^[78] After the second TEOS addition, a new emulsion-template is formed, producing new primary particles alongside the already existing ones. As the growth rate of silica particles is a surface limited reaction, surface-to-volume ratio is the critical factor for the final size of the particles.^[79]

As shown in Fig. 3.12, granular hybrids of polysilicate-protein particles were observed in the intermediate stage after the first addition. At this stage, no agglomeration occurred due to its low concentration and mild stirring. This was also observed for non-biocatalyzed studies where TEOS droplets acted both as template and precursor.^{[81] [82]}

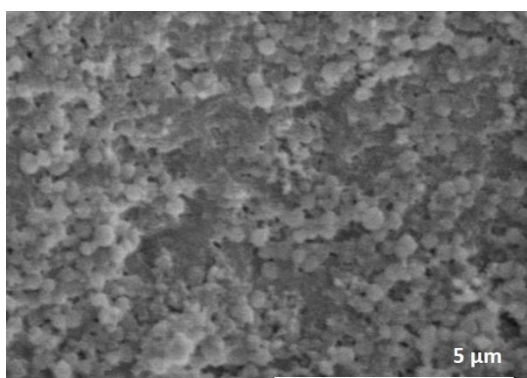


Fig. 3.12: SEM image of the template product formed at intermediate stage in the two-step procedure after the first addition of 20 μL TEOS and 30 min of mild stirring.

By adding the second part of TEOS (80 μL) a new emulsion templated system is generated. Here the initially formed hybrid oligomers assemble around the emulsion

3 Lysozyme-silica hybrid capsules

droplets creating hollow silica-hybrid capsules in a regular manner. When the two step procedure is followed, different types of capsule structures emerge depending on the type of emulsification without changing the overall reaction composition or reaction time with respect to the single addition procedure.

While the one-step addition of TEOS and mild stirring led to the formation of solid nanoparticles (**HS4**, Fig. 3.11D), the two-step addition provided hollow structures. The capsules shell seems to resemble primary particles grown together around the emulsion template. The diameter of the capsules is about 250 nm which is smaller than that of the solid particles in the one step method and significantly smaller than previously reported,^{[27] [28]} and more homogeneous in size (**HS5**, Fig. 3.13A). When 15 min sonication was applied the shell morphology became smoother and more homogenous (**HS6**, Fig. 3.13B).

These sequences can be varied even more *e.g.* by 15 min sonication directly after the second addition (**HS7**) to introduce more energy into the system. While all other parameters are the same as for **HS6**, the additional treatment with ultrasound for 15 min after the second addition resulted in capsules with more homogenous shell and a diameter between 500-2000 nm (**HS7**, Fig. 3.13C). The larger size of **HS7** than **HS6** can be explained by droplet-fusion due to enhanced collisions.^[83] Surprisingly, lowering the lysozyme concentration from 5 to 2.5 mg/mL resulted in nanocapsules with a diameter between 300~500 nm (**HS8**, Fig. 3.13D).

3 Lysozyme-silica hybrid capsules

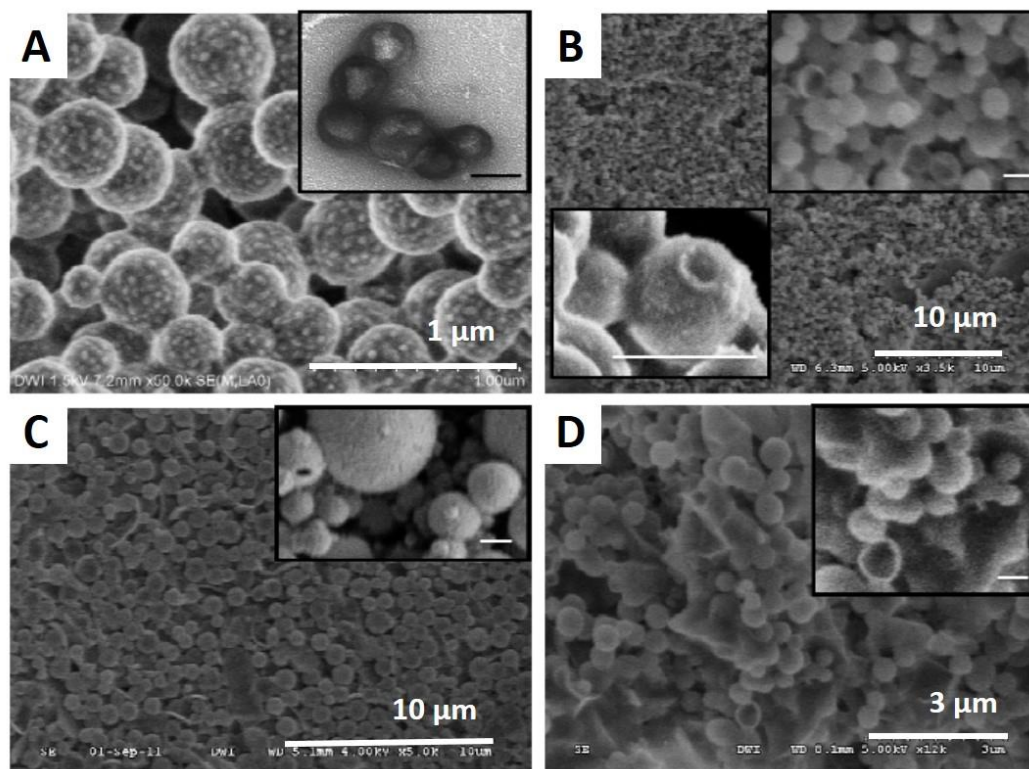


Fig. 3.13: SEM images of hybrid structures (A) HS5 (B) HS6 (C) HS7 (D) HS8 prepared by two-step addition of TEOS into lysozyme solution with different emulsification methods. Insets are higher magnifications showing more details of corresponding capsules (all inset scale bars are 300 nm and inset in A is a TEM image). Reprinted with permission from reference [75]. Copyright 2012 the Royal Society of Chemistry.

3.4 Inverted emulsion and double emulsion lysozyme-silica capsules

For the encapsulation of active agents in capsules synthesized from o/w emulsions a hydrophobic compound is needed or an additional step is necessary to change the polarity of the core. Since many active agents like drugs are hydrophilic, it would be

more convenient to apply an inverse emulsion in which capsules with aqueous core should be formed.

3.4.1 Inverted emulsion (w/o) capsules

When the ratio of lysozyme/TEOS is changed from 900 μL (5 mg/mL)/100 μL to 100 μL (300 mg/mL)/900 μL , a w/o instead of o/w emulsion can be formed. The higher concentration at 300 mg/mL is necessary to compensate for the lower overall amount of lysozyme because of the lower content of aqueous phase. *Via* optical microscopy many capsules were observed which appeared to be highly clustered inside a much larger capsule (Fig. 3.14A). However, SEM images (Fig. 3.14B) do not show those large capsules but many smaller ones grown together. Since the lysozyme solution is the minor phase, the capsules displayed in SEM image should be with an aqueous interior, which was confirmed by fluorescence microscope (inset in Fig. 3.14A) where Nil Red indicates TEOS. However, in this w/o emulsion the final structures after mineralization are not separated capsules anymore, because TEOS is the continuous phase.

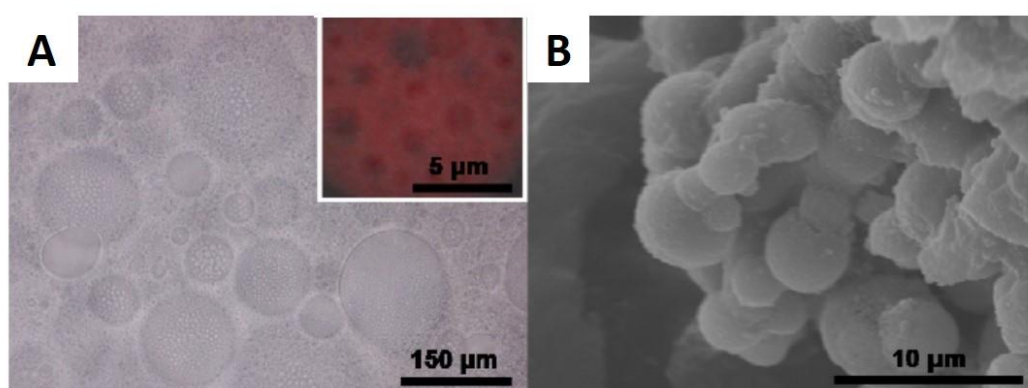


Fig. 3.14: (A) Fluorescence microscopy and (B) SEM images of inverted emulsion capsules. Reprinted with permission from reference ^[75]. Copyright 2012 the Royal Society of Chemistry.

3.4.2 Double emulsion (o/w/o) capsules

Compared with conventional o/w or w/o emulsions, w/o/w or o/w/o double emulsions might be more interesting in the controlled released field, since the double emulsion can provide better stability for the active substances entrapped chemical compound in the internal capsules and more precise release mechanism.^[84]

By using higher lysozyme content (lysozyme solution 990 μL /TEOS 10 μL instead of 900 μL /100 μL), longer sonication time and glass vial (instead of Eppendorf tube), it is possible to prepare double emulsions. Firstly there are more lysozyme molecules available to stabilize interface. Secondly the longer sonication time and the use of glass vial increase the total energy input to the emulsion. As a result, aqueous micro droplets are pushed into the oil droplet to form w/o/w double emulsion.

The double emulsion was analyzed by fluorescence microscopy and Nile Red was added to visualize the oil phase. Fig. 3.15A shows both interface were stained red as TEOS condensed to SiO_2 and Nile Red was incorporated in the capsule shells, which was the proof for the double emulsion. SEM image (Fig. 3.15B) also confirms the double mineralization process with the “small capsules in big capsule” structure.

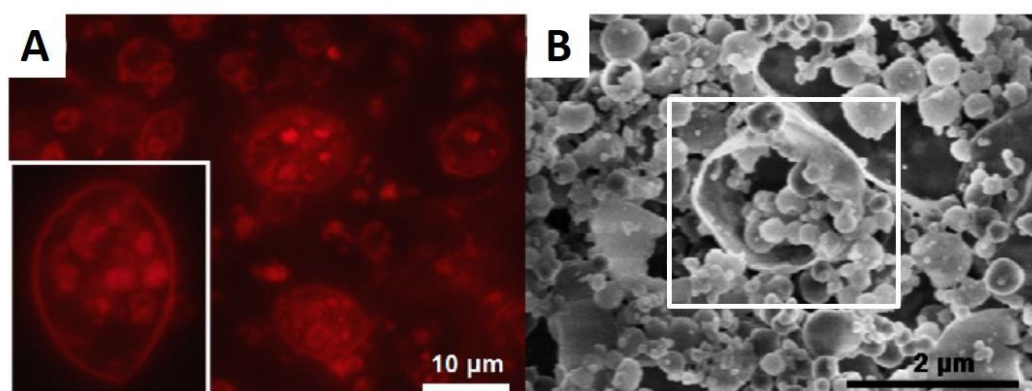


Fig. 3.15: (A) Fluorescence microscopy and (B) SEM images of double emulsion capsules. Reprinted with permission from reference ^[75]. Copyright 2012 the Royal Society of Chemistry.

Section 3.3 and 3.4 demonstrate that without changing the specific chemical components but by changing the sequence of addition, the emulsification method (vortex, stirring or sonication) and relative amount of lysozyme and TEOS, silica particles/capsules with controlled size exhibiting various surface morphologies, inverted capsules and double emulsion mineralized capsules were formed. The next two sections will describe the influence of buffer and additive on size and morphology of lysozyme-silica hybrid capsules.

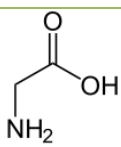
3.5 Influence of buffer solution on the size and morphology of lysozyme-silica hybrid capsules

Both one-step and two-step approaches were applied for the preparation of capsules. With the one-step approach 100 μL TEOS was added into 900 μL lysozyme and the mixture was treated in ultrasonic bath for 15 min. With the two-step approach 20 μL TEOS was added into the 900 μL lysozyme solution first. The mixture was then stirred for 30 min. After that 80 μL TEOS was added into the mixture and sonication was applied to the whole sample for 15 min.

Glycine buffer and phosphate buffer were employed to prepare lysozyme solutions. Their major components and pH values are summarized in Tab. 3.2. Tab. 3.3 and Fig. 3.16 show the considerable changes in both size and morphology of formed capsules by using different buffer. The use of phosphate buffer resulted in larger capsules compared to glycine buffer both with one-step and two-step method. Furthermore, use of phosphate buffer provided a rough capsule shell on which small particles are clearly seen, while the shell of the capsules formed in glycine buffer is relatively homogeneous and smooth.

3 Lysozyme-silica hybrid capsules

Tab. 3.2: Buffers used for the synthesis of lysozyme-silica hybrid capsules.

Buffer	Major component	pH value
Glycine buffer		9
Phosphate buffer	Na ₂ HPO ₄	9

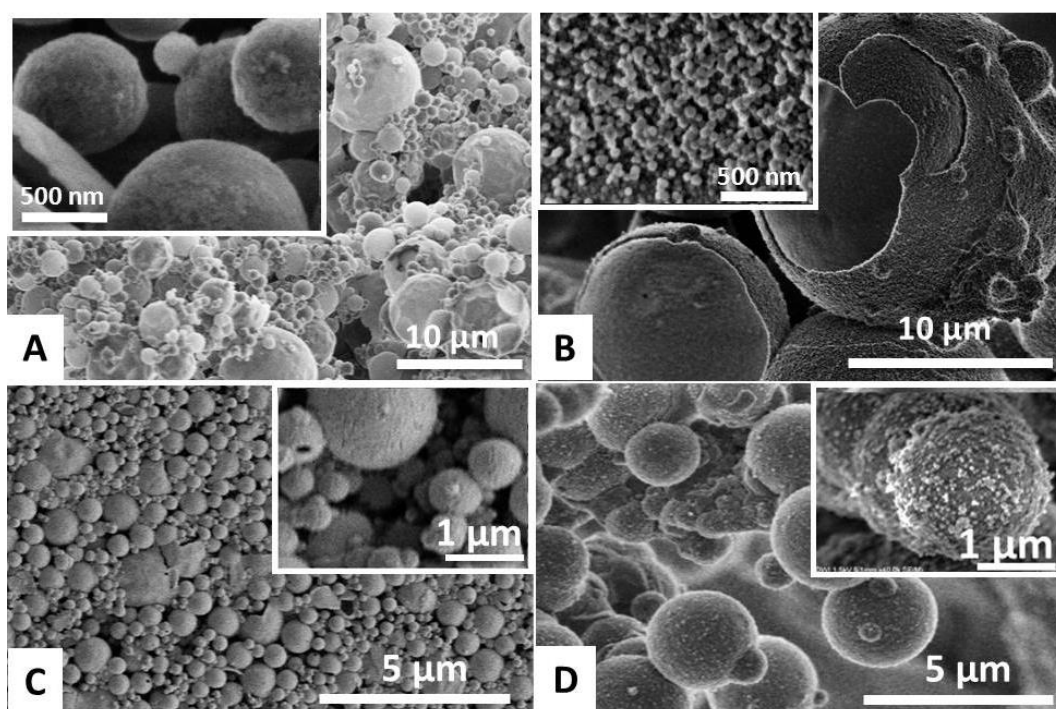


Fig. 3.16: SEM images of lysozyme-silica capsules prepared *via* (A) one-step approach using glycine buffer and (B) one-step approach using phosphate buffer and *via* (C) two-step approach using glycine buffer and (D) two-step approach using phosphate buffer. Insets show magnifications of the shell surface. Reprinted with permission from reference [3]. Copyright 2013 the Royal Society of Chemistry.

3 Lysozyme-silica hybrid capsules

Tab. 3.3: Changes in size and morphology by using different buffers.

	Glycine buffer		Phosphate buffer	
	Size	Morphology	Size	Morphology
One-step	300 nm ~ 15 μm	Smooth	5 ~ 30 μm	Rough
Two-step	< 2 μm	Smooth	1 ~ 5 μm	Rough

Despite of the different surface morphologies, both buffers led to amorphous SiO_2 , which was identified by XRD analysis (Fig. 3.17).

From the purified capsules with phosphate buffer, Na and P elements were detected by EDX analysis (Fig. 3.18B), which indicates these are incorporated from the phosphate buffer into the capsules while these signals were absent in the glycine buffer (Fig. 3.18A). An interaction between the buffer ions and lysozyme molecules or/and silicon compounds is considered to cause the different sizes and morphologies of the capsules. The major difference between glycine buffer and phosphate buffer is the ionic strength (see the major components in Tab. 3.2). The second most abundant element K in phosphate buffer is not detected in the EDX measurement. It would be expected that other additives in the form of sodium salts also affect the capsule formation. The next section will describe how the capsule size and morphology are influenced by an addition of NaCl and NaF.

3 Lysozyme-silica hybrid capsules

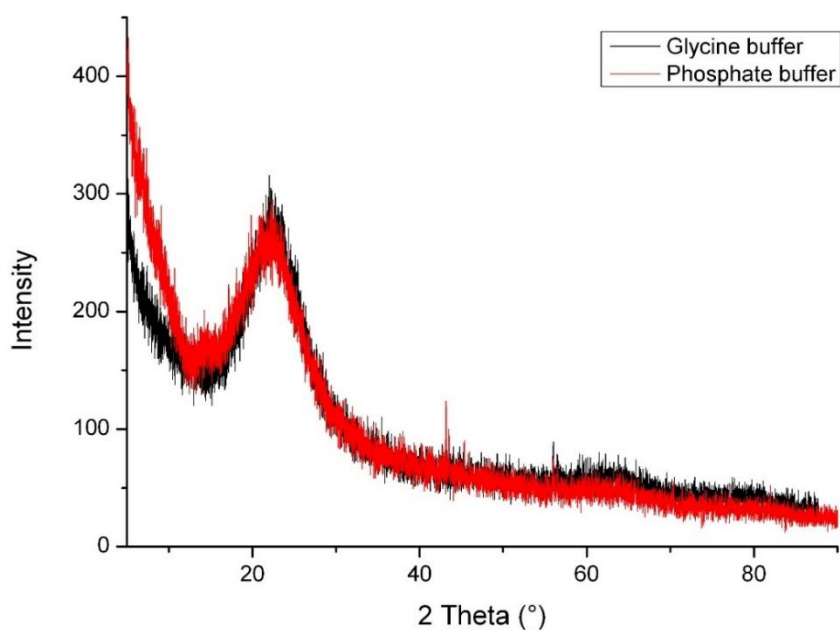


Fig. 3.17: XRD diffractograms of lysozyme-silica capsules prepared in different buffers.

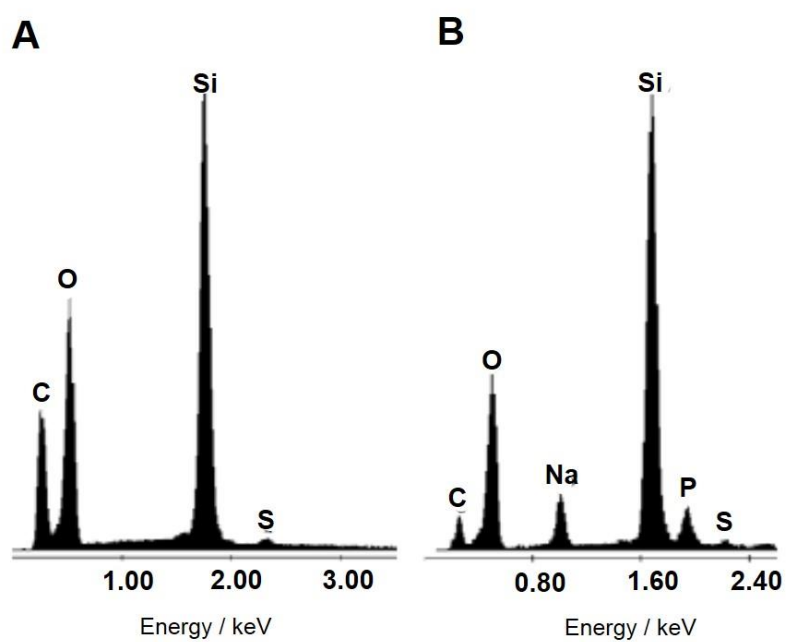


Fig. 3.18: EDX spectra of capsules by using (A) glycine buffer (B) phosphate buffer. Reprinted with permission from reference ^[3]. Copyright 2013 the Royal Society of Chemistry.

3.6 Influence of additives on the size and morphology of the lysozyme-silica hybrid capsules

3.6.1 Sodium salts as additive

Sodium salts NaCl and NaF were added to the lysozyme-TEOS mixture to investigate how they affect the formation of lysozyme-silica hybrid capsules during the reaction in glycine buffer with the two-step method. 20 μL TEOS and 900 μL lysozyme solution (5 mg/mL in glycine buffer) were mixed and then stirred gently with a platform shaker for 30 min. NaCl (2.9 mg, 0.5 mmol) or NaF (2.1 mg, 0.5 mmol) was added with together 80 μL TEOS in the mixture and sonication was applied for 15 min. The samples were stirred again for 24 hours. After purification SEM-analysis was performed.

The addition of sodium salts changes the size and morphology of the capsules significantly (Fig. 3.19). By using NaCl the capsule size increases from $<2\ \mu\text{m}$ (Fig. 3.16C) to 5~10 μm (Fig. 3.19A). The addition of NaF decreases the proportion of capsules dramatically and the capsules are even bigger ($>20\ \mu\text{m}$) with a fragile shell (Fig. 3.19B).

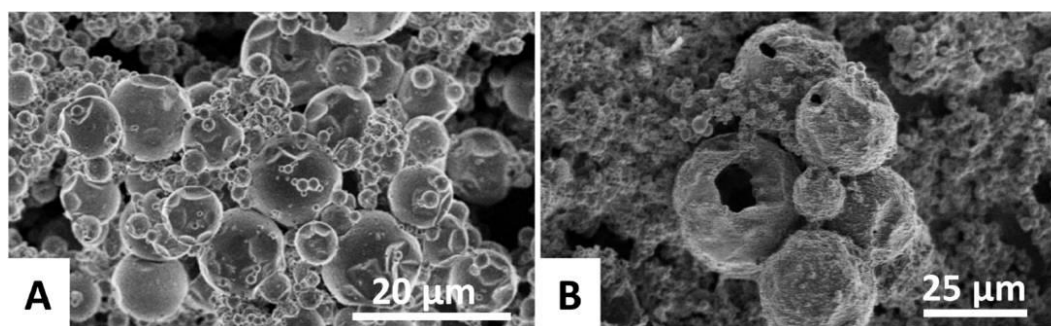


Fig. 3.19: SEM images of lysozyme-silica capsules *via* two-step approach with (A) NaCl (B) NaF as additive. Reprinted with permission from reference ^[3]. Copyright 2013 the Royal Society of Chemistry.

3 Lysozyme-silica hybrid capsules

The change in size and morphology can be explained by the influence of additives on the stability of the lysozyme/TEOS emulsion. Generally there are two major types of intermolecular forces which affect the stability of emulsions: Van der Waals force and electrostatic force. The small suspended droplet particles attract each other naturally due to Van der Waals forces. They coalesce into less stable, larger droplets at first. If the coalescence continues, phase separation occurs. Electrostatic force is a repulsive force, which counterbalances the Van der Waals force and stabilizes the emulsion. When total repulsive forces > total attractive forces, the emulsion is stable (Fig. 3.20). The lysozyme is positively charged at pH 9,^[85] which causes electrostatic repulsion between the TEOS droplets in the Lysozyme/TEOS emulsion. As a result, the emulsion is stable enough to provide a large amount of capsules with small size (Fig. 3.16C). When the total attractive forces > total repulsive forces, the emulsion is instable. Upon addition of NaCl to the emulsion, the interaction between Cl^{-1} and lysozyme reduces the electron density on the surface of TEOS droplets. The small TEOS droplets coalesced into larger ones. That is the reason why the addition of NaCl resulted in bigger capsules. With NaF a large amount of silica cluster and a few capsules with even larger size were formed. Compared to Cl^{-1} , F^{-1} has a higher electron density. So the interaction between NaF and lysozyme is even stronger and the emulsion is dramatically destabilized.

The signal of the element P in EDX spectrum for the sample performed in phosphate buffer without additive (Fig. 3.18B) and the signal of Cl for the one in glycine buffer with NaCl as additive (Fig. 3.21A) indicate that the corresponding counter-ion was incorporated into the lysozyme-silica capsules. Despite the interaction between the sodium salts and lysozyme, the enzymatic activity of lysozyme seems not to be affected since a similar amount of silica was obtained after the same reaction time with and without additives.

However, in the sample with NaF as additive only a low signal of Na was detected and F could not be proven by EDX. The reason could be the difference in relative association strengths of F and Cl towards Na or the cationic amino acids of lysozyme

3 Lysozyme-silica hybrid capsules

(mostly lysines). The relative affinity of F for Na compared to positively charged lysine is higher than that of Cl towards Na and lysine. Hence more NaCl is incorporated and in the NaF addition only Na is detected since the affinity of Na towards negatively charged silicate of the capsule surface is higher than towards F and therefore Na is confined to the surface of the capsules and F is not detected in the EDX. This suggests that several interactions play a role and that the overall system is more complex than simple anion-protein interactions.

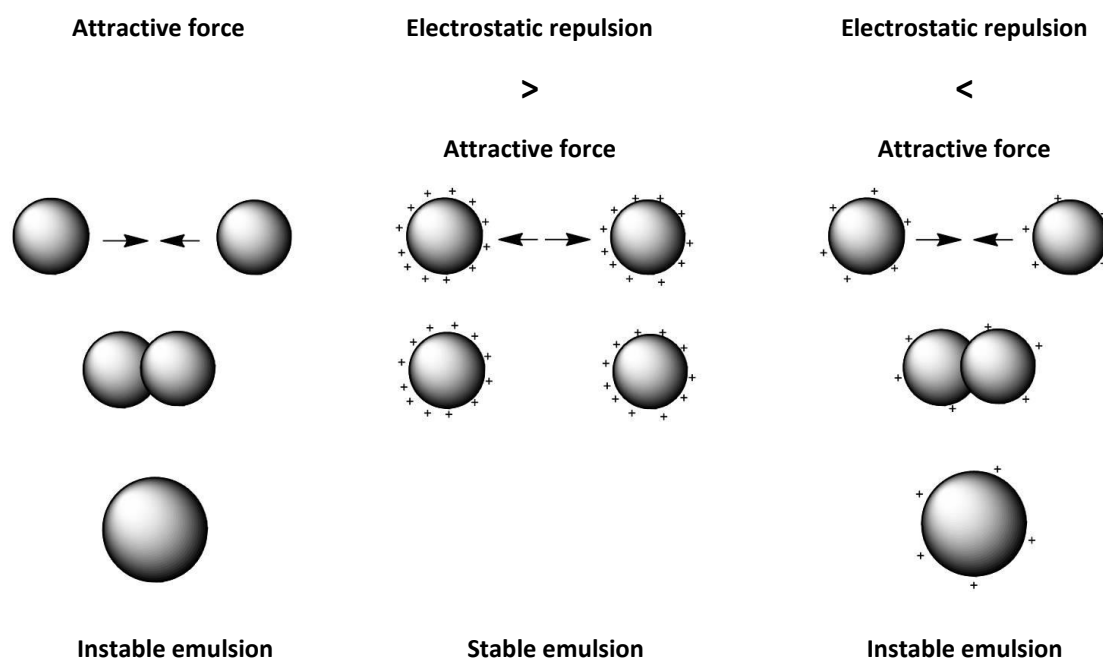


Fig. 3.20: Schematic representation of emulsion stability influenced by electrostatic repulsion.

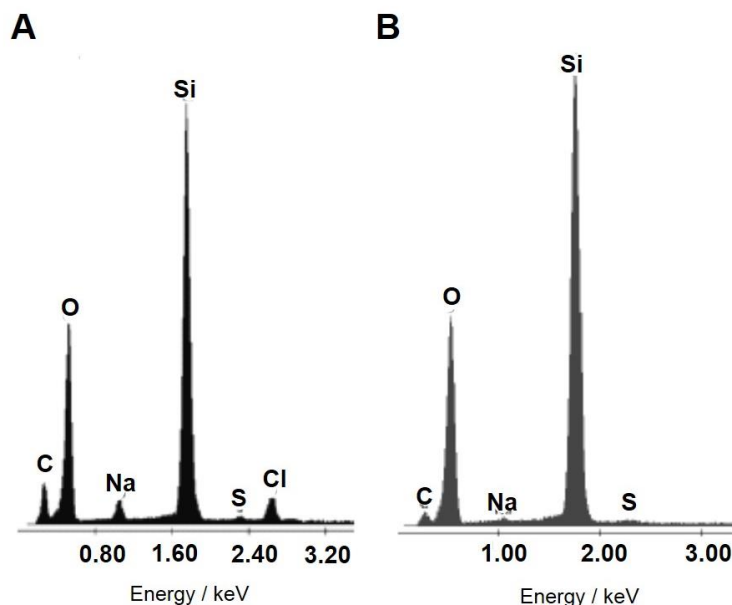


Fig. 3.21: EDX spectra of lysozyme-silica capsules by using (A) NaCl (B) NaF. Reprinted with permission from reference ^[3]. Copyright 2013 the Royal Society of Chemistry.

3.6.2 Ionic surfactants as additive

It is known that specific ion-coordination to polypeptides or polyamines affects the rate of SiO₂ formation as well as the morphology of the SiO₂ structure.^[86] As lysozyme is positively charged and SiO₂ species are negatively charged,^[87] the electrostatic interactions and/or other interactions of the ions with lysozyme and SiO₂ also influence the sizes and morphologies of the protein-SiO₂ hybrid capsules. However, the salts destabilize the emulsion and therefore an ion-pair with additional stabilizing features should be applied to avoid the loss of emulsion stability. An anionic surfactant sodium dodecylsulphate (SDS) as well as a cationic surfactant cetyltrimethylammonium bromide (CTAB) was chosen instead of salts as additive (both at 6.67 mM). SDS and CTAB were used to monitor the influence of charges in capsule formation and SDS is promising since this is also a sodium salt. Although the critical micelle concentration (cmc) of these two surfactants is quite different (1 mM for CTAB and 7-10 mM for SDS), this can be neglected since surfactant aggregates

3 Lysozyme-silica hybrid capsules

and monomers are in a dynamic equilibrium. This means that after adsorption of a monomer surfactant in solution onto the interface, the loss of monomer is compensated by the disassembly of micellar aggregates. So even though the concentration of SDS is below its cmc, it should not affect the emulsification property as compared to CTAB of which the concentration is above the cmc.

The addition of SDS did not result in capsule formation and only unidentified liquid-like structures were obtained. Probably the coordination of SDS to lysozyme *via* ionic interactions is similar as for the other anions. It was reported that SDS associates to lysozyme up to a molar ratio of 100:1 (SDS:lysozyme) before significantly denaturing the protein and coordination occurs between the positively charged amino acids on the surface and the negative charge of the SDS.^[88] This forms an apolar layer around the lysozyme. Although this still enables the lysozyme-SDS complex to stabilize the interface, SDS is much bigger than other anions and the hydrophobic tails of SDS surrounding the lysozyme can shield the enzyme, inhibiting the catalytic activity and prevent SiO₂ formation.

After addition of CTAB, nanocapsules were obtained with diameters between 200 and 600 nm (Fig. 3.22A). The silicification process is not compromised by the addition of the surfactant and the additional stabilizing effect of the CTAB provides smaller capsules with a smooth and rather thick shell. Additionally, a large amount of SiO₂-nanoparticles of about 50 nm in diameter was formed which were observed along with the nanocapsules by TEM analysis (Fig. 3.22B). CTAB forms micellar aggregates and can act as a template for SiO₂ deposition on its own and because the concentration of CTAB used in the experiment is about 7 times higher than its cmc, a large amount of micelles and hence smaller nanoparticles can be expected.^[89]

3 Lysozyme-silica hybrid capsules

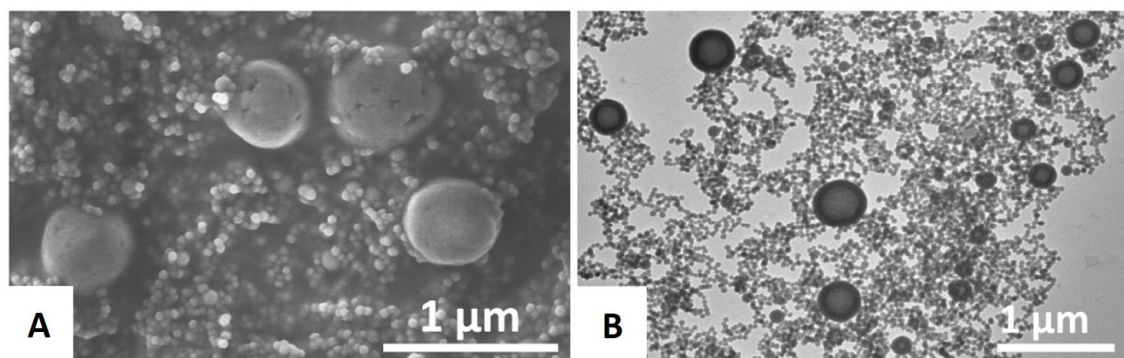


Fig. 3.22: (A) SEM image of lysozyme-silica capsules *via* two-step approach with CTAB; (B) the corresponding TEM analysis of (A). Reprinted with permission from reference ^[3]. Copyright 2013 the Royal Society of Chemistry.

Tab. 3.4: Changes in size and morphology by using different additives.

Additive	Size	Morphology
No additive	< 2 μm	Smooth shell, capsules are highly spherical
NaCl	5 ~ 10 μm	Thin and smooth shell
NaF	Cluster + capsules > 20 μm	Thin and fragile shell, the capsules are deformed
SDS	No silica was formed.	~
CTAB	Nanoparticle 50 nm + capsules 200 ~ 600 nm	Smooth and thick shell

3.7 Surface functionalization of lysozyme-silica hybrid capsules *via* a one-step approach

SiO₂ surface functionalization can be easily performed with the Stöber-method in an ammonia-ethanol mixture at 80 °C.^[90] However, an incorporation of new functionality can also be achieved using lysozyme in aqueous phase at room temperature, which avoids the use of organic solution and high temperature.

For the modification the conventional one-step method was applied. A small amount of APTMS was added together with TEOS in the lysozyme solution as precursor. APTMS provides an amine functionality on the capsules surface (Fig. 3.23).

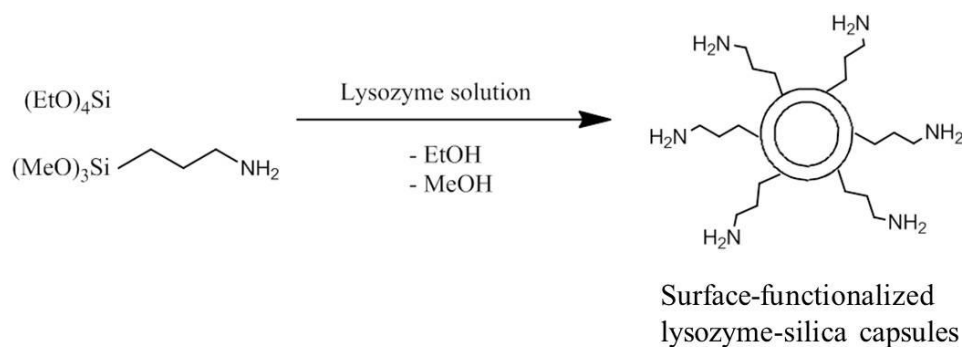


Fig. 3.23: Reaction scheme of surface functionalization with APTMS *via* the one-step approach.

To determine the proper amount of APTMS for the modification, 7 samples (Tab. 3.5, samples 1-7) were prepared first. When the TEOS contents were below 90 wt% a gelled reaction mixture instead of solid silica was formed. Only with TEOS content above 90 wt% dispersible structures were isolated. Another 3 samples (Tab. 3.5, sample 8-10) were prepared, with a TEOS/APTMS (wt %) ration of 98/2, 95/5 and 92/8 separately. Silica capsules were obtained from all the 3 samples (Fig. 3.24). The ration 92/8 was found most promising for the further testing on reactivity, because it contains the highest amount of APTMS bearing functional amine. Fig. 3.25 shows

3 Lysozyme-silica hybrid capsules

SEM and TEM images of capsules formed with 92 % TEOS/8 %APTMS. The capsules were purified *via* decantation. The solid phase was washed subsequently with ethanol and water to remove the remaining APTMS for the further reactivity tests of the amine functionality.

Tab. 3.5: Samples with different TEOS/APTMS ratios.

Sample	TEOS/APTMS Ratio (in weight)	Result
1	100 % / 0 %	Silica capsules
2	90 % / 10 %	Silica cluster
3	80 % / 20 %	Gel
4	70 % / 30 %	Gel
5	50 % / 50 %	Gel
6	25 % / 75 %	Gel
7	0 % / 100 %	Gel
8	98 % / 2 %	Silica capsules
9	95 % / 5 %	Silica capsules
10	92 % / 8 %	Silica capsules

3 Lysozyme-silica hybrid capsules

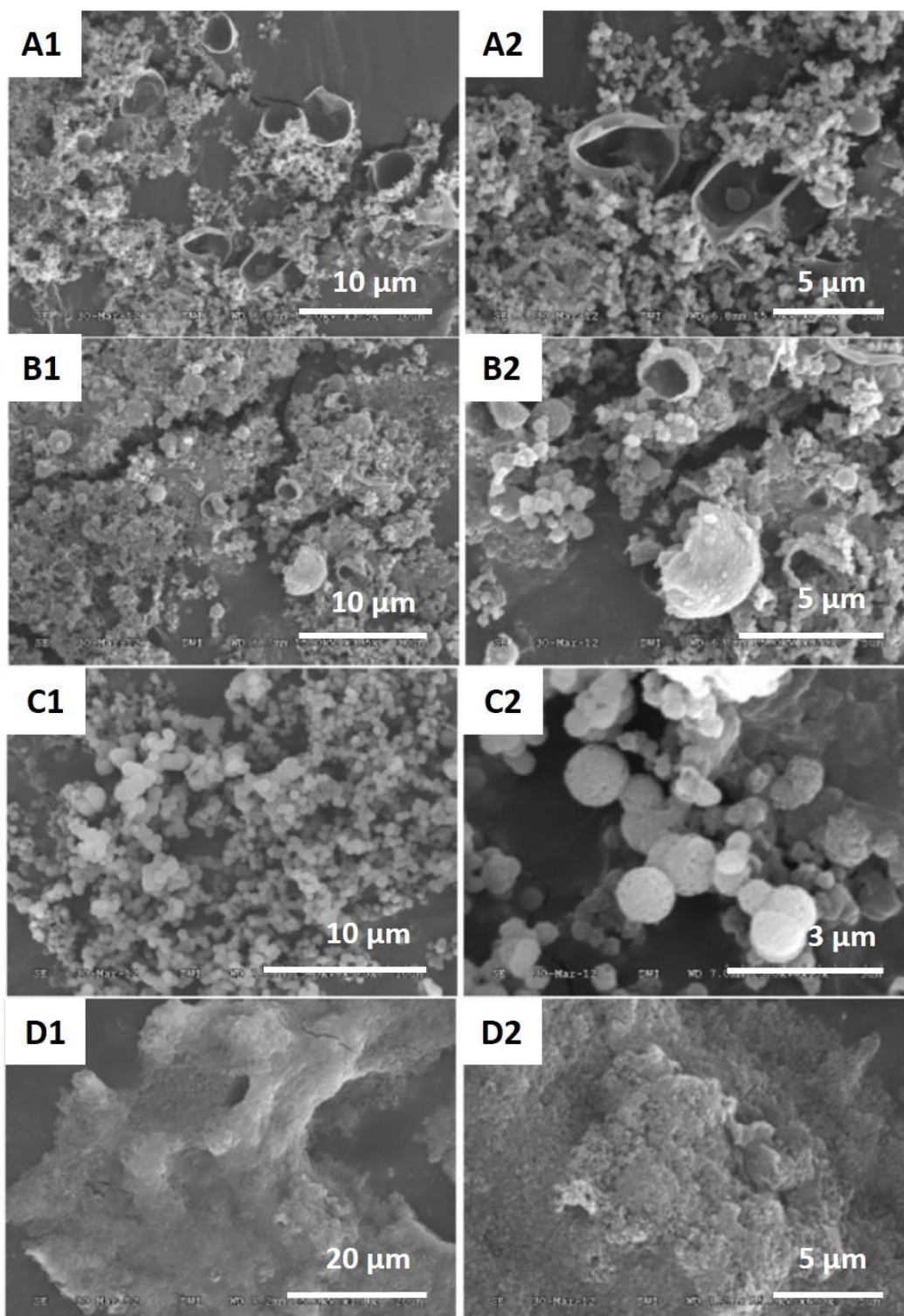


Fig. 3.24: SEM images of samples with different TEOS/APTMS ratios: (A) 98 %/2 %, (B) 95 %/5 %, (C) 92 %/8 % and (D) 90 %/10 % *via* the one-step approach.

3 Lysozyme-silica hybrid capsules

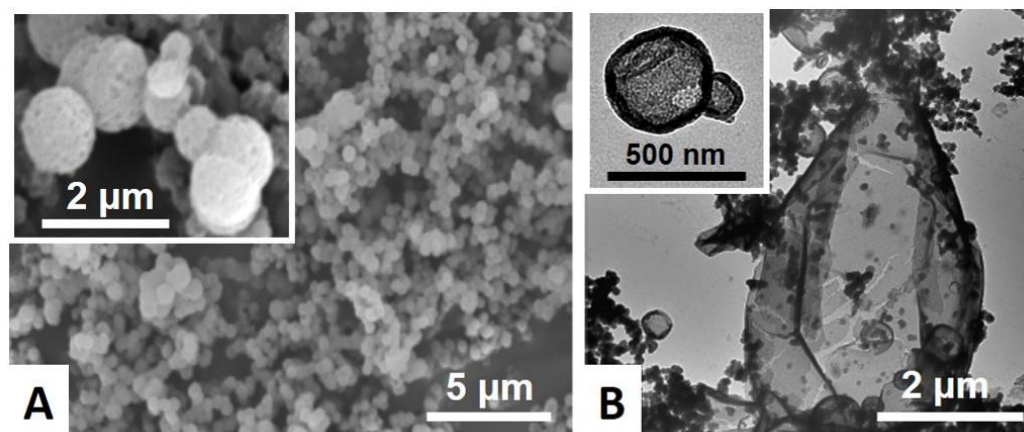


Fig. 3.25: SEM images (A) and TEM images (B) of silica-lysozyme capsules prepared *via* mixing TEOS and APTMS (92 wt%/8 wt%). Reprinted with permission from reference [3]. Copyright 2013 the Royal Society of Chemistry.

To determine the functionalization of the lysozyme-silica hybrid capsules with amine groups *via* APTMS, dabsyl chloride and calcein were applied to test the amine group reactivity.

100 μL dabsyl chloride solution in Dimethylformamide (DMF, 5 mg/mL) was added to 900 μL of a suspension of modified capsules (92 wt% TEOS and 8 wt% APTMS). The reaction mixture was shaken at 37 °C for 24 h and the product was washed with DMF and water. Fig. 3.26 shows the reaction scheme of dabsyl chloride with primary amine groups.

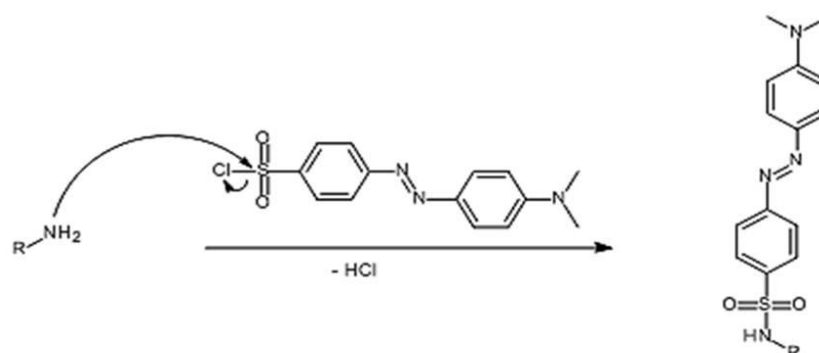


Fig. 3.26: Reaction scheme of primary amine with dabsyl chloride.

3 Lysozyme-silica hybrid capsules

When primary amine groups are introduced on the capsule surface, they should react with dabsyl chloride and the product should show absorption in the UV-Vis range at about 465 nm.

To determine whether unmodified silica or lysozyme is also capable to react with dabsyl chloride, four control reactions were also performed with 1) lysozyme, 2) silica NP (commercial) 3) silica NP functionalized with APTMS 4) lysozyme-silica hybrid capsules from 100 % TEOS under same condition.

Pure dabsyl chloride absorbs at about 465 nm (Fig. 3.27A). In the case of pure silica NP no absorption was detected, which means silica itself is not able to react with dabsyl chloride (Fig. 3.27B). However, in the silica NP functionalized with APTMS and pure lysozyme a shoulder at about 465 nm is visible, indicating a reaction with dabsyl chloride (Fig. 3.27C/D). The unmodified silica capsules from 100 % TEOS show no absorption, which means the incorporated lysozyme is not on the surface of the shell or is not active any more towards dabsyl chloride (Fig. 3.27E). In the spectrum of the modified capsules (Fig. 3.27F) a shoulder at 465 nm is present. Because the incorporated lysozyme is not active so the only reason for the absorption is the amine groups from the APTMS. This reveals a successful surface functionalization with primary amine groups on silica capsules.

3 Lysozyme-silica hybrid capsules

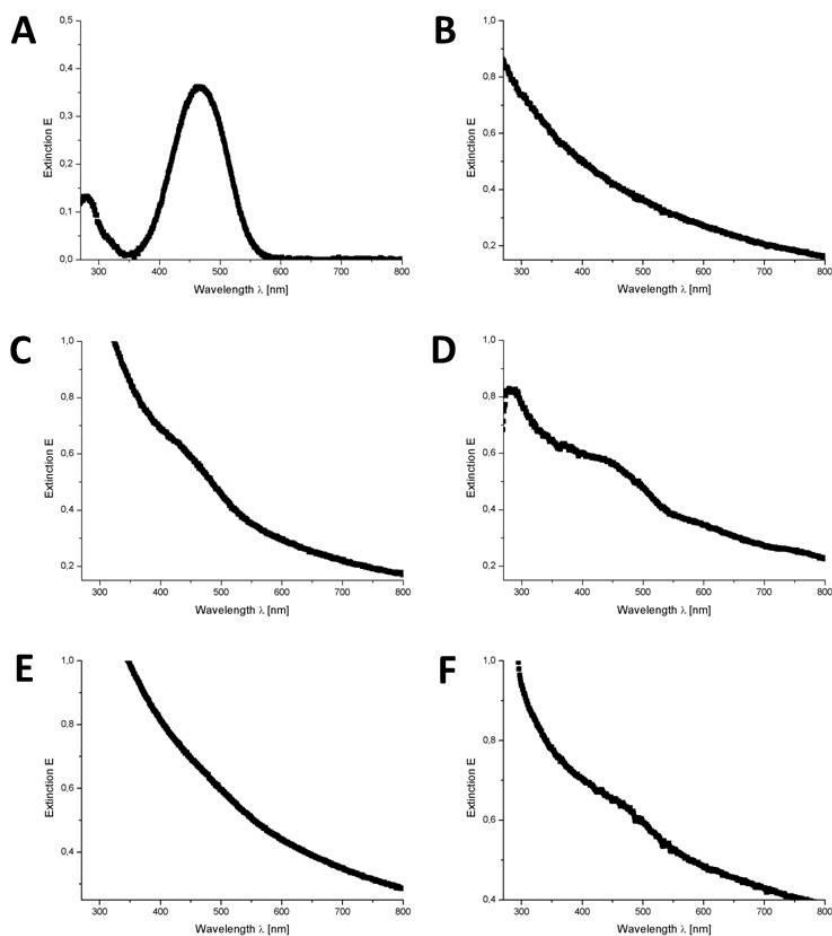


Fig. 3.27: UV-Vis spectra of (A) pure dabsyl chloride (measured in EtOH), (B) dabsyl chloride reacted with silica NP (measured in EtOH), (C) dabsyl chloride reacted with APTMS functionalized silica NP (measured in EtOH), (D) dabsyl chloride reacted with lysozyme (measured in DMF), (E) dabsyl chloride reacted with normal lysozyme-silica (100 % TEOS) capsules (measured in H₂O) and (F) dabsyl chloride reacted with functionalized lysozyme-silica (92 % TEOS 8 % APTMS) (measured in H₂O).

For a further test, a fluorescent dye calcein was used and for this reaction a carbodiimide coupling reagent (EDC) is necessary which represents a standard peptide coupling reaction (Fig. 3.28). 1 mg calcein together with 1 mg *N*-(3-Dimethylaminopropyl)*N*-ethylcarbodiimide hydrochloride was added to 1 mL

3 Lysozyme-silica hybrid capsules

aqueous modified capsules (92 wt% TEOS and 8 wt% APTMS) suspension and the mixture was shaken at 37 °C for 24 h. The product was washed with water and centrifuged to remove the excess of calcein and coupling reagent. Two control reactions with modified silica NP and unmodified silica capsules were performed under the same reaction conditions.

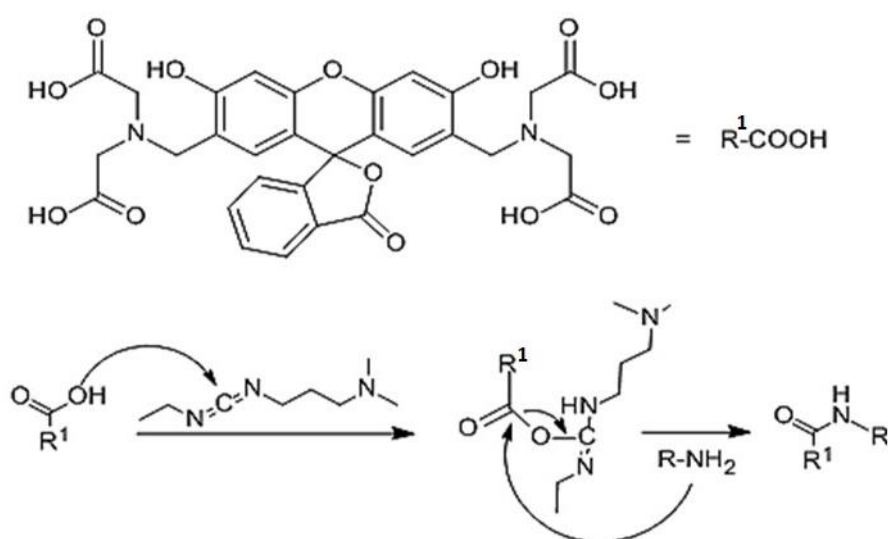


Fig. 3.28: Reaction scheme of calcein and a coupling reagent with primary amine groups.

Fig. 3.29 shows the three reaction mixtures, the liquid fractions after each wash and centrifugation step and the dispersions of the products after 5 centrifugation processes. After the reaction and purification by several washing and centrifugation steps, all three samples remained coloured indicating that calcein attaches to all three samples. However, the liquid fraction of the modified silica NP displays no colour after the first centrifugation. This is because that calcein is bound covalently with the modified silica nanoparticles so that the reaction mixture did not lose its color.

3 Lysozyme-silica hybrid capsules

The unmodified capsule continued to lose colour even after 5 centrifugation steps indicating a physisorption of the dye on the capsules, which is probably due to the interaction of the positively charged lysozyme and negatively charged dye calcein.

In the case of the modified capsules, the upper liquid fraction was slightly coloured after 2 steps, but after 5 steps the fraction was almost colourless. It can be concluded that the calcein was bounded to the modified capsules *via* covalent binding as well as physisorption.

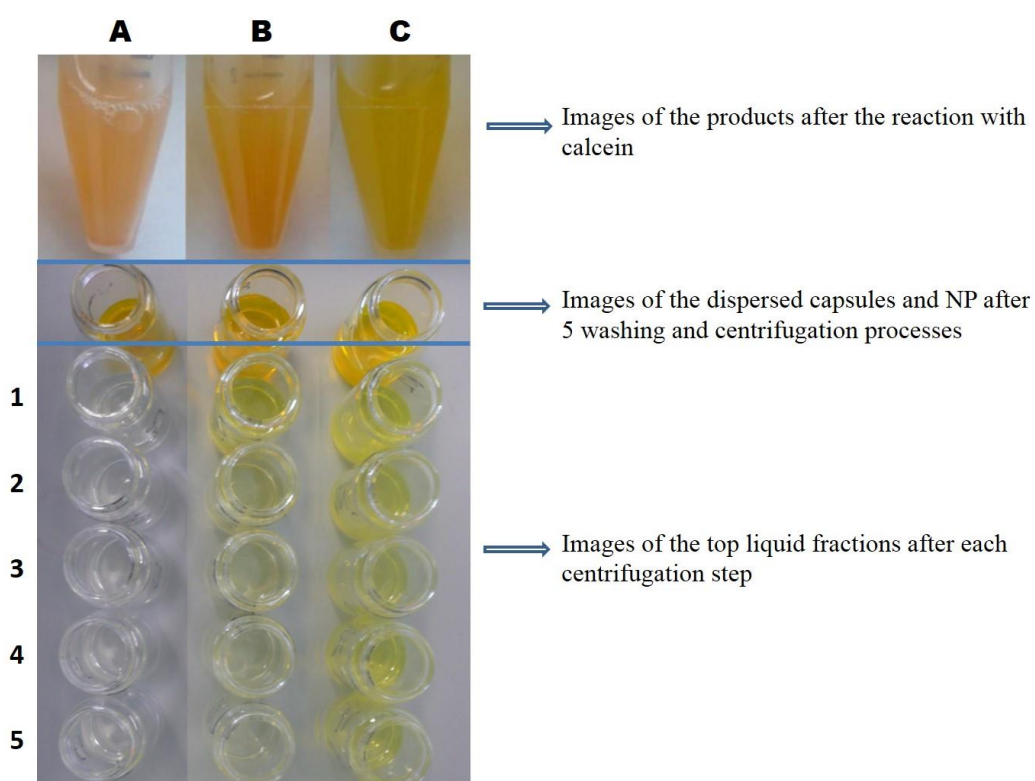


Fig. 3.29: Reaction mixture and supernatant collected after each washing step after a reaction of calcein with: column (A) silica nanoparticles modified with APTMS; column (B) modified silica capsules with APTMS; column (C) silica capsules without modification.

A bathochromic shift in absorption was observed probably due to inter-molecular π -interaction/stacking in the covalently bound system as compared to the physisorbed

3 Lysozyme-silica hybrid capsules

one, indicating a high surface concentration of calcein (Fig. 3.30). Such bathochromic shifts were also observed in other calcein-based systems.^[91]

The bathochromic shift also explains the difference in fluorescent behaviour which was observed in the fluorescence microscopy analysis of the unmodified and modified lysozyme-silica capsules treated with calcein (Fig. 3.31). The emission wavelength of calcein is 515 nm. For the unmodified capsules onto which the calcein is merely physisorbed, the fluorescence was detected in the green channel which is normally the case for pure calcein, while in the red channel no signal was observed. In the case of modified capsules where calcein is partially covalently bound, the aqueous phase was green, presumably originating from desorbed calcein moieties. The modified capsules did not display any fluorescence in the green but only in the red channel.

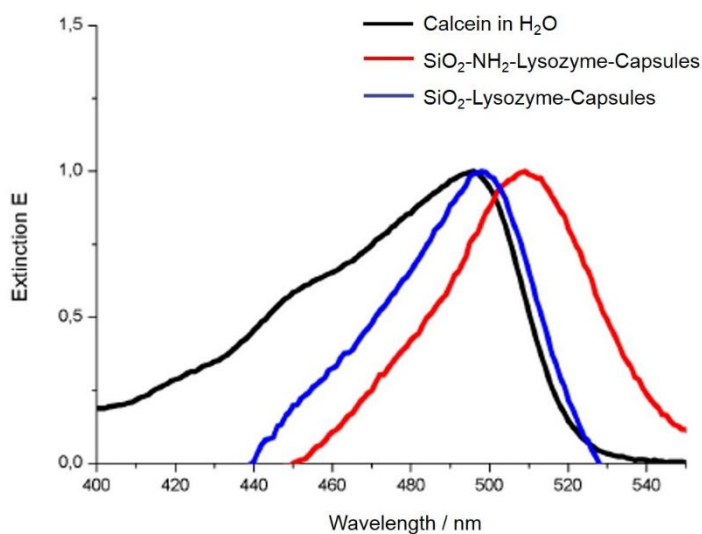


Fig. 3.30: UV-Vis spectra of calcein (black line), unmodified lysozyme-silica capsules (blue line) and modified lysozyme-silica capsules (red line). Reprinted with permission from reference ^[3]. Copyright 2013 the Royal Society of Chemistry.

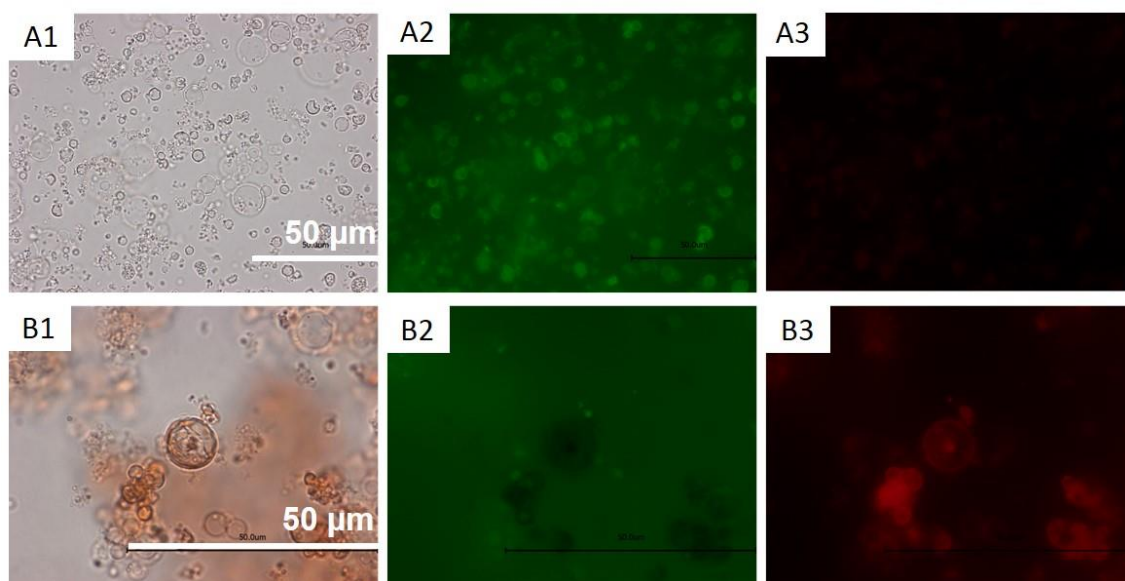


Fig. 3.31: Optical and fluorescent micrographs of unmodified (A) and modified (B) capsules after the treatment with calcein in bright field, green and red channels. Adapted with permission from reference ^[3]. Copyright 2013 the Royal Society of Chemistry.

3.8 Double/multilayer structure of capsule shell

Natural seashell structures have achieved outstanding toughness and strength despite their lightweight. These improved properties base on the alternating layers of flexible biopolymers like chitin or silk-like proteins and hard inorganic layers like calcium carbonate. While the calcium carbonate layer alone is brittle, the thin layers of biopolymer increase the toughness and strength significantly. Nacre, for example, is composed of calcium carbonate platelets, arranged in a continuous parallel lamina. These layers are separated by sheets of organic matrix composed of elastic biopolymers. The multilayer structure make the shell almost as strong as silicon.^[92] Another example for composite structures is the abalone shell, composed of approximately 1 % polymer and 99 % aragonite (CaCO₃) by volume, is two times harder and 1,000 times stronger than pure aragonite.^[85]

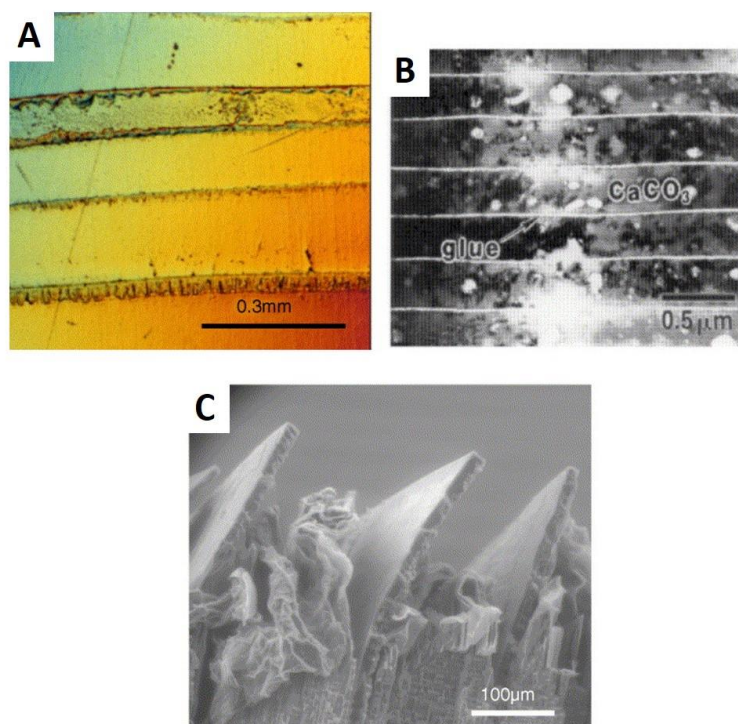


Fig. 3.32: Sections normal to abalone shell surface showing nacreous layer: (A) optical micrograph showing mesostructures with 0.3 mm thick inorganic layers separated by 20 μm thick protein layers; (B) TEM showing the microstructure of tiles;^[93] (C) partially demineralized specimen showing mesolayers (rigid “fins”) and nano-layers (crumbled sheets) of organic material. Reprinted with permission from reference ^[94]. Copyright 2005 Elsevier.

3.8.1 Double layer structure

Inspired by the seashell structures and the layer by layer (LbL) technique in polyelectrolyte for multilayer thin films fabrication^[61], synthesis of capsules with double layers was designed (Fig. 3.33).

Lysozyme-silica hybrid capsules were prepared with the conventional one-step approach. After 3 days the same amount of lysozyme solution was added into the capsule dispersion and the mixture was stirred gently for 15 min. As silica is negatively charged and lysozyme is positively charged at pH 9, the added lysozyme molecules should be absorbed onto the silica capsules. Subsequently 100 μL TEOS

3 Lysozyme-silica hybrid capsules

was also added and the whole mixture was stirred at room temperature for 3 days. Due to the absorbed protein, TEOS is expected to condense on the capsule surface to form the second layer. After the second addition of lysozyme or/and TEOS no sonication was performed because the new lysozyme/TEOS may probably form new emulsion droplets instead of adsorb onto the surface of the capsules.

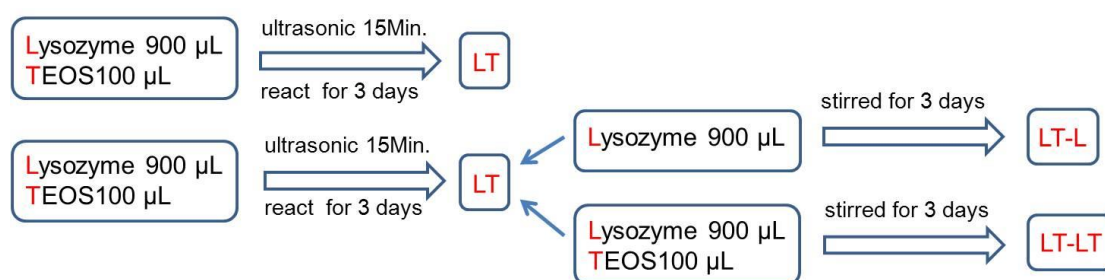


Fig. 3.33: Different samples for the investigation of double layer structure. LT stands for the conventional lysozyme-silica capsules with the one-step method. If only the second part of lysozyme solution is added to the sample LT, LT-L is obtained after 3 days. LT-LT is the abbreviation for the sample with a second addition of lysozyme and TEOS together to the sample LT.

Tab. 3.6: Zeta-potential measurements for double layer structure.

	Zeta-Potential / mV at pH 9 and 25 °C		
	Glycine buffer	Phosphate buffer	Milli-Q water
Lysozyme	- 4.23	- 1.03	28.4
LT	- 17.80	- 15.80	-
LT-L	- 7.80	- 8.40	-
LT-LT	- 22.70	- 23.30	-

3 Lysozyme-silica hybrid capsules

The isoelectric point of lysozyme is at about pH 11 and lysozyme is positively charged when $\text{pH} < 11$.^[85] At pH 9 the Zeta-potential of lysozyme in Milli-Q water is 28.4. However, the results measured in either glycine buffer or phosphate buffer at pH 9 are negative, indicating a net negative surface charge. A possible explanation is that lysozyme molecules are surrounded by buffer ions due to the protein-ion interaction. The outer shell of buffer ions such as HPO_4^{2-} screens the surface charge of lysozyme so that the lysozyme molecules are lightly negatively charged.

Silica usually is strongly negatively charged (zeta-potential between -50 and -80).^[95] The lysozyme-silica hybrid capsules LT were also negatively charged, but not as strong as pure silica. After the second addition of lysozyme solution to the sample LT the zeta potential changed from -17.8 to -7.8 in glycine buffer and from -15.8 to -8.4 in phosphate buffer separately, which indicates the absorption of the new lysozyme molecules on the LT surface. When lysozyme and TEOS were added together to LT, the zeta potential of the sample LT-LT became more negative in both glycine and phosphate buffer. Probably new silica was formed on the capsule surface (Tab. 3.6).

SEM micrographs were measured for the morphology investigation of sample LT-L and LT-LT in detail. Fig. 3.34A and B show no significant difference between normal sample LT and the one with second lysozyme addition LT-L. The shell thicknesses are almost identical at about 100 nm, which confirms again that TEOS is completely converted after 3 days so that a further reaction with the new lysozyme is not possible. However, when TEOS was added together with lysozyme to LT, after 3 days the new sample LT-LT (Fig. 3.34C) is different from LT and LT-L. Firstly, unlike the well separated capsules in sample LT and LT-L, there is much more bulk material besides capsules. Secondly, the capsule surface is not smooth anymore. It seems like the major part of the second lysozyme/TEOS condensed in the solution and a minor part on the capsule surface, but the condensation of new silica on the surface was not homogeneous so that the surface is not smooth anymore and no increase of shell thickness is observed.

3 Lysozyme-silica hybrid capsules

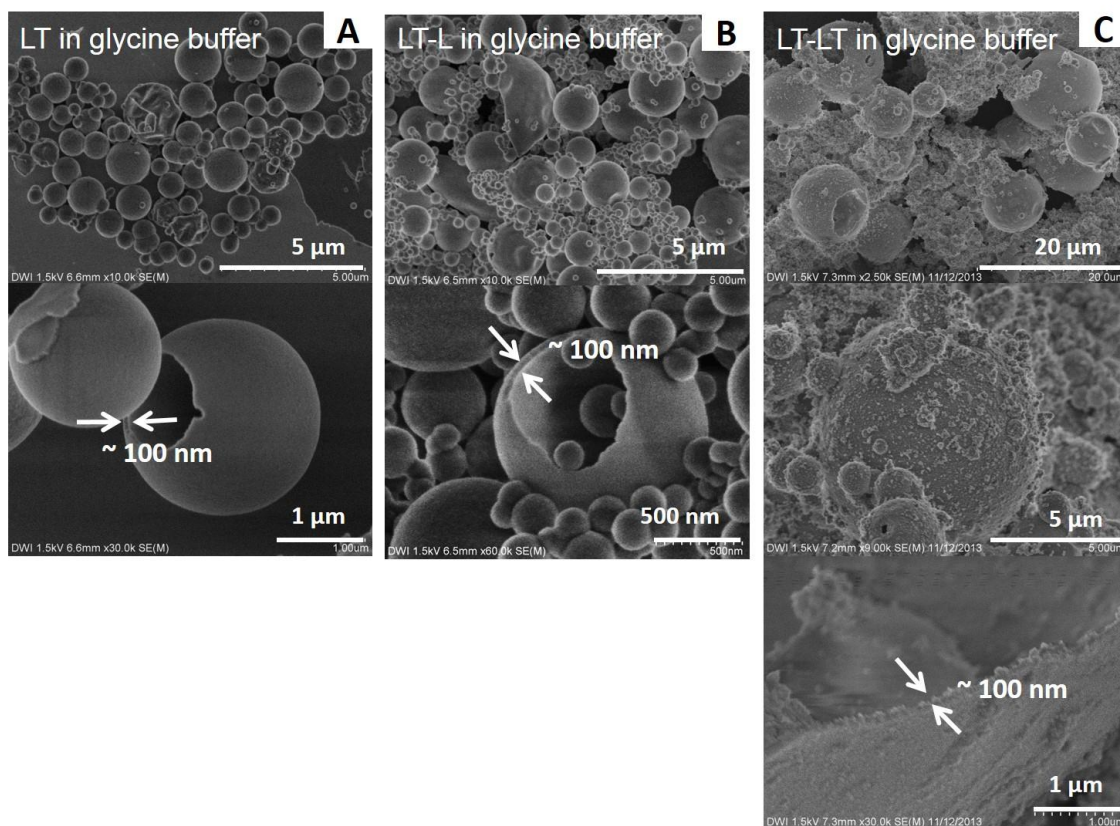


Fig. 3.34: SEM images of the overview and the magnification of (A) LT, (B) LT-L and (C) LT-LT in glycine buffer.

SEM images of the sample in phosphate buffer are displayed in Fig. 3.35. Similar to the samples prepared in glycine buffer, there is no obvious difference between normal sample LT and the one only with addition of lysozyme LT-L. The shell thickness of both samples is about 300 nm (Fig. 3.35A/B). The sample with second lysozyme-TEOS addition LT-LT, however, shows some changes.

Different from the sample in glycine buffer, no large cluster was formed here in LT-LT. Furthermore, the thickness of capsule shell increased, indicating the second part of TEOS condensed very homogeneously on the LT capsule surface so that an increase of thickness is observed (Fig. 3.35C).

3 Lysozyme-silica hybrid capsules

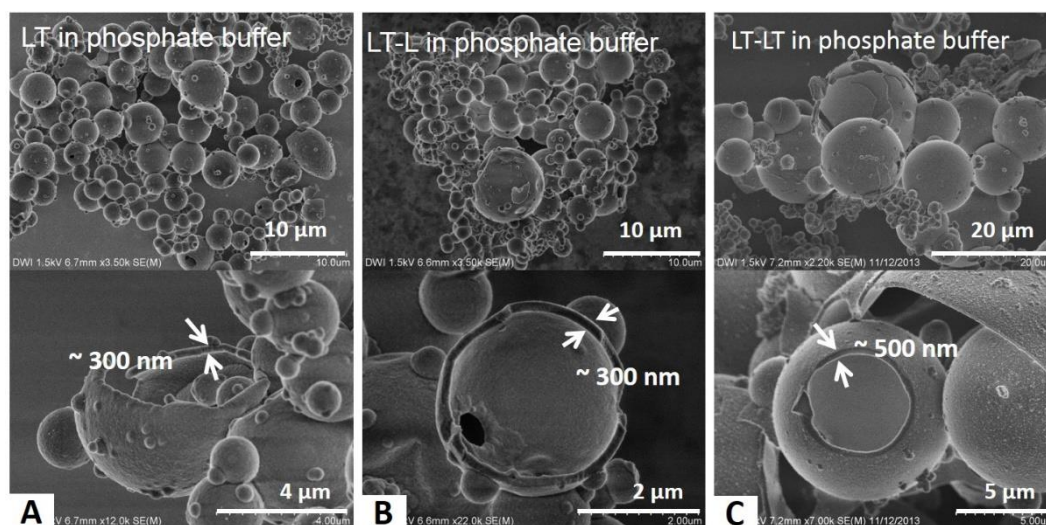


Fig. 3.35: SEM images of the overview and the magnification of (A) LT, (B) LT-L and (C) LT-LT in phosphate buffer.

Fig. 3.36 show two capsules from sample LT-LT with more details. In Fig. 3.36A a line could be clearly seen within the capsule shell, which is, besides the increasing thickness for a double layer structure, an additional proof. In Fig. 3.36B the inside view of the broken capsule reveals that the second condensation of TEOS also occurred in the inner side homogeneously.

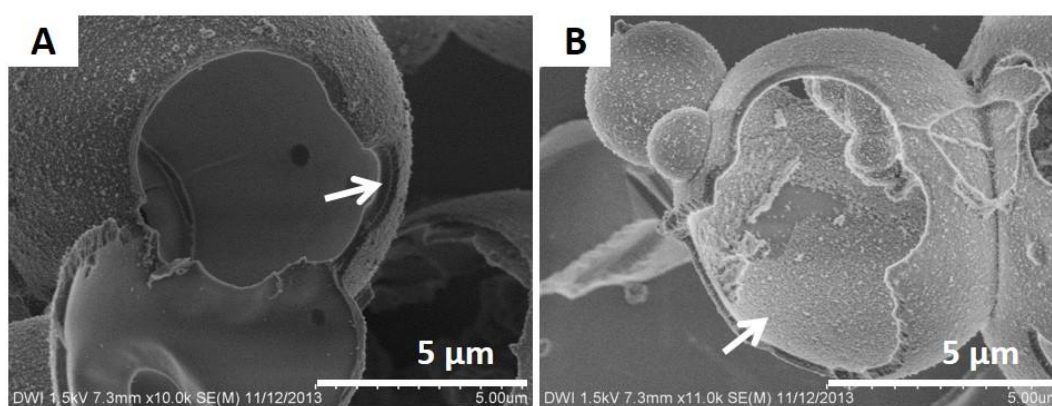


Fig. 3.36: SEM images of two capsules from sample LT-LT in phosphate buffer.

Based on the results above, it can be concluded that the synthesis of silica capsules with double-layer shell in phosphate buffer is successful.

3.8.2 Multilayer structure

To investigate the possibility of structure formation with more than two layers, samples LT-LT-LT and LT-LT-LT-LT were also prepared in the phosphate buffer with the same methods as described above (Fig. 3.37).

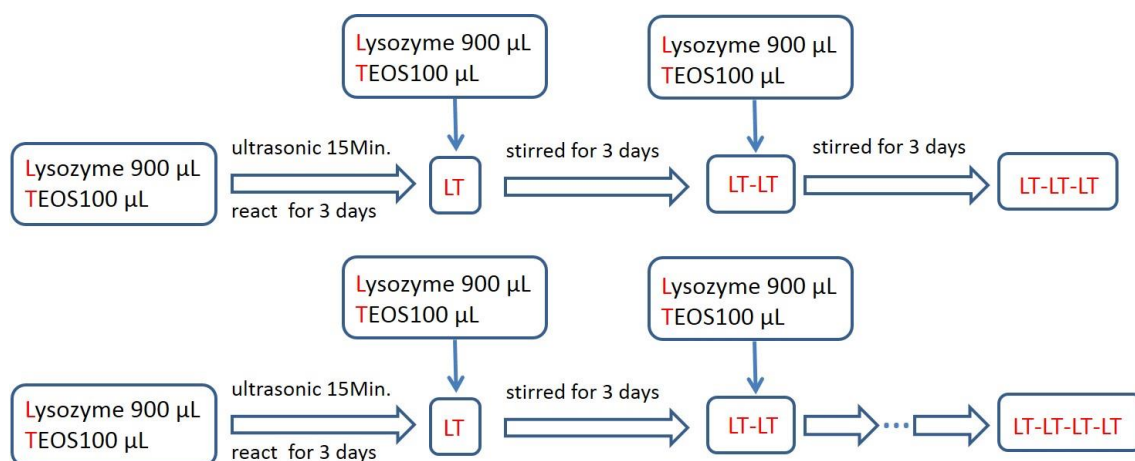


Fig. 3.37: Preparation of sample LT-LT-LT and LT-LT-LT-LT in phosphate buffer.

The SEM images (Fig. 3.38) show that the shell of LT-LT-LT is still about 500 nm, which is similar as LT-LT, however, the surface morphology has changed. LT-LT has homogeneous surfaces (Fig. 3.35C), while the surface of LT-LT-LT is rather rough (Fig. 3.38C). The third addition of lysozyme/TEOS still condensed on the capsule surface. If the condensation was homogeneous, an increase of shell thickness should be observed. However, the new lysozyme/TEOS built solid particle on the surface of LT-LT-LT, resulting in the rough surface morphology. The average thickness of LT-LT-LT must have increased, which is difficult to be determined though.

3 Lysozyme-silica hybrid capsules

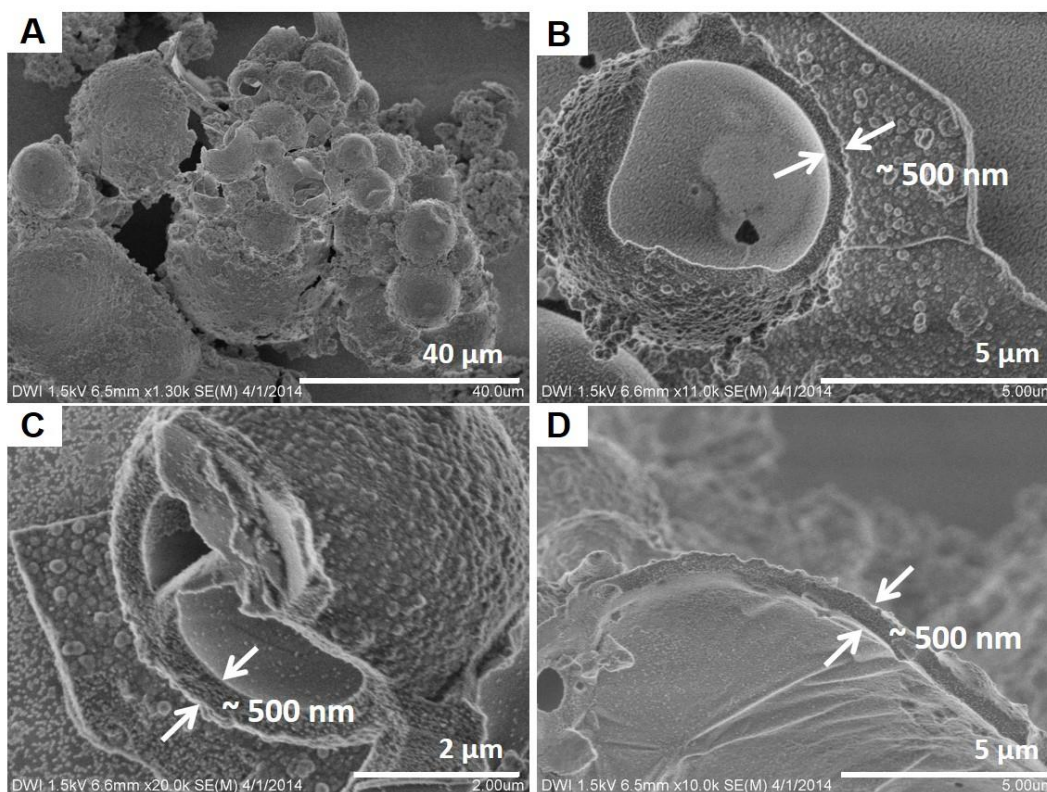


Fig. 3.38: SEM images of sample LT-LT-LT prepared in phosphate buffer.

The SEM images of sample LT-LT-LT-LT prove a clear increase of the shell thickness (Fig. 3.39B (~1 μm) and Fig. 3.39C (~700 nm)). However, the amount of capsules has decreased dramatically in LT-LT-LT-LT. Only a few big capsules remained and silica cluster were formed (Fig. 3.39A/B). The similar tendency can also be observed with sample LT-LT-LT, yet less pronounced. Since the preparation of LT-LT-LT-LT needs 12 days and it was reported in our research paper that the capsules *via* one-step approach are stable up to 10 days but not for longer periods.^[75] Many capsules were broken and a large amount of silica cluster can be observed. Fig. 3.39C and D show two cross sections of LT-LT-LT-LT. It can be concluded that the shell has a multilayer structure, however, it is not possible to determine the exact number of layers.

3 Lysozyme-silica hybrid capsules

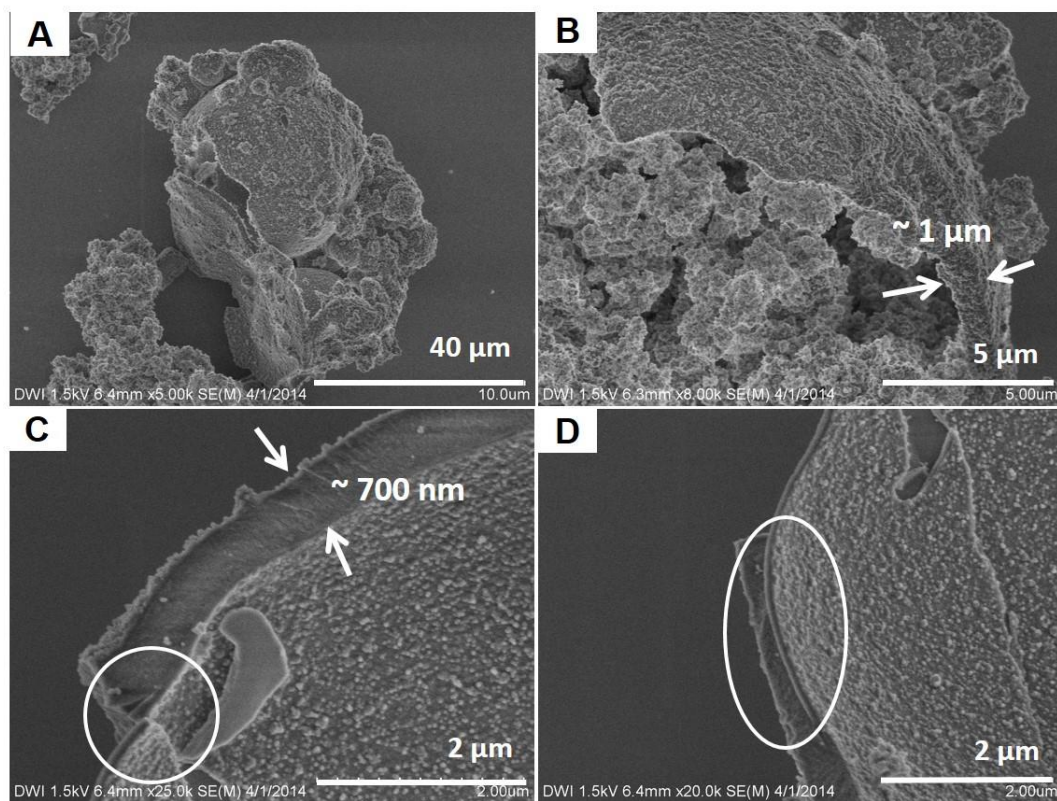


Fig. 3.39: SEM images of sample LT-LT-LT-LT prepared in phosphate buffer.

4 Silicatein-silica hybrid capsules

4.1 Silicatein as effective biocatalysts and templates for the synthesis of silica capsules

To prove the catalytic ability of silicatein, 4 samples were prepared (Fig. 4.1). 100 μL TEOS was mixed separately with 400 μL Milli Q H_2O , 400 μL Tris buffer (pH 8), 400 μL hydrophobin B* solution (a very surface active amphiphilic protein, 5 mg/mL in Tris buffer, pH 8) and recombinant silicatein solution (0.15 mg/mL in Tris buffer, pH 8). After 3 hours incubation at room temperature, white precipitate was isolated from the mixture of recombinant silicatein and TEOS, while in the other 3 samples no precipitate was observed. After purification and lyophilization, IR measurement was applied with the precipitate and the spectrum of the sample D is identical with that of pure silica (Fig. 4.2).

4 Silicatein-silica hybrid capsules

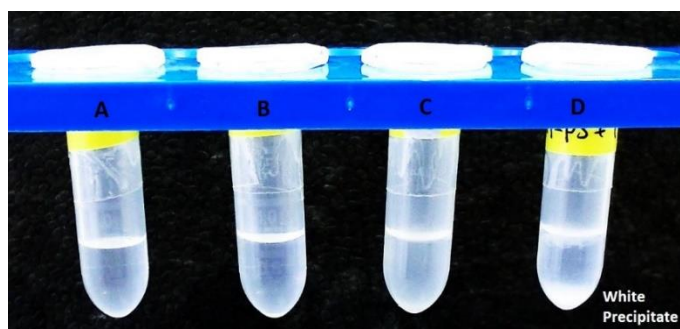


Fig. 4.1: (A) Milli Q H₂O, (B) Tris buffer, (C) hydrophobin solution in Tris buffer (5 mg/mL), (D) recombinant silicatein solution in Tris buffer (0.15 mg/mL) incubated with TEOS after 3 hours at room temperature.

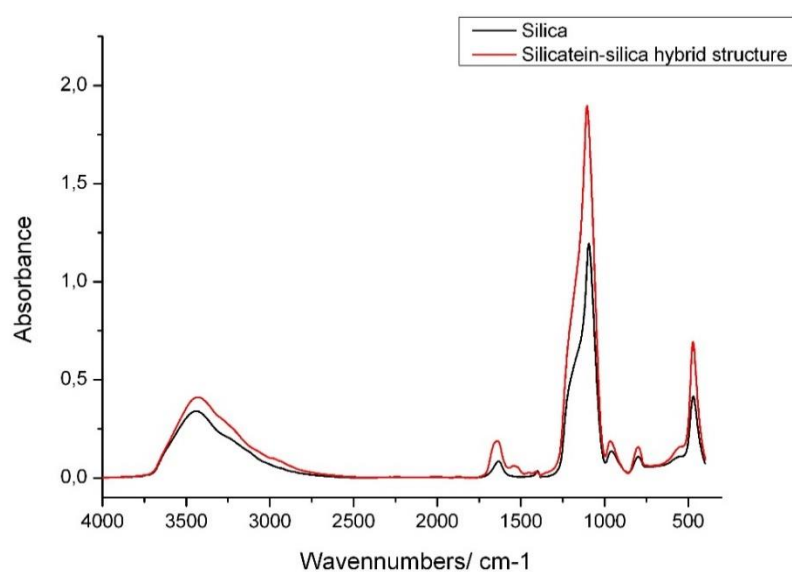


Fig. 4.2: IR spectra of pure silica and the precipitate isolated from recombinant silicatein after 3 hours incubation with TEOS.

4 Silicatein-silica hybrid capsules

It can be concluded from the experiments and the IR measurements that the synthesized silicatein is active towards silica formation.

Pendant drop measurement was used to check whether the recombinant silicatein is also interfacial active to serve as templates for capsules. Due to the limited amount of silicatein solution, TEOS was set as the environment and the pendant drop was formed from protein solution. The red line in Fig. 4.3 shows that the interfacial tension between the water phase and the TEOS can be significantly reduced by recombinant silicatein solution. Therefore it is capable to work as effective biocatalyst for the templated synthesis of silica capsules.

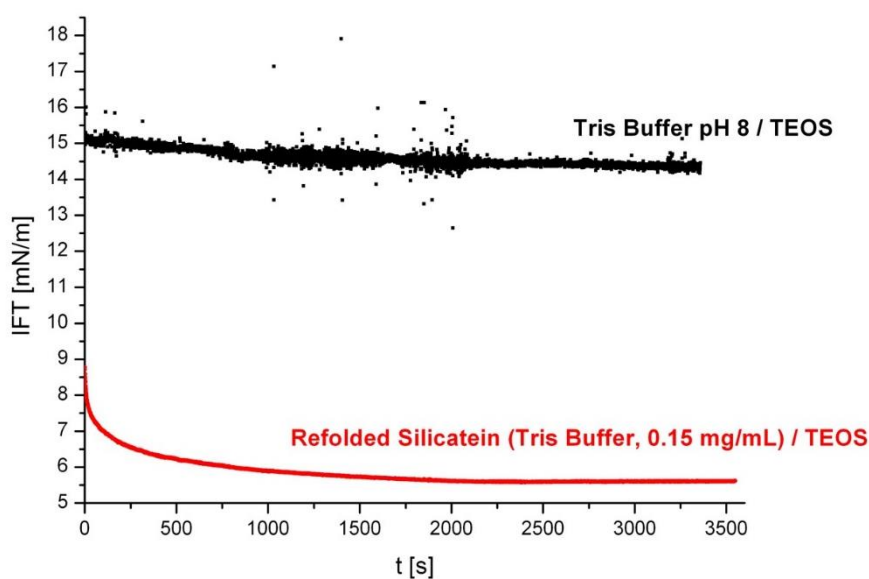


Fig. 4.3: Dynamic interfacial tension at the interface between Tris buffer and TEOS (black); refolded silicatein solution and TEOS (red).

Furthermore, the pendant drop was changing over time (Fig. 4.4). Within the first 60 minutes the drop was transparent and the shape stayed the same, however, changes of the drop could be observed after one hour. At first the pendant drop was becoming turbid which probably indicates a reaction and the product was soluble neither in

4 Silicatein-silica hybrid capsules

aqueous phase nor in TEOS. As from 120 min onwards a phase separation in the droplet is clear to be seen and the shape changed significantly. Obviously the interface was solidifying over time. The change of the pendant drop corresponded to the process of the enzymatic polycondensation of TEOS (Fig. 1.3 and 1.5 the reaction scheme of polymerization of TEOS). The TEOS was hydrolyzed at the interface in the presence of silicatein. The (partially) hydrolyzed TEOS became hydrophilic and diffused into the pendant drop (aqueous phase). The condensation between Si-OH groups formed intermediates e.g. dimer, trimer and oligomer (straight or hyperbranched), which possibly occurred between 60 and 120 min after drop formation. At the same time the silicatein in the pendant drop catalyzed the hydrolysis of remaining ethoxy groups of the intermediate. The hydrolyzed intermediates condensed continually and the chains grew forward, which correlated to the phase separation observed from 120 to 420 min. The interface also turned from liquid to solid during the polycondensation.

This process is not exactly the same as the formation of silica capsules in an o/w Pickering emulsion, because the droplets in a Pickering emulsions are much smaller than a pendant drop and the water is the continuous phase. However, it proves that the TEOS is hydrolyzed at the interfaces in a short time in the presence of protein.

4 Silicatein-silica hybrid capsules

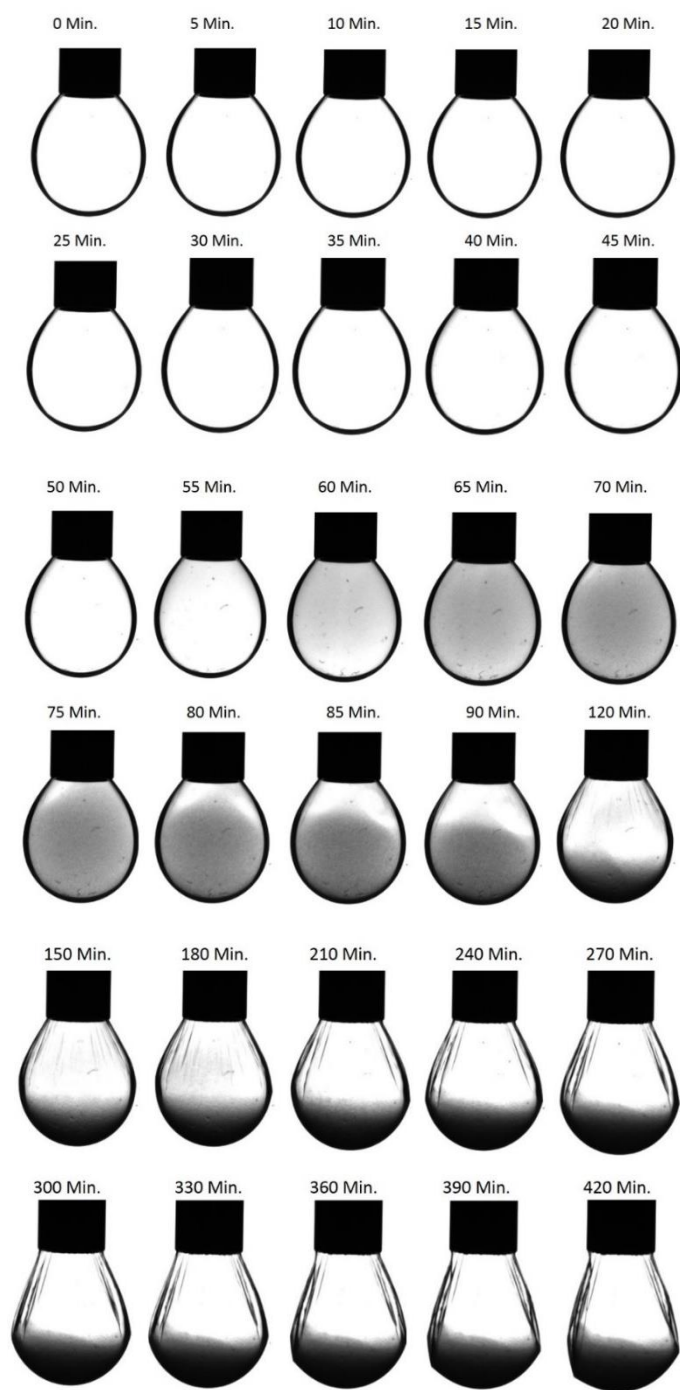


Fig. 4.4: Change of a pendant drop over time (pendant drop: silicatein solution 0.15 mg/mL in Tris buffer pH 8, environment: TEOS).

4.2 Silicatein vs. lysozyme

In chapter 1 it was discussed that lysozyme has similar active sites as silicatein, therefore it also shows excellent ability for silica formation. Comparing the IFT measurement of recombinant silicatein solution in Tris buffer against TEOS with those of lysozyme and other enzymes (Fig. 4.5), recombinant silicatein solution is apparently more active, despite of the much lower concentration.

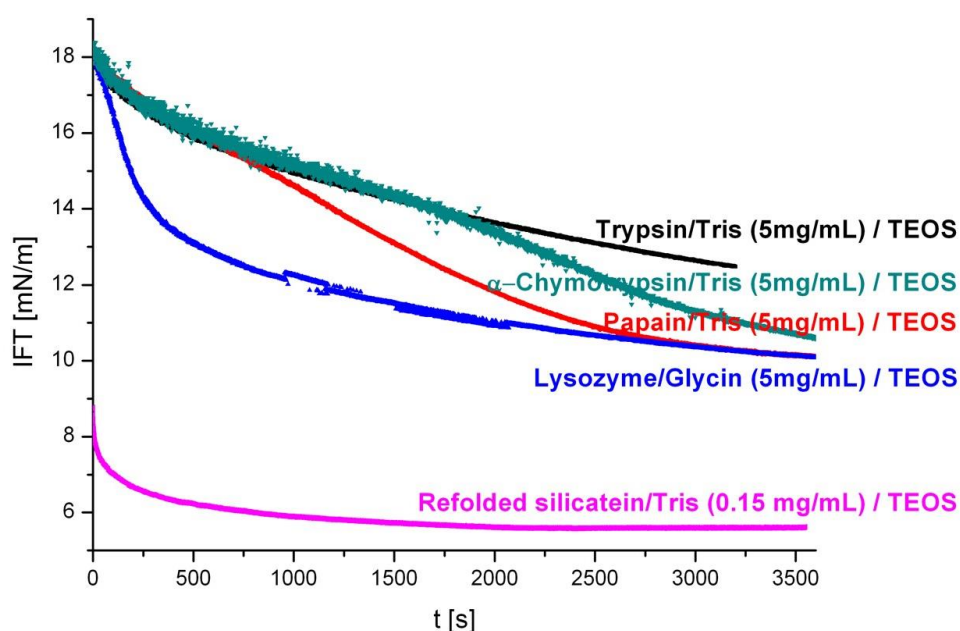


Fig. 4.5: Dynamic interfacial tensions at the interface between different enzymes solutions and TEOS.

The change of a lysozyme pendant drop (5 mg/mL in glycine buffer) was also analyzed with the Tensiometer and compared with a silicatein pendant drop (0.15 mg/mL in Tris buffer). The lysozyme drop showed a similar development as silicatein, but the reaction in the presence of silicatein seemed faster even with a much lower concentration. (Fig. 4.6).

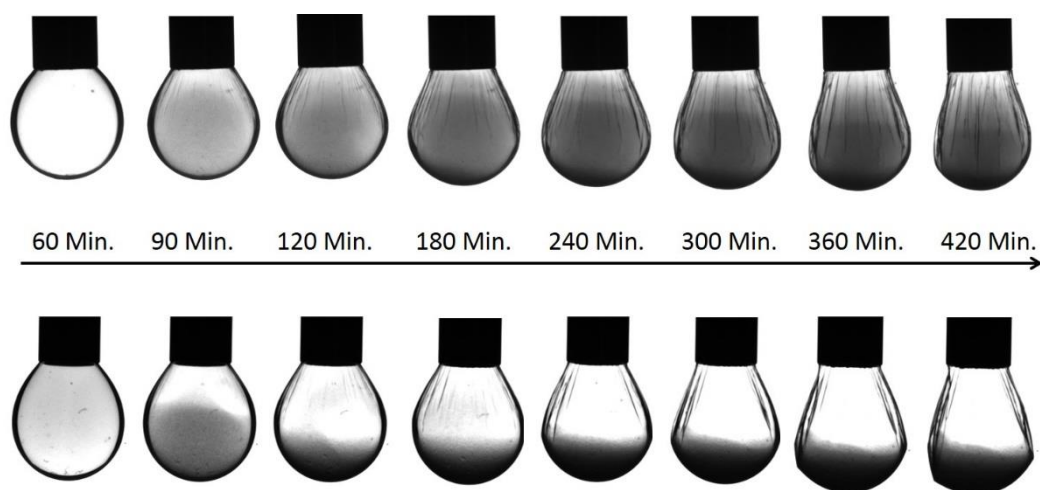


Fig. 4.6: Change of a lysozyme (5 mg/mL in glycine buffer) pendant drop (top) and a recombinant silicatein (0.15 mg/mL in Tris buffer) pendant drop (bottom) in the TEOS environment.

4.3 Size and morphology control of silicatein-silica capsules influenced by emulsification method and precursors

The recombinant silicatein achieves the two requirements for the enzymatic synthesis of silica capsules. Firstly, it can enzymatically catalyse the silicification. Secondly, it can stabilize the interface between water and TEOS.

Four samples were prepared with recombinant silicatein and two different silica precursors, TEOS and PEOS. (Tab. 4.1) Instead of 900 μL lysozyme solution here only 500 μL silicatein solution were employed for each sample due to the limited amount of silicatein. The difference between sample 1 and 2 is the emulsification method. Sample 2 and 3 have different silicatein/TEOS ratio. Sample 3 and 4 differ from each other in the using of two different silica precursors TEOS and PEOS. After 24 hours incubation at room temperature all four samples were purified and characterized with SEM (Fig. 4.7).

4 Silicatein-silica hybrid capsules

Tab. 4.1: Silica capsules prepared with silicatein solution after a reaction of 24 hours at room temperature.

Sample	Result
1 Silicatein 500 μ L + TEOS 20 μ L Vortex 15 min	Big capsules (>50 μ m) with thick and rough shell (Fig. 3.46 A1 and A2)
2 Silicatein 500 μ L + TEOS 20 μ L Sonication 15 min	Small capsules (<20 μ m) with thin and smooth shell (Fig. 3.46 B1 and B2)
3 Silicatein 500 μ L + TEOS 100 μ L Sonication 15 min	Middle capsules (5~50 μ m) with thin and smooth shell (Fig. 3.46 C1 and C2)
4 Silicatein 500 μ L + PEOS 100 μ L Sonication 15 min	Small capsules (<10 μ m) with special surface structure (Fig. 3.46 D1 and D2)

Sample 1 was treated with vortex while sample 2 with sonication. It was observed that vortex led to much bigger capsules than sonication. Furthermore, the vortex provided much thicker shell and rougher surface while capsules formed by sonication had thin and smooth shell. If the amount of TEOS was increased from 20 μ L to 100 μ L and still treated with sonication (sample 2 and 3), the average diameter of capsules also increased but the capsules had similar shell thickness and surface morphology. By the using of the same amount of PEOS instead of TEOS (sample 4), smaller capsules were obtained and they showed a totally different surface morphology. Instead of smooth surface, sample 4 provided shell surface with many wrinkles. Additionally, the yield of silica capsules with PEOS as precursor was significantly lower than that of the other 3 samples, where TEOS was applied as precursor.

In summary, different emulsification method can influence the size of the capsules and the thickness of the shell. By changing the amount of precursor the size of the capsules changes correspondently. Different precursor can also affect the size as well as the morphology of the capsules.

4 Silicatein-silica hybrid capsules

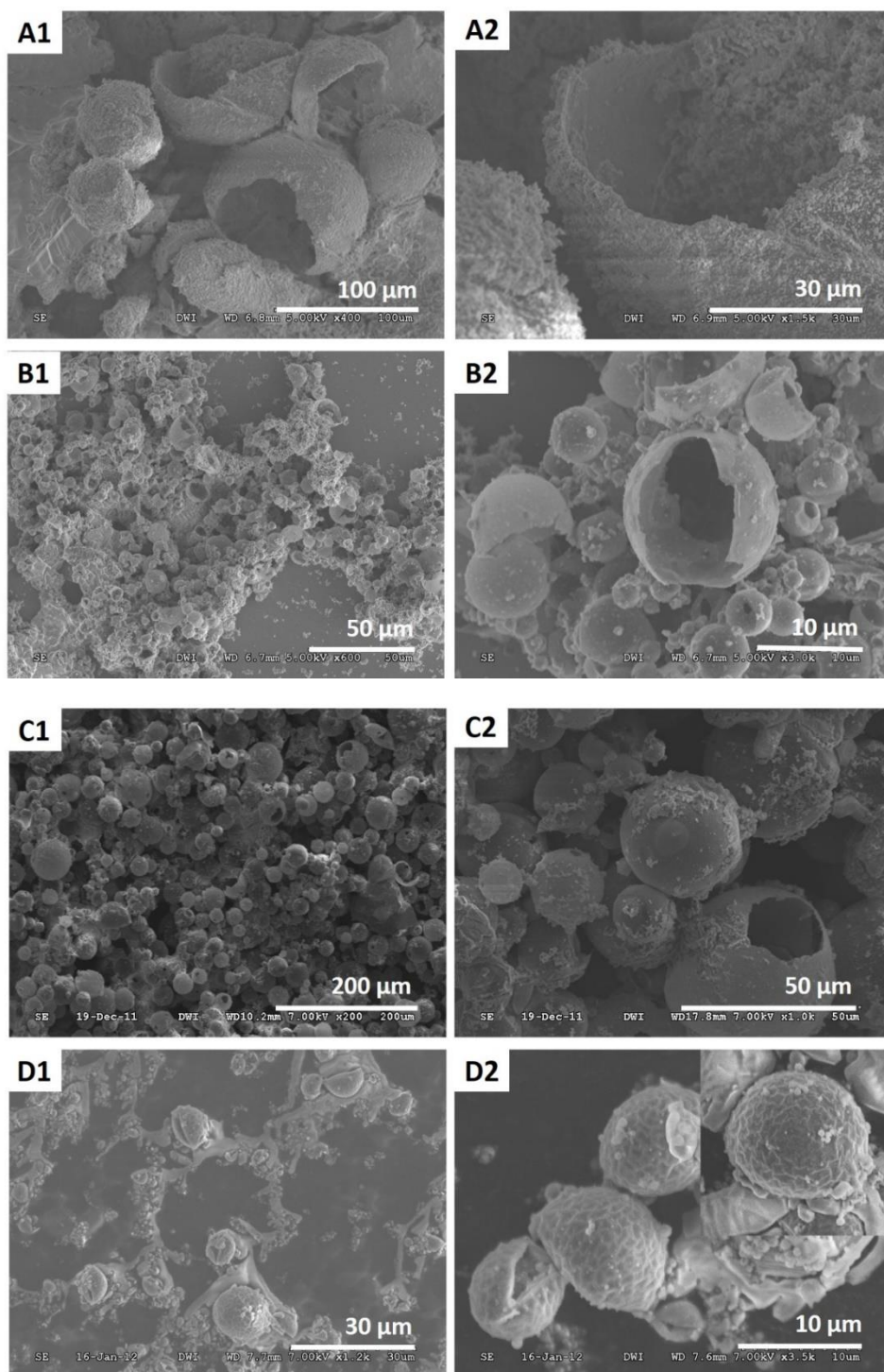


Fig. 4.7: SEM images of capsules prepared with recombinant silicatein and (A) 20 μL TEOS and vortex; (B) 20 μL TEOS and sonication; (C) 100 μL TEOS and sonication; (D) 100 μL PEOS and sonication.

5 PNIPAAm-silica hybrid capsules

In Chapter 1 PNIPAAm microgels were introduced as potential analogue of catalyst for silicification. This section will discuss how PNIPAAm microgels provide Pickering emulsion templates and work at interface as catalyst for the synthesis of silica capsules.

5.1 PNIPAAm microgels as effective catalyst and template for the synthesis of silica capsules

The dispersion polymerization of *N*-isopropylacrylamides was performed by Dr. Andreea Balaceanu. 2,2'-azobis(2-methylpropionamidine)dihydrochloride was used as initiator and *N,N'*-methylenebisacrylamide as cross-linker.^[38] The PNIPAAm microgels were received as dispersion in deionized water (8 mg/mL, pH 7). PVCL (poly(*N*-vinylcaprolactam)) microgels (8.5 mg/mL, pH 7) were applied as reference, in which amide groups are replaced with lactam groups. The chemical structures of PNIPAm and PVCL are shown in Fig. 5.1. Due to the steric hindrance, PVCL is probably not catalytic active towards silicification.

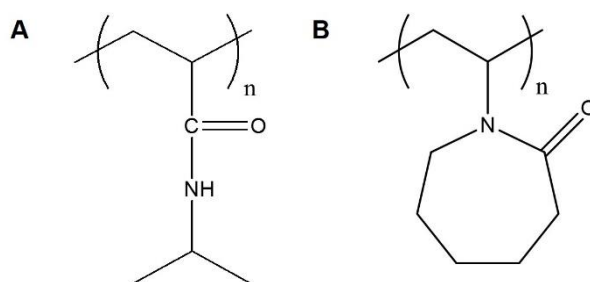


Fig. 5.1: Chemical structure of (A) PNIPAAm and (B) PVCL.

Dynamic interfacial tensions at the interface between TEOS and two microgel-dispersions were measured with pendant drop methods. Both microgels are interfacially active and their IFTs are comparable with lysozyme glycine solution (Fig. 5.2).

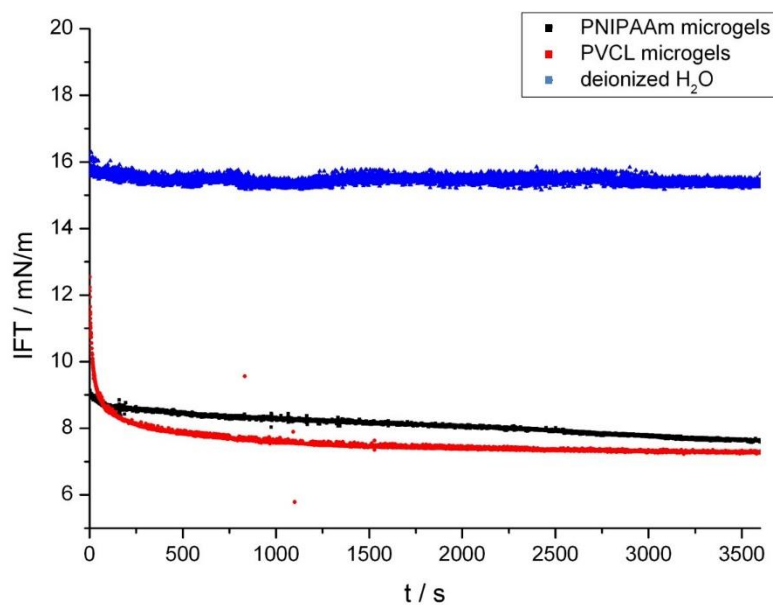


Fig. 5.2: Dynamic interfacial tension measurements of interface between PNIPAAm microgels and TEOS, PVCL microgels and TEOS, deionized H₂O and TEOS.

5 PNIPAAm-silica hybrid capsules

After the measurements of interfacial tensions, PNIPAAm and PVCL microgels were employed for the Pickering emulsion templated synthesis of silica capsules. Vortex and ultrasonic bath were applied as emulsification methods. The results are summarized in Tab. 5.1.

With PVCL there was no silica precipitate observed regardless of emulsification method, which confirms the assumption that PVCL has no catalytic activity for silicification. In contrast, the synthesis of silica capsules with PNIPAAm microgels was successful. However, vortex does not seem like an ideal emulsification method, which only led to a few strongly deformed capsules with large size. (Fig. 5.3A) In the sample treated with sonication, hollow spheres with a diameter about 1~5 μm were observed. (Fig. 5.3B)

Tab. 5.1: Samples prepared with PNIPAAm and PVCL.

Sample	Emulsification	Result
PNIPAAm 900 μL + TEOS 100 μL	vortex	Deformed silica capsules with large size (30~50 μm)
PNIPAAm 900 μL + TEOS 100 μL	ultrasonic bath	Silica capsules (1~5 μm)
PVCL 900 μL + TEOS 100 μL	vortex	No silica
PVCL 900 μL + TEOS 100 μL	ultrasonic bath	No silica

*PNIPAAm dispersion: 8 mg/mL, pH 7; PVCL dispersion 8.5 mg/mL, pH 7

*Emulsification time: 15 min

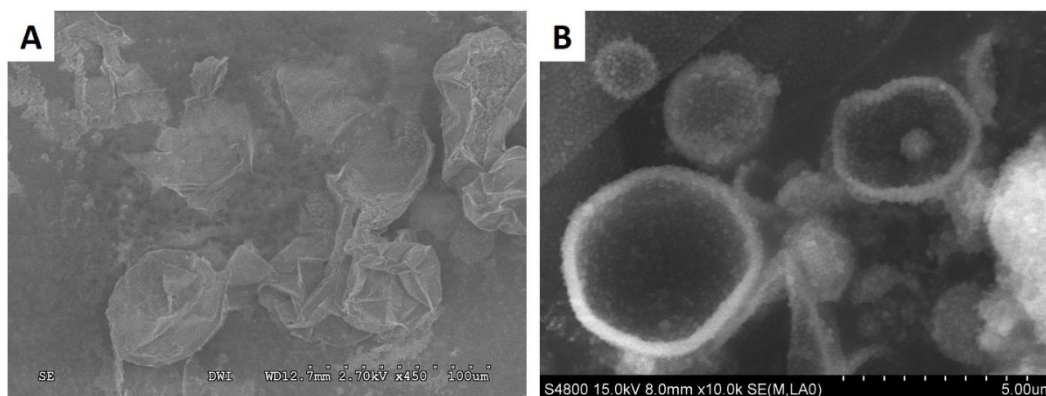


Fig. 5.3: SEM images of PNIPAAm-silica capsules prepared with (A) vortex and (B) sonication.

Fig. 5.4 shows the EDX analysis of the PNIPAAm-silica capsules treated with sonication. A is an SEM image showing the area where EDX measurements were performed, C is the corresponding EDX spectrum. The presences of Si and O signals

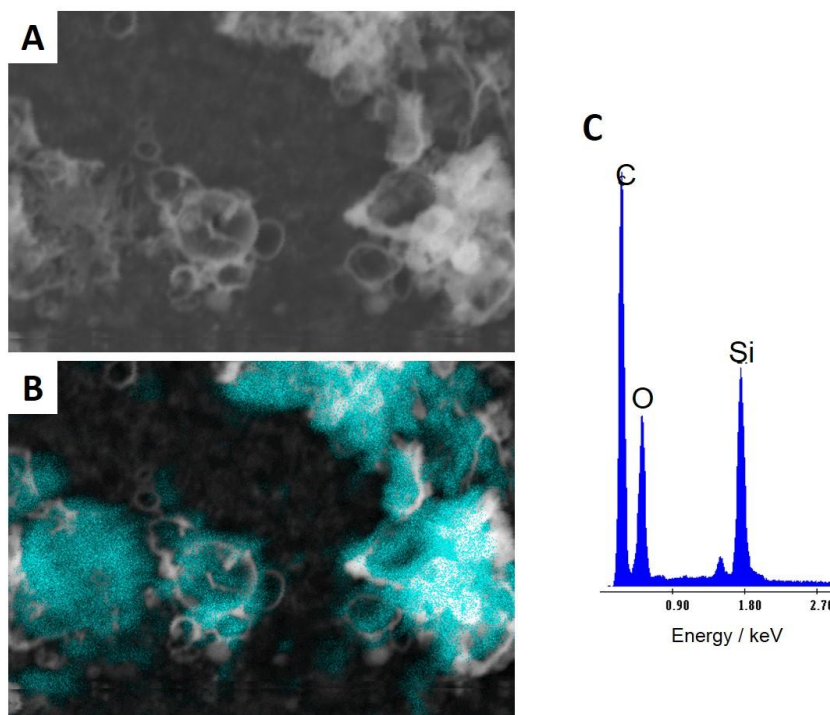


Fig. 5.4: EDX analysis of PNIPAAm-silica hybrid capsules. (A) SEM image for the sample area where EDX was performed, (B) mapping of Si (in blue) in the same area, (C) corresponding EDX spectrum of (A).

prove that PNIPAAm can catalyse silica formation. B is an EDX-mapping measurement for the same area, which demonstrates the distribution of silicon with blue points and indicates the uniform distribution of silicon dioxide in the hybrid capsules.

The TGA analysis about the composition of two samples prepared with vortex and sonication reveals that different emulsification methods have no obvious influence on the composition of the hybrid structure. The degradation curves of both samples and the compositions of the hybrid structures based on TGA measurements are presented in Fig. 5.5 and Tab.5.2. The first degradation in TGA measurements belongs to H₂O, the second degradation represent PNIPAAm and the mass remaining at 800 °C is from SiO₂ and few residue of PNIPAAm after thermal decomposition.

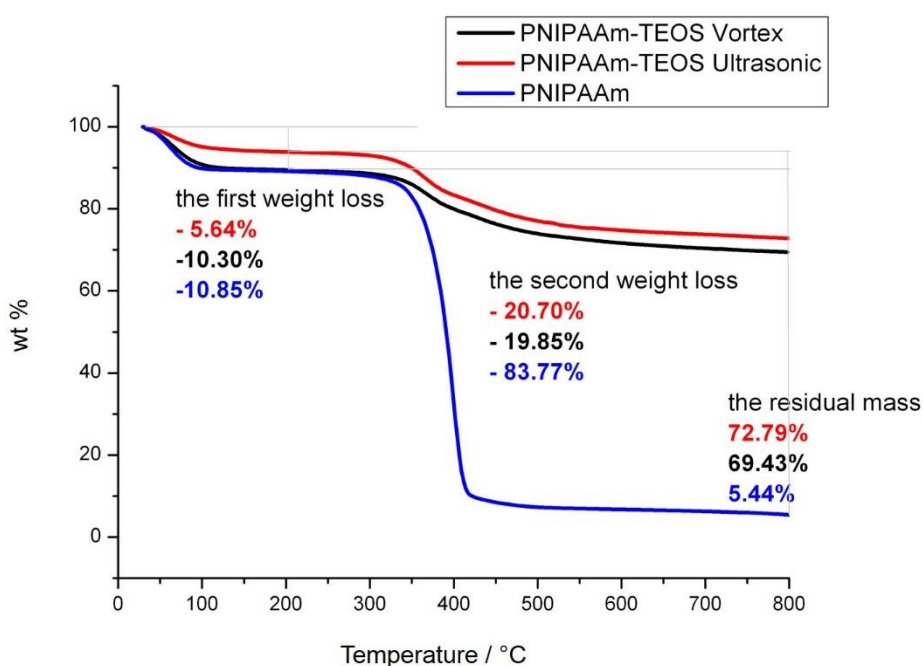


Fig. 5.5: TGA measurements of PNIPAAm-silica hybrid prepared with vortex and sonication.

5 PNIPAAm-silica hybrid capsules

Tab. 5.2: Composition of PNIPAAm-Silica hybrid structures.

Emulsification	PNIPAAm (wt %)	SiO ₂ (wt %)*	PNIPAAm/SiO ₂
Vortex	19.85	68.24	0.29
Sonication	20.70	68.19	0.30

*The part of the PNIPAAm residue at 800 °C is excluded.

A further SEM investigation of the PNIPAAm-silica capsules reveals a hexagonal arrangement of PNIPAAm microgels particles on the capsule shell. Fig. 5.6B shows a close up of the shell structure. This observation corresponds to the interfacial behaviour of PNIPAAm microgel particles in emulsions. (Chapter 1, Section 1.2.3) It also confirms that Pickering emulsions emulsified by PNIPAAm particles are very stable and the reaction at the interface has less influence on the closed array.

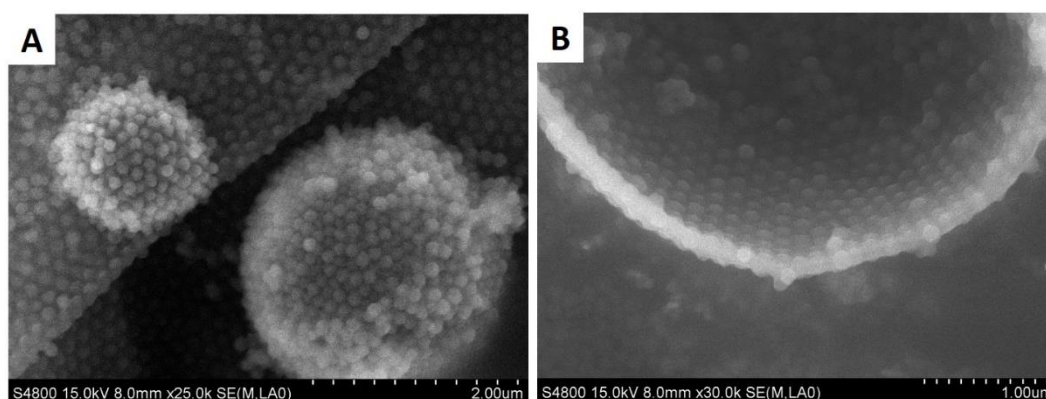


Fig. 5.6: (A) Hexagonal arrangement of PNIPAAm microgels on the capsule shell, (B) a close-up view of the capsules shell, which represents the interface in the emulsion.

5.2 Synthesis of silica capsules with PNIPAAm microgels

Although PNIPAAm microgels proved to be effective catalysts for the Pickering-emulsion templated synthesis of silica capsules, the yield of the reaction is not as good as with lysozyme and silicatein. Both enzymes provided capsules in large amount and few clusters. However, in the PNIPAAm sample, bulk materials as well as capsules were observed. Furthermore sample made with PNIPAAm microgels required repeating purification steps, otherwise the capsules were buried under the excess microgels and almost invisible with SEM. Probably the concentration of the dispersion 8 mg/mL is too high and should be decreased. To circumvent that problem, 1/2, 1/5, 1/10, 1/20, 1/50 and 1/100 dilutions were prepared from the original PNIPAAm microgel dispersion with the concentration c_0 of 8 mg/mL

Fig. 5.7 illustrates the interfacial tensions at the interface between TEOS and PNIPAAms dispersion with different concentrations. While the 1/10 dilution shows nearly no influence on the IFT, the 1/100 dilution increases the IFT slightly.

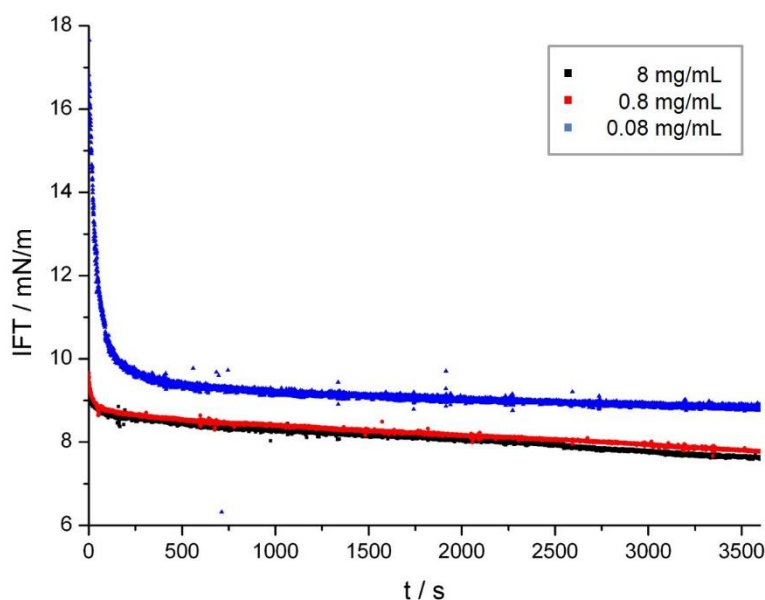


Fig. 5.7: IFT between TEOS and PNIPAAm microgel dispersion with different concentration.

5 PNIPAAm-silica hybrid capsules

Subsequently, samples with 900 μL diluted PNIPAAm dispersion and 100 μL TEOS were prepared. 15 min sonication was applied for each sample. Fig. show the samples after a reaction time of 24 hours. Obviously, the samples with higher concentration are more turbid than the ones with lower concentration, which indicates that more silica is formed with a high concentration of PNIPAAm. (Fig. 5.8) With low concentration $c_0/10$, $c_0/20$, $c_0/50$ and $c_0/100$ silica could be isolated only in very small amount and capsules could hardly be observed under SEM.

With $c_0/2$ and $c_0/5$, however, a high yield of silica capsules were obtained. (Fig. 5.9) Again, the hexagonal arrangement of the microgels on the shell can be observed in these samples.

$c_0/2$ and $c_0/5$ seem to be the proper concentration for the synthesis of silica capsules *via* Pickering emulsions, providing a large amount of capsules. If $c \leq c_0/10$, there are not sufficient PNIPAAm microgels to catalyse the condensation of TEOS and/or to stabilize the emulsion, therefore the yields were very low with the concentration $c_0/10$, $c_0/20$, $c_0/50$ and $c_0/100$.

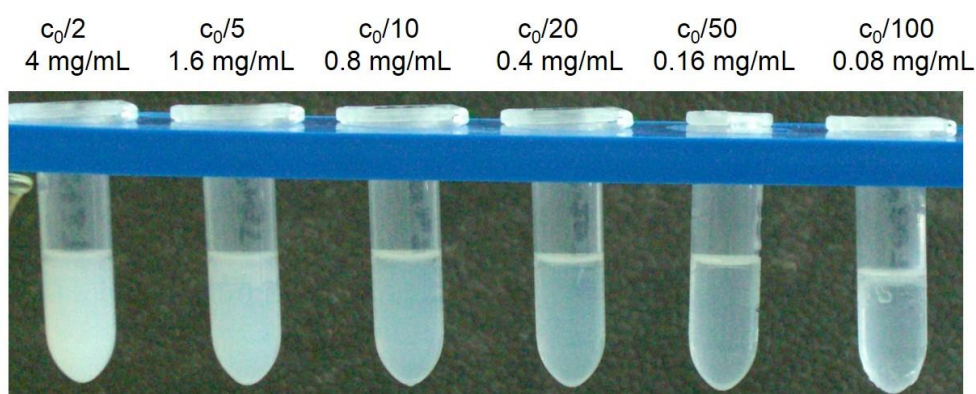


Fig. 5.8: TEOS reacted with dilute PNIPAAm dispersion for 1 day. ($c_0=8$ mg/mL)

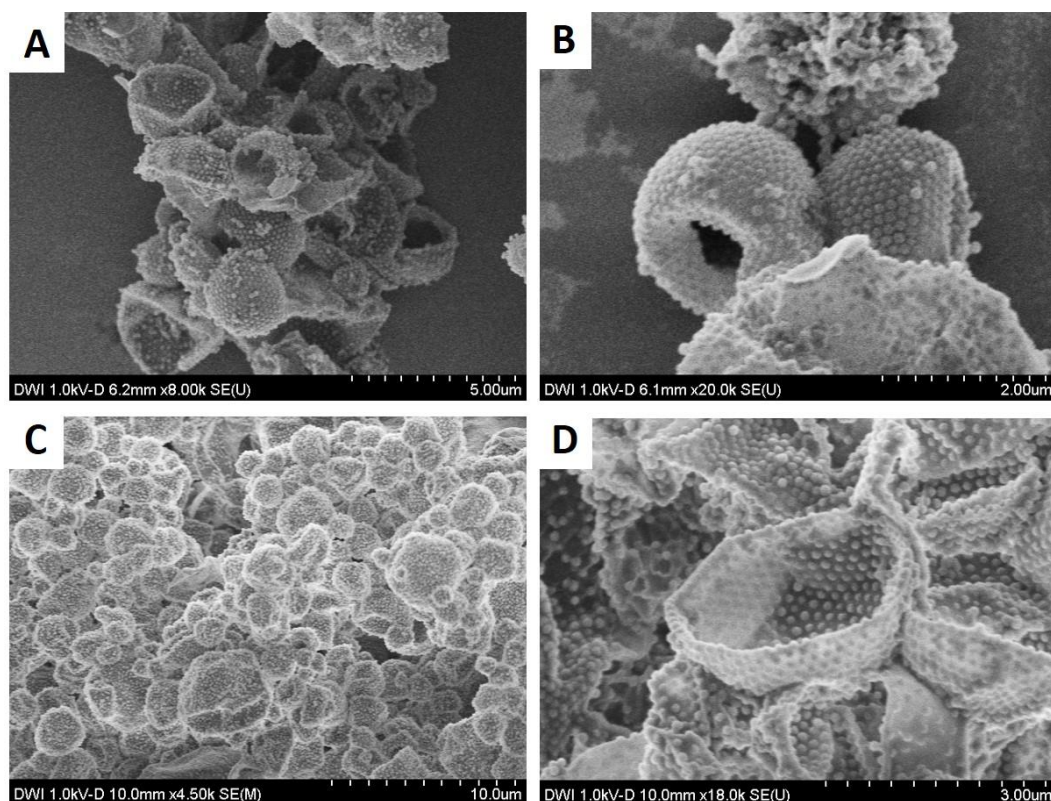


Fig. 5.9: SEM images of PNIPAAm-silica hybrid capsules prepared with PNIPAAm dispersion with different concentrations: (A) (B) $c_0/2$ and (C) (D) $c_0/5$ ($c_0=8$ mg/mL).

5.3 Thermal treatment of PNIPAAm-silica capsules

In the chapter 3 about lysozyme-silica capsules, the change of surface morphology after TGA measurements (Fig. 3.8), because of protein removal at high temperature was described. The TGA measurements also show that pure PNIPAAm microgels start to decompose at about 350 °C and above 450 °C the decomposition is almost done (Fig. 3.3). Combining the TGA result with the interfacial behaviour of PNIPAAm microgels, namely dense hexagonal array of microgels on the shell, it could be expected that TGA or a similar heating process would lead to a cage-like hollow sphere with arranged and uniform pores. However, after heating to 800 °C, no

5 PNIPAAm-silica hybrid capsules

cage-like structure was obtained (Fig. 5.10). The possible explanation is that TEOS condensed in the space between microgel particles as well as on the surface of microgels to form a very thin silica layer which prevents the formation of a porous structure. Furthermore, the capsule form seems not stable enough at high temperature because few capsules and more bulk material were observed after heating.

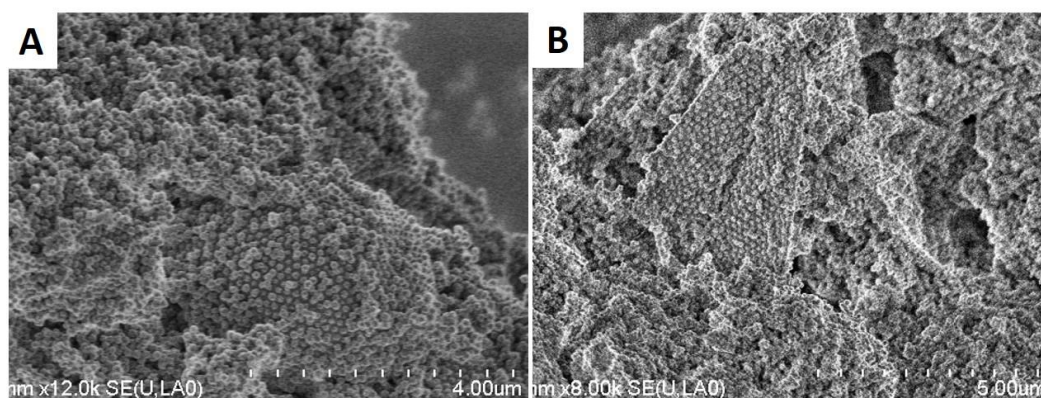


Fig. 5.10: SEM images of PNIPAAm-silica hybrid structures after heating at 800 °C.

6 Immobilized lysozyme within microgel matrix for the synthesis of silica capsules

Enzymes are very sensitive to their environment and they can easily lose their activity by changing of polarity of the solution, temperature or pH value. Therefore the immobilization of enzymes in an active conformation is of considerable interest for an improved performance, namely solubility, stability and recyclability of enzymes.^[96]
[97] [98]

The features of carrier materials (size, surface area, permeability, hydrophilicity/hydrophobicity, mechanical stability and functional groups etc.) have strong influence on the performance of enzymes and they can be divided into two classes: inorganic and organic carriers.^[96] Inorganic carriers, for example glass, silica gel, bentonite, titania, often show high physical and chemical stability. However, organic carriers are more often applied for the industrial processes as their physical and chemical characters can be easily adapted to the requirements of enzymatic process.^[96] [97] [99]
The organic carriers consist of natural polymers and synthetic polymers.^[100] Microgels as synthetic polymer networks show various advantages for immobilization of enzymes. Their porous structure is beneficial for a high enzyme loading and their pore distribution can be controlled with cross link density. They are stable in aqueous media, which is also advantageous for the immobilization of enzymes since most enzymes are hydrophilic. Furthermore, the self-assembly of microgels at interfaces extends the application of immobilized enzymes in biphasic reactions.^[39] [98]

6 Immobilized lysozyme in microgel matrix for the synthesis of silica capsules

The methods of immobilization of enzymes can be classified with irreversible (covalent binding, entrapment or encapsulation, cross linking etc.) and reversible (physical absorption like hydrogen bonding, van der Waals forces, electrostatic or hydrophobic forces) attachments.^[101] The reversible immobilization of enzymes *via* physical adsorption attracts many interests because the attachment does not change the conformation of enzymes strongly and hence their enzymatic activities are not reduced after immobilization.^{[102] [103]} By changing conditions (*e.g.* pH, temperature or ionic strength), the immobilized enzymes can be easily released from the carriers.^[97]
[98]

This chapter describes experiments performed in cooperation with the research group of Prof. Pich. The immobilized lysozyme in microgel (Fig. 6.1) was provided by Andrea Götz. The enzymatic activity of lysozyme after loading should be investigated *via* application for the synthesis of silica capsules.

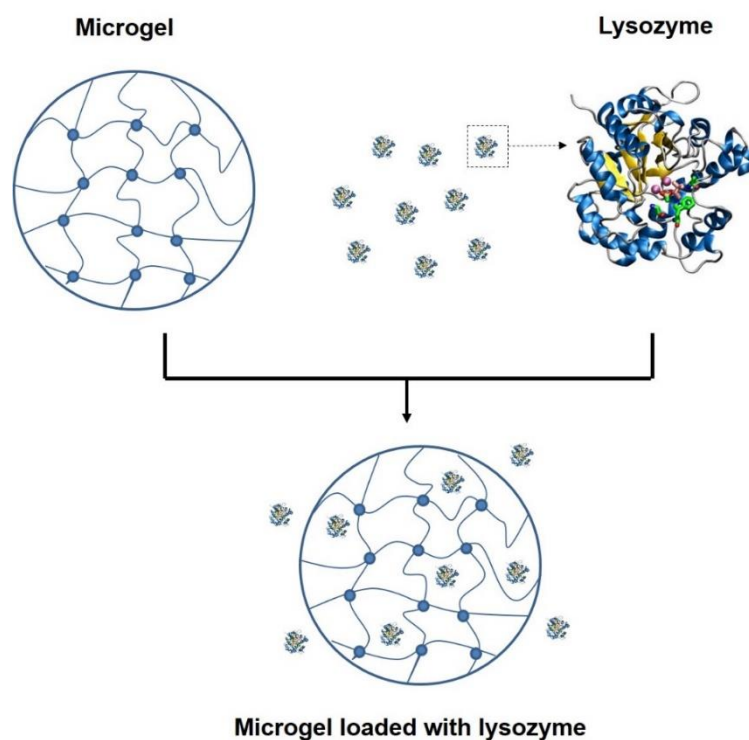


Fig. 6.1: Schematic representation of the immobilization of lysozyme in a microgel matrix.

6 Immobilized lysozyme in microgel matrix for the synthesis of silica capsules

The carrier material, poly(*N*-vinylcaprolactam-*co*-2-methoxyethylacrylat-*co*-acrylic acid) microgels (PVCL/MEA/AA), consisting mainly of the monomer *N*-vinylcaprolactam (VCL) and two comonomers 2-methoxyethylacrylat (MEA) and acrylic acid (AA), was synthesized by a radical polymerization, in which 2,2'-azobis[*N*-(2-carboxyethyl)-2-methylpropionamide] (ACMA) was applied as initiator and *N,N'*-methylenebisacrylamid (BIS) as cross linker (Fig. 6.2). As acrylic acid exhibits a pK_s value of 4.25, when $pH > 4.25$ acrylic acid is deprotonated and hence negatively charged. The isoelectric point of lysozyme is at pH 11.35, lysozyme is positively charged when $pH < 11.35$. Therefore over a broad pH range 4.24~11.35, acrylic acid and lysozyme attract each other. The electrostatic interaction will be used here as the force for the immobilization of lysozyme in the microgel matrix.

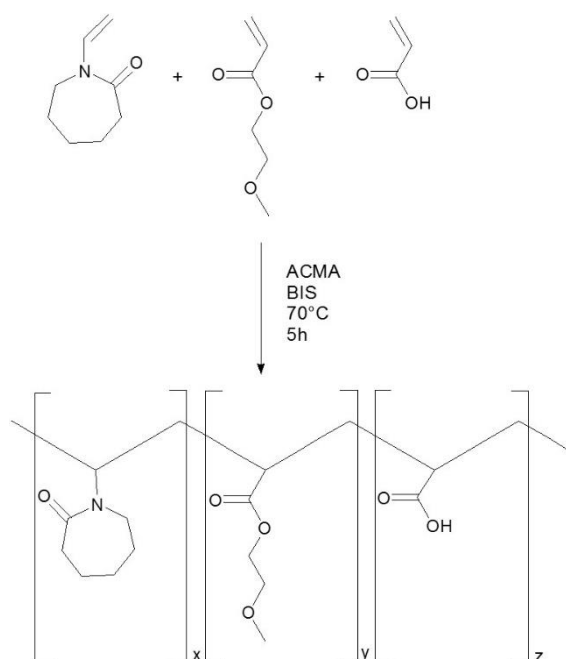


Fig. 6.2: Synthesis of PVCL/MEA/AA microgels *via* radical polymerisation.* (VCL: *N*-vinylcaprolactam, MEA: 2-Methoxyethylacrylat, AA: Acryl acid, ACMA: 2,2'-azobis[*N*-(2-carboxyethyl)-2-methylpropionamide], BIS: *N,N'*-methylenebisacrylamid)

*The synthesis of PVCL/MEA/AA and the immobilization of lysozyme was performed by Andrea Götz.

6.1 Immobilization of lysozyme in PVCL/MEA/AA microgels

Six different microgel-dispersions (in Na₃PO₄ buffer) were provided for the reaction with TEOS (Tab. 6.1). Sample 1, 2 and 3 are microgels without lysozyme at pH 6.7, 8.5 and 9.0 separately (lysozyme is active between pH 6.0 and 9.0).^[104] Sample 1a, 2a and 3a are corresponding microgels loaded with lysozyme. Due to the different concentration of microgel-dispersions and the different loading capacity of microgels at different pH value, the lysozyme concentration varied slightly around 3 mg/mL.

Tab. 6.1: Pure carriers and immobilized lysozyme in the carrier materials at three different pH.

Sample (in Na₃PO₄ buffer)	
1	PVCL/MEA/AA 80:20:4.2 mol % 13.3 mg/mL pH 6.7
1a	PVCL/MEA/AA 80:20:4.2 mol % loaded with lysozyme 3.1 mg/mL pH 6.7
2	PVCL/MEA/AA 80:20:4.2 mol % 10.8 mg/mL pH 8.5
2a	PVCL/MEA/AA 80:20:4.2 mol % loaded with lysozyme 2.8 mg/mL pH 8.5
3	PVCL/MEA/AA 80:20:4.2 mol % 12.7 mg/mL pH 9.0
3a	PVCL/MEA/AA 80:20:4.2 mol % loaded with lysozyme 3.3 mg/mL pH 9.0

Since the immobilization of lysozyme in microgels is mainly based on electrostatic interactions, the zeta-potential of the dispersion should change upon loading. Tab. 6.2 summarizes the zeta-potential of all the dispersions measured at room temperature. Without lysozyme the three dispersions were negatively charged and the charge rose with increasing pH value. After loading with lysozyme, they were still negatively charged but their charge declined significantly. As lysozyme is positively charged when pH<11.35,^[85] the positively charged lysozyme would be absorbed to negatively

6 Immobilized lysozyme in microgel matrix for the synthesis of silica capsules

charged PVCL/MEA/AA microgels, which is the reason for the change of zeta-potential. The immobilization of lysozyme in microgels is therefore successful.

Tab. 6.2: Zeta potential before and after immobilization of lysozyme.

Sample (in Na₃PO₄ buffer)	Zeta-potential (at 25 °C) / mV
1 PVCL/MEA/AA pH 6.7	-21.4
1a PVCL/MEA/AA loaded with lysozyme pH 6.7	-7.04
2 PVCL/MEA/AA pH 8.5	-24.1
2a PVCL/MEA/AA loaded with lysozyme pH 8.5	-8.97
3 PVCL/MEA/AA pH 9.0	-29.5
3a PVCL/MEA/AA loaded with lysozyme pH 9.0	-11.9

6.2 Immobilized lysozyme in PVCL/MEA/AA as effective catalysts and templates for the synthesis of silica capsules

The dynamic interfacial tension at the interface between PVCL/MEA/AA dispersion and TEOS, PVCL/MEA/AA+lysozyme dispersion and TEOS, and pure lysozyme solution and TEOS were measured with pendant drop tensiometry (Fig. 6.3). The PVCL/MEA/AA microgels with three different pH values exhibit better interfacial activity at the H₂O/TEOS interface than pure lysozyme. The results of immobilized lysozyme in PVCL/MEA/AA lay between pure microgels and pure lysozyme. Therefore their interfacial activity is sufficient to serve as the emulsifiers.

6 Immobilized lysozyme in microgel matrix for the synthesis of silica capsules

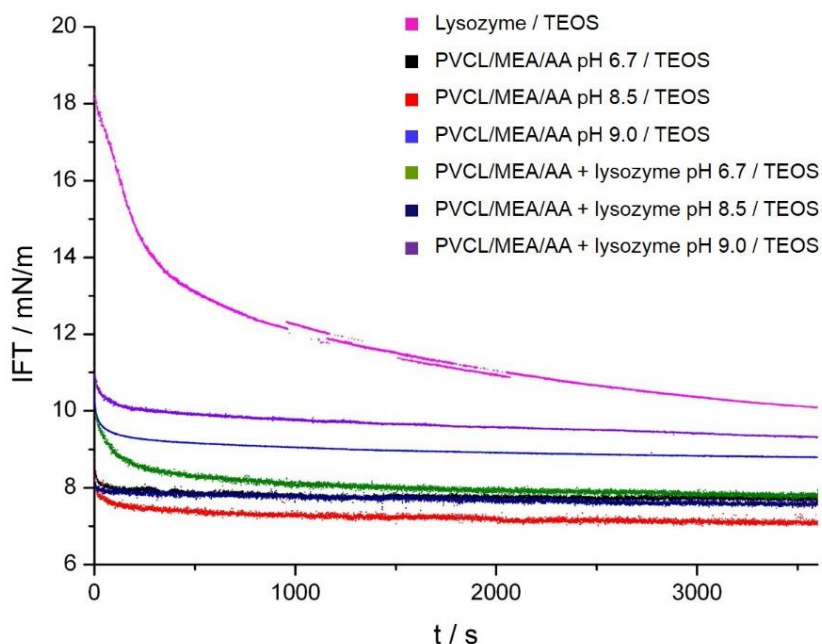


Fig. 6.3: Dynamic interfacial tension measurements of PVCL/MEA/AA microgels without and with lysozyme at the interface between H₂O and TEOS.

Conventionally 900 μ L microgel-dispersion and 100 μ L TEOS were mixed together and 15 min sonication was applied. Emulsification with vortex was not applied here since vortex is not the best agitation for the hollow sphere structure. As expected, PVCL/MEA/AA microgels alone showed no catalytic activity towards TEOS because no precipitate could be isolated after reaction. Lysozyme remained active after immobilizing in PVCL/MEA/AA matrix at all three pH values. IR spectra compare the pure silica, silica formed from TEOS in the presence of pure lysozyme and the product isolated from the reaction of immobilized lysozyme with TEOS (Fig. 6.4). It is very obvious that the immobilized lysozyme is catalytic active for silicification. However, only at pH 9.0 capsules were formed besides bulk material (Tab. 6.3, Fig. 6.5). It seems that at pH 6.7 and 8.5 silicification occurred directly on every single microgel particle to form cluster. The reason that no capsules were observed in these two samples remains unclear.

6 Immobilized lysozyme in microgel matrix for the synthesis of silica capsules

Tab. 6.3: Results of pure carriers and immobilized lysozyme after incubation with TEOS.

Sample	Result
PVCL/MEA/AA 900 μ L + TEOS 100 μ L pH 6.7	No silica
PVCL/MEA/AA loaded with lysozyme 900 μ L + TEOS 100 μ L pH 6.7	Silica cluster no capsules
PVCL/MEA/AA 900 μ L + TEOS 100 μ L pH 8.5	No silica
PVCL/MEA/AA loaded with lysozyme 900 μ L + TEOS 100 μ L pH 8.5	Silica cluster no capsules
PVCL/MEA/AA 900 μ L + TEOS 100 μ L pH 9.0	No silica
PVCL/MEA/AA loaded with lysozyme 900 μ L + TEOS 100 μ L pH 9.0	Silica cluster and capsules

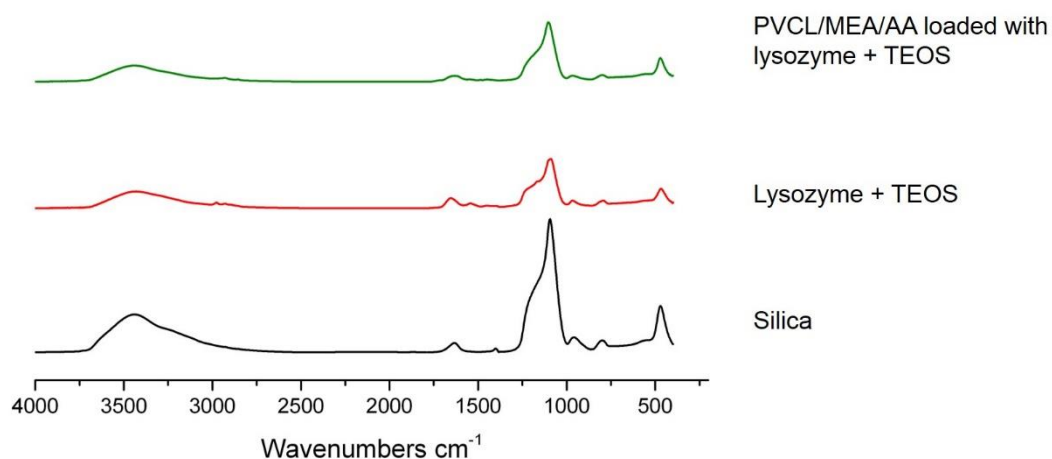


Fig. 6.4: IR spectra of pure silica, precipitate isolated from the reaction of pure lysozyme with TEOS and immobilized lysozyme with TEOS.

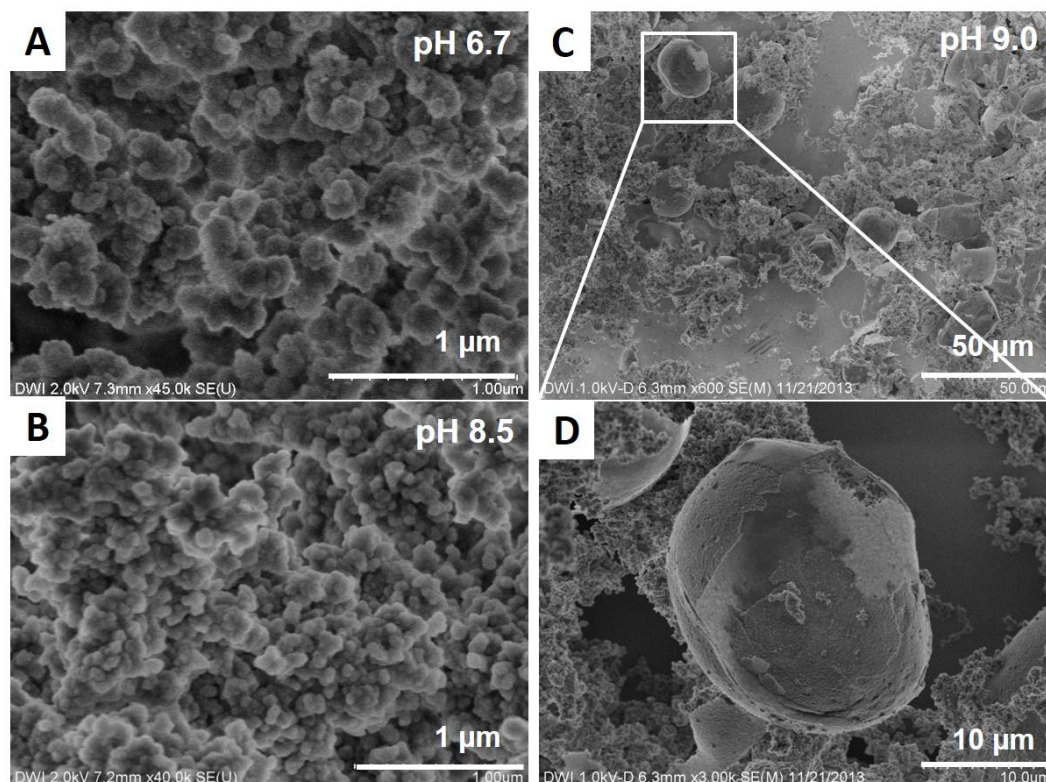


Fig. 6.5: SEM images of immobilized lysozyme in PVCL/MEA/AA-silica hybrid structure A) at pH 6.7, B) at pH 8.5, C) at pH 9.0 and D) close-up image of a capsule at pH 9.0.

6.3 PNIPAAm vs. PVCL/MEA/AA-lysozyme

Through the immobilization of lysozyme, active sites were introduced into PVCL/MEA/AA microgels, which are naturally inactive towards silicification. However, the capsules synthesized with those PVCL/MEA/AA-lysozyme microgels show different features from the capsules obtained with PNIPAAm microgels (Fig. 6.6).

6 Immobilized lysozyme in microgel matrix for the synthesis of silica capsules

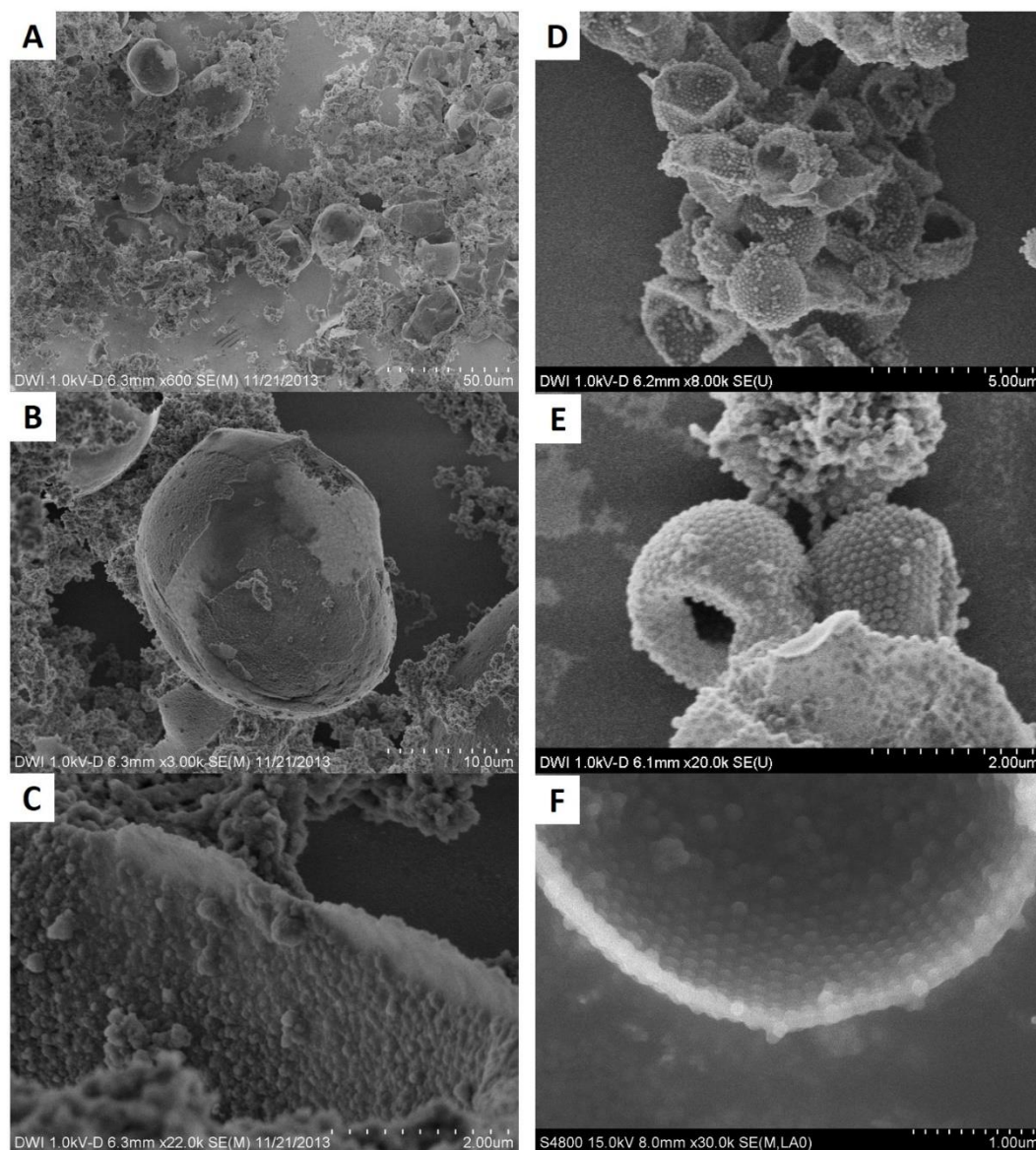


Fig. 6.6: Comparison between capsules synthesized with (A) (B) (C) PVCL/MEA/AA-lysozyme (D) (E) (F) PNIPAAm microgels.

Firstly, the capsules have different sizes. The ones with PVCL/MEA/AA-lysozyme have a diameter about 20~30 μm and the ones with PNIPAAm are much smaller with a diameter about 2~3 μm . It can probably be caused by the difference in the microgel

6 Immobilized lysozyme in microgel matrix for the synthesis of silica capsules

diameter. PNIPAAm microgels have a hydrodynamic radius of ~130 nm at 25 °C and PVCL/MEA/AA are much bigger with a radius of ~550 nm.

Secondly, the capsules have different surface morphologies. The closed hexagonal packing of microgel particles is absent on the capsule shell in the PVCL/MEA/AA-lysozyme sample. The loading of lysozyme changes the size of the microgels and the loading process in each single microgel particle may not be identical. Therefore after immobilization the dispersity of microgels is increased considerably (PDI of PVCL/MEA/AA=0.09, PDI of PVCL/MEA/AA+lysozyme=0.33, pH 9.0), thus a compact array of microgel particles on the interface is not achievable.

In addition, the locations of the catalytic center of PNIPAAm microgel and PVCL/MEA/AA-lysozyme may be different. The amide groups of PNIPAAm microgel are on the polymer chains while the lysozyme molecules are immobilized into the PVCL/MEA/AA network. As mentioned before, the immobilization of lysozyme molecules in each single microgel cannot be identical so that the mineralization reaction on each PVCL/MEA/AA microgel is also different. In the contrary, the active centers of PNIPAAm microgels are regularly distributed and the catalytic reaction procedure on each PNIPAAm microgel should be similar, which might also explain the better regularity of the PNIPAAm-silica hybrid capsules.

7 Enzymatic activity assay of lysozyme

7.1 Hydrolysis of bis(*p*-aminophenoxy)-dimethylsilane catalyzed by silicatein

The enzymes silicatein and lysozyme are used to catalyze the formation of silica capsules in the course of this thesis. However, the conditions during these catalysis reactions differ much from the natural environment of proteins. In this respect it is advantageous to have a proof of the activity of the enzymes under the conditions present during the biosilicification. Besides the enzymatic activity expressed in terms of the weight of condensed silica after the reaction with TEOS,^[105] another assay based on UV-Vis absorption was reported by Müller *et al.* Fig. 7.1 shows the hydrolysis of bis(*p*-aminophenoxy)-dimethylsilane catalyzed by silicatein.^[13] This process is similar to the TEOS hydrolysis, in which ethoxy groups are also hydrolyzed (Fig. 1.3).

7 Enzymatic activity assay of lysozyme and immobilized lysozyme

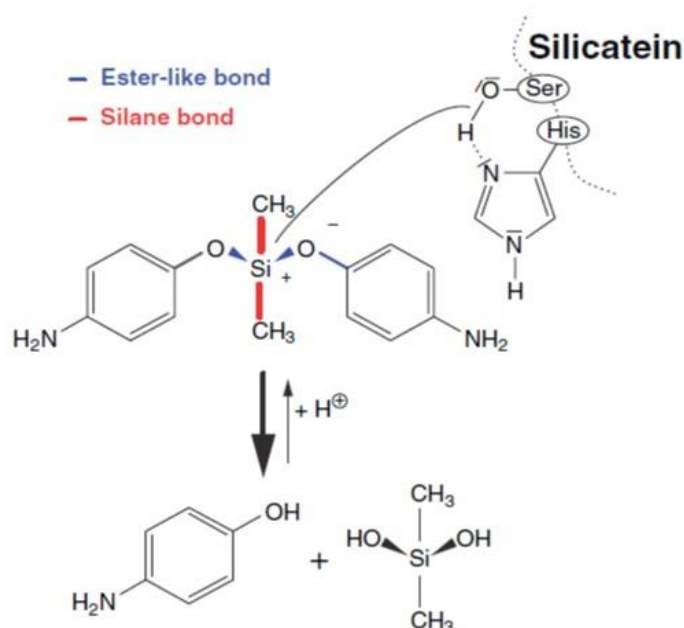


Fig. 7.1: Proposed hydrolysis mechanism of bis(*p*-aminophenoxy)-dimethylsilane catalyzed by Ser/His active site of silicatein. In the catalytic center of silicatein, the serine oxygen proceeds a nucleophilic attack on the silicon atom of the substrate, resulting in release of *p*-aminophenol and formation of an (alkoxy)-monosilane. This reaction is facilitated by hydrogen bonding between the imidazole nitrogen of the conserved histidine and the hydroxyl of the serine. Reprinted with permission from reference ^[13]. Copyright 2008 John Wiley & Sons, Inc.

The advantage of this reaction is that the concentration of the product *p*-aminophenol can be measured by UV-Vis spectroscopy, which exhibits two absorptions with maxima at 230 and 300 nm respectively. Fig. 7.2 represents the increase of absorbance through the formed *p*-aminophenol during the reaction. Since lysozyme has a similar catalytic center compared to silicatein, it is expected that this assay could also be operated with lysozyme.

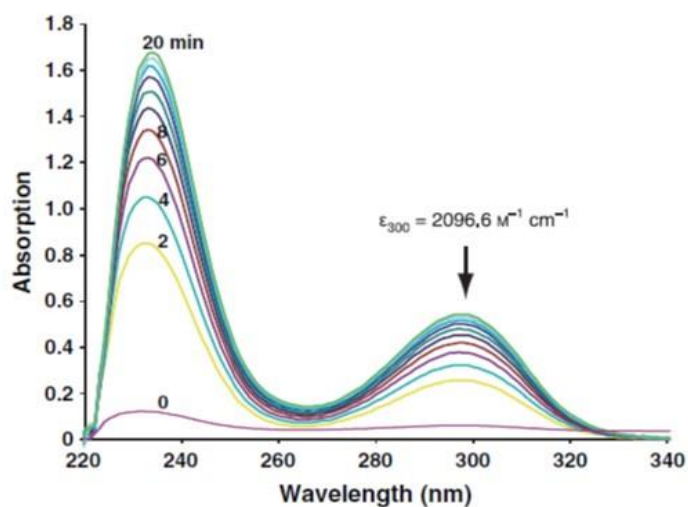


Fig. 7.2: Change of absorption spectra during incubation of silicatein in the presence of 140 μM bis(*p*-aminophenoxy)-dimethylsilane. At time zero, the absorbance at $\lambda = 300$ nm is very low. The absorbance increases steadily during the subsequent 20 min of incubation. The molar absorption coefficient (ϵ) of *p*-aminophenol at 300 nm is indicated. Reprinted with permission from reference [13]. Copyright 2008 John Wiley & Sons, Inc.

7.2 Enzymatic activity assay of lysozyme by using bis(*p*-aminophenoxy)-dimethylsilane

The measurements were carried out with the phase transfer principle and adopted in the same way to be performed in the presence of lysozyme instead of silicatein which is shown in Fig. 7.3B. Bis(*p*-aminophenoxy)-dimethylsilane is not soluble in water but in diethyl ether, however, the enzyme and the *p*-aminophenol are water soluble. The reaction proceeded at the interface where the enzyme molecules from the aqueous phase were in contact with the reagent in the upper organic phase. The released product *p*-aminophenol diffused from the interface into the aqueous phase, because *p*-aminophenol is only slightly soluble in diethyl ether. The UV light went through the water phase and was absorbed only by *p*-aminophenol.

7 Enzymatic activity assay of lysozyme and immobilized lysozyme

1 mL of 1 mg/mL (5 mg/mL would be too high for a proper absorption intensity) lysozyme glycine solution (pH 9, blue phase in Fig. 7.3B) was added in a quartz cuvette first, then 300 μ L bis(*p*-aminophenoxy)-dimethylsilane (abbreviated as NH₂-silane) diethyl ether solution (yellow phase in Fig. 7.3B) were injected carefully into the cuvette to form a separated two-phase system. The absorption of the aqueous phase was measured with a UV-Vis spectrometer immediately after the addition of NH₂-silane. Between each measurement the sample was stirred gently with a magnetic stirrer for a homogeneous distribution of the product in the aqueous phase. A control sample without lysozyme was also analysed, whose spectra show nearly no absorption at 300 nm. (Fig. 7.3A) However, in the presence of lysozyme in buffer solution, a continuous increase of absorption at 300 nm was observed during the reaction (Fig. 7.3B).

Since the synthesis of silica capsules was performed *via* an emulsion-templated method, an assay with the same composition, namely 1 mL lysozyme glycine solution (1 mg/mL) and 300 μ L NH₂-silane diethyl ether solution, was shaken for 30 s to form an o/w emulsion. Then the whole sample was allowed to stand for 1 min so that the droplets could diffuse upwards, which ensured the UV-light was only absorbed by the release product NH₂-phenol in the aqueous phase (Fig. 7.3C). The other measurement conditions were the same as those for a two-phase system.

Instead of a steady increase of absorption, the sample showed strong absorption from the beginning of the measurement and the absorption intensity remained almost unchanged during the measurement time. An emulsion exhibits much more interface area than a separated two-phase system which is furthermore strengthened through the shaking of the sample. Therefore the overall reaction in the emulsion proceeded much faster than in a two-phase system and seems to be already finished after 1 min (Fig. 7.3C).

The plots of absorption maxima at 300 nm against reaction time show the different reaction procedures of a two-phase system and an emulsion system, (Fig. 7.4) which indicates that the interface area probably determines the reaction rate.

7 Enzymatic activity assay of lysozyme and immobilized lysozyme

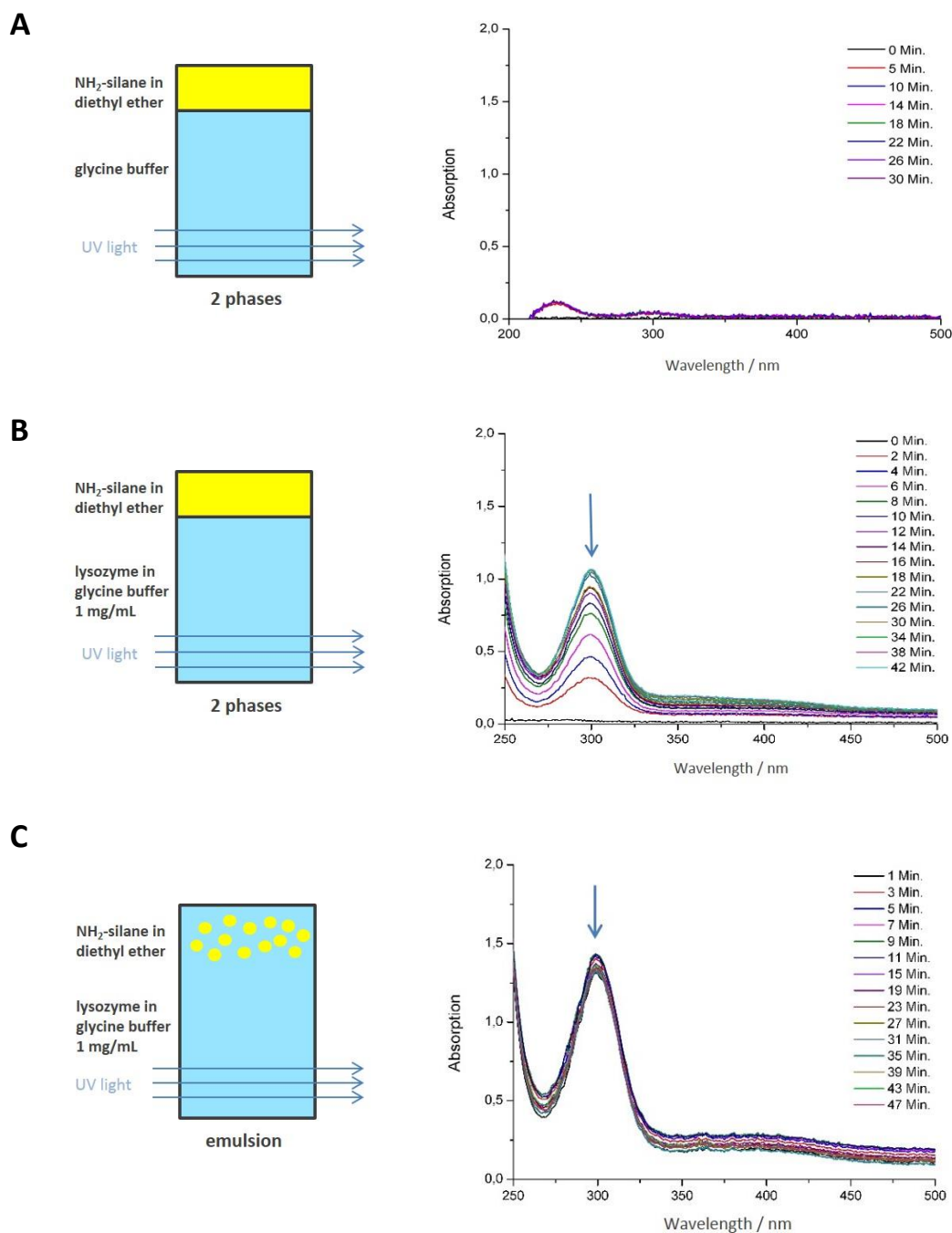


Fig. 7.3: UV-Vis measurements during incubation of lysozyme (in glycine buffer, pH 9) in the presence of bis(*p*-aminophenoxy)-dimethylsilane. (A) control sample without lysozyme in the two-phase system, (B) sample with lysozyme in the two-phase system, (C) sample with the same composition as B) but in an emulsion system.

7 Enzymatic activity assay of lysozyme and immobilized lysozyme

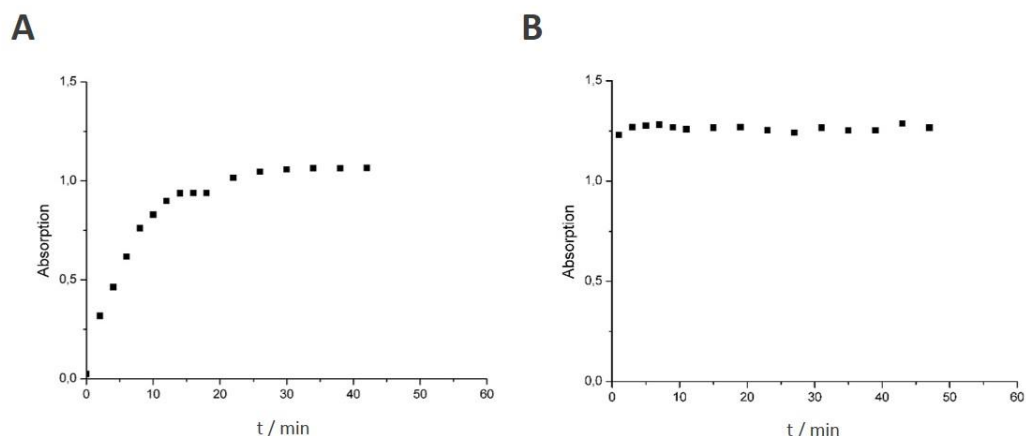


Fig. 7.4: Change of absorption at 300 nm during the incubation of lysozyme with bis(*p*-aminophenoxy)-dimethylsilane in (A) a two-phase system and (B) an emulsion.

Instead of glycine buffer, phosphate buffer at pH 9 was also used for the UV-Vis measurements in the two-phase system. The results reveal that the buffer has no significant influence on the reaction rate, compared to the sample in glycine buffer (Fig. 7.4A and Fig. 7.5B).

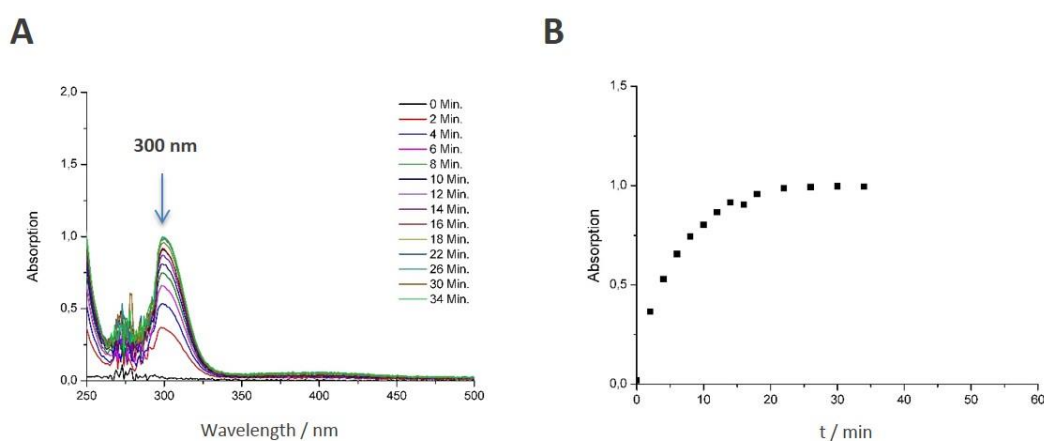


Fig. 7.5: (A) UV-Vis spectra of the hydrolysis of bis(*p*-aminophenoxy)-dimethylsilane in the presence of lysozyme by using phosphate buffer at pH 9. (B) Change of absorption at 300 nm during the reaction.

7.3 Enzymatic activity assay of immobilized lysozyme by using of bis(*p*-aminophenoxy)-dimethylsilane

The chapter 6 described the application of immobilized lysozyme for the synthesis of silica. To study the influence of immobilization process on enzymatic activity, this assay was also applied with lysozyme after the loading in PVCL/MEA/AA microgels.

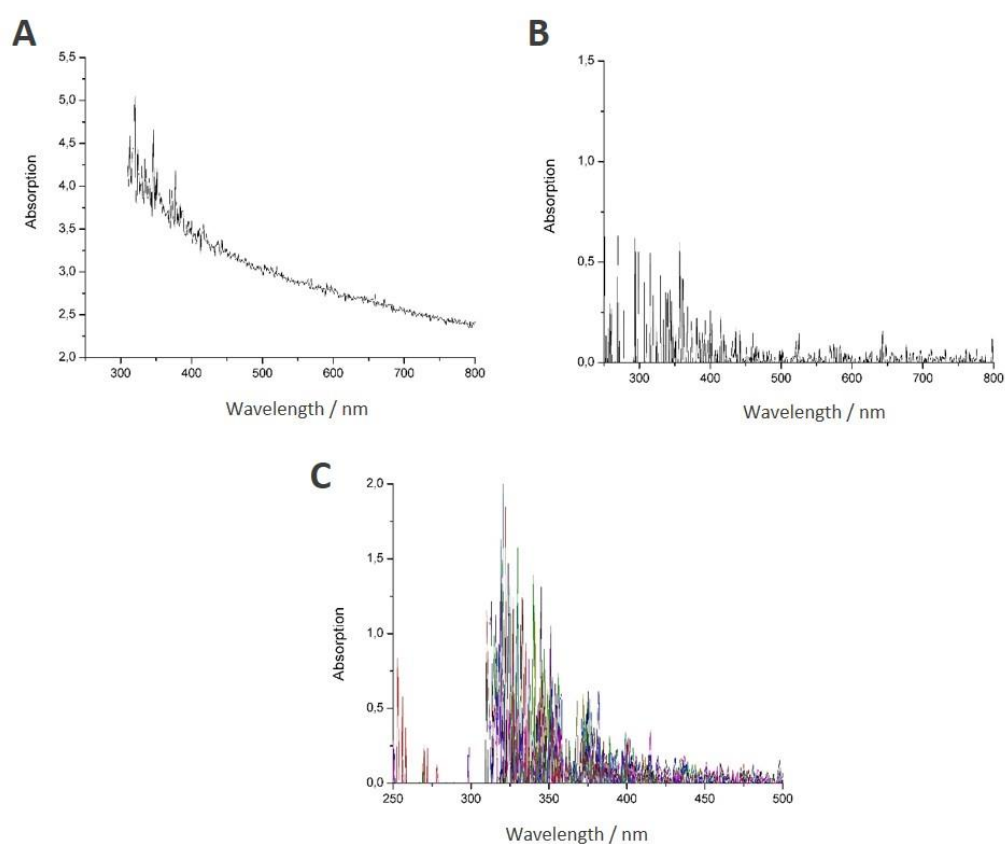


Fig. 7.6: UV-Vis spectra of (A) immobilized lysozyme in PVCL/MEA/AA microgel dispersion as background, (B) background after baseline correction, (C) hydrolysis of bis(*p*-aminophenoxy)-dimethylsilane in the presence of immobilized lysozyme in a two-phase system.

The sample composing of 1 mL of immobilized lysozyme (1 mg/mL) in PVCL/MEA/AA dispersion solution and 300 μ L NH_2 -silane diethyl ether solution

was measured in a two-phase system. However, due to the colloidal features of microgels, the incoming light was scattered strongly. Fig. 7.6A is the background spectrum from immobilized lysozyme in microgel dispersion. The high background noise around -300 nm could not be reduced by performing a baseline correction (Fig. 7.6B). Therefore it is not possible to monitor the hydrolysis of NH₂-silane by immobilized lysozyme with UV-Vis spectroscopy (Fig. 7.6C).

7.4 Enzymatic activity assay of lysozyme by using of bis(*p*-nitrophenoxy)-dimethylsilane

Based on the knowledge that the molar absorption coefficient of *p*-nitrophenol is much higher than that of *p*-aminophenol,^[106] it is expected that lysozyme and other similar enzymes could also catalyze the cleavage of the Si-O bonds in bis(*p*-nitrophenoxy)-dimethylsilane (abbreviated here as NO₂-silane) (Fig. 7.7). The concentration of the releasing product *p*-nitrophenol could be measured with UV-Vis spectroscopy in the same way like described before. This would be a more sensitive assay for silicatein and hydrolases like lysozyme or even for esterases since Si-O bond is an ester-like bond.^[13]

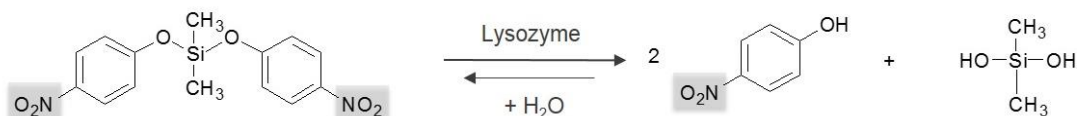


Fig. 7.7: Proposed hydrolysis of bis(*p*-nitrophenoxy)-dimethylsilane catalyzed by lysozyme.

7 Enzymatic activity assay of lysozyme and immobilized lysozyme

While *p*-aminophenol absorbs at a wavelength of 300 nm, *p*-nitrophenol exhibits an absorption maximum at 400 nm. The molar absorption coefficient of *p*-aminophenol (ϵ at $\lambda = 300$ nm) was determined to be $2 \cdot 10^3 \text{ M}^{-1} \text{ cm}^{-1}$ in glycine buffer (Fig. 7.8A), which conforms to the literature value.^[13] The molar absorption coefficient of *p*-nitrophenol (ϵ at $\lambda = 400$ nm) was determined to be $18 \cdot 10^3 \text{ M}^{-1} \text{ cm}^{-1}$ in glycine buffer, which means *p*-nitrophenol absorbs 9 times as much light as *p*-aminophenol at the same concentration (Fig. 7.8B).

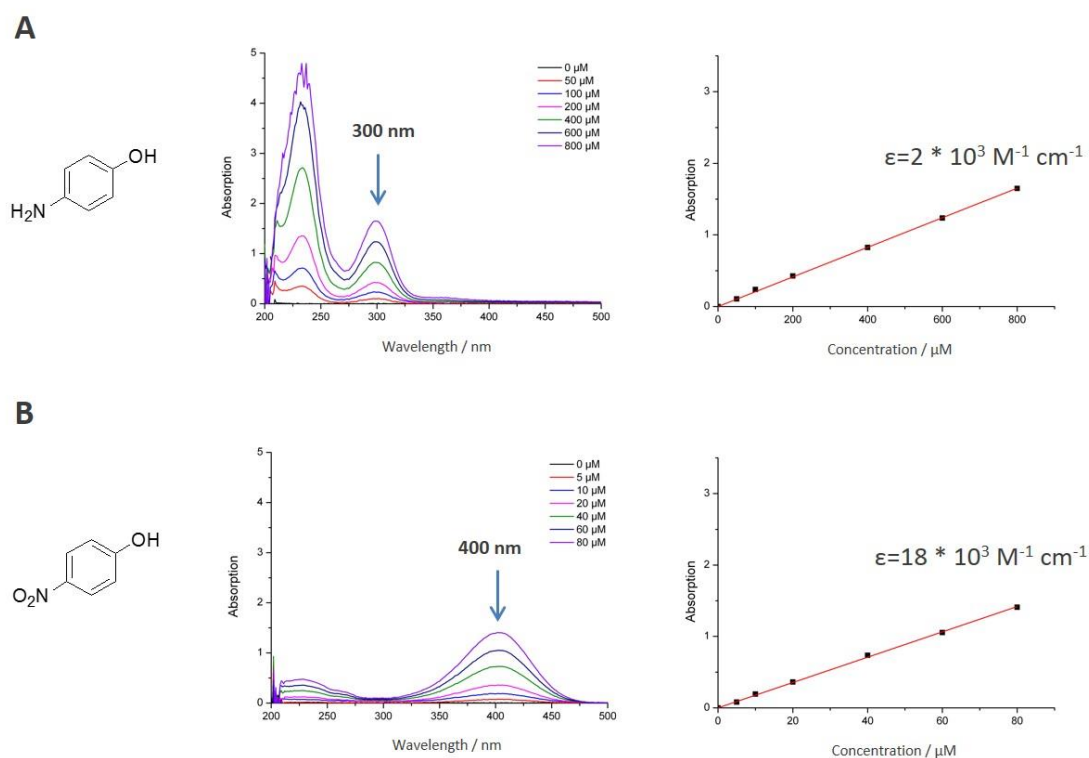


Fig. 7.8: Determination of the molar absorption coefficient ϵ of (A) *p*-aminophenol at 300 nm and (B) *p*-nitrophenol at 400 nm in glycine buffer (pH 9).

7 Enzymatic activity assay of lysozyme and immobilized lysozyme

Bis(*p*-nitrophenoxy)-dimethylsilane was synthesized from *p*-nitrophenol and dichlorodimethylsilane (Fig. 7.9) in a similar way like it was reported for bis(*p*-aminophenoxy)-dimethylsilane.^[107] 694 mg (5.00 mmol) *p*-nitrophenol was dissolved in 7 mL THF, 2 mL toluene and 693 μ L (5.00 mmol) triethylamine. A solution of 0.31 mL (2.55 mmol) dichlorodimethylsilane in 3 mL THF was added drop wise over a period of 15 min at 75 °C. After 6 hours reflux, the formed salt was removed by filtration and the solvents in vacuum. The solid material was purified by column chromatography using silica gel and THF as eluent. After removal of the solvent in vacuum, the product was obtained as a slightly yellow solid.

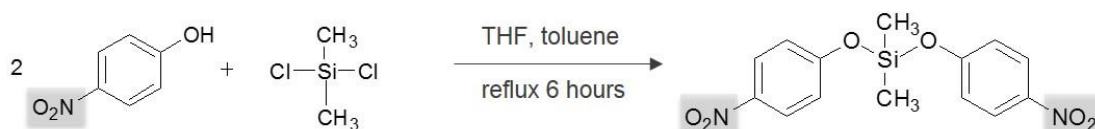


Fig. 7.9: Synthesis of bis(*p*-nitrophenoxy)-dimethylsilane.*

*The synthesis of bis(*p*-nitrophenoxy)-dimethylsilane was performed by Dr. Ulrich Glebe.

However, unlike NH₂-silane, which is water-insoluble, NO₂-silane dissolves in water quite well and exhibits an absorption at the same wavelength of 400 nm as *p*-nitrophenol. Fig. 7.10 represents the UV-Vis spectra of NO₂-silane at different concentrations in glycine buffer and the indicated molar absorption coefficient at 400 nm, which was determined to be $38 \cdot 10^3 \text{ M}^{-1} \text{ cm}^{-1}$ and almost 2 times of that of *p*-nitrophenol.

7 Enzymatic activity assay of lysozyme and immobilized lysozyme

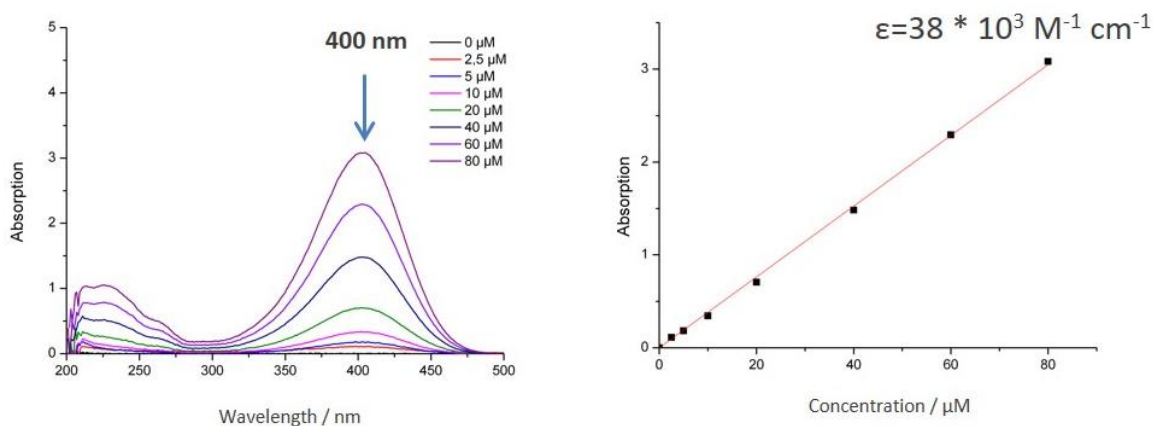


Fig. 7.10: UV-Vis spectra of NO₂-silane at different concentrations in glycine buffer at pH 9 (left) and the determination of the molar absorption coefficient at 400 nm (right).

Therefore it is no longer possible to apply the hydrolysis of NO₂-silane for the quantitative determination of the enzymatic activity of lysozyme. The measurements of a control sample in a two-phase system without lysozyme were done in a similar way as it was presented in Fig. 7.3A and they are shown in Fig. 7.11. The continuously increasing absorption reveals that the NO₂-silane diffused from diethyl ether into the aqueous phase. Thus, the lysozyme activity assay cannot be performed using bis(*p*-nitrophenoxy)-dimethylsilane as substrate.

7 Enzymatic activity assay of lysozyme and immobilized lysozyme

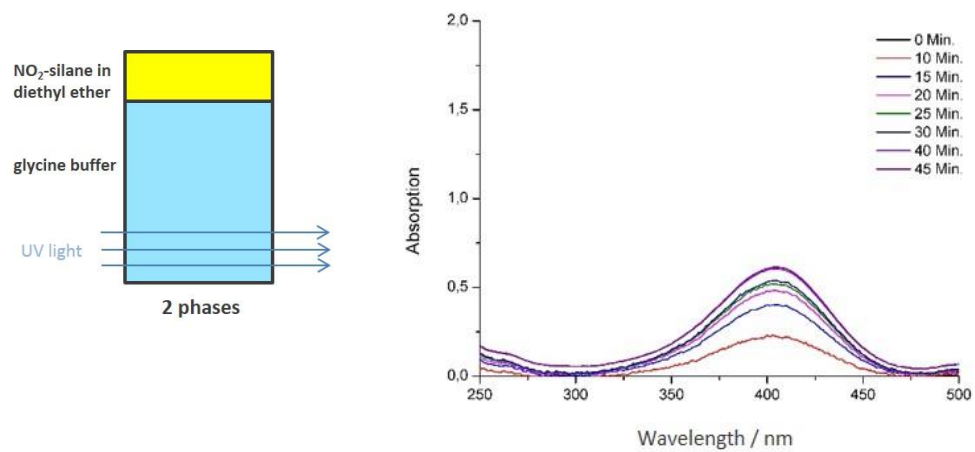


Fig. 7.11: UV-Vis measurements of the control sample without lysozyme in the presence of bis(*p*-nitrophenoxy)-dimethylsilane in the two-phase system (pH 9).

8 Summary

In the process of biomineralization, the formation of the mineral phase and the final structure depend on involved proteins because of their catalytic activities, specific sizes and colloidal behaviors. This natural synthetic pathway inspired this work to use similar approaches which lead to the formation of various synthetic protein-silica hybrid structures.

The adaption of recombinant silicatein for the synthesis of protein-silica hybrid capsules *via* Pickering emulsion templates was studied. The recombinant silicatein shows outstanding catalytic activity towards the polycondensation of TEOS or PEOS. Its interfacial activity allows the formation of hollow sphere structures from Pickering emulsions. By using different emulsification methods (mechanical or ultrasonic mixing), capsules with different sizes and shell-thicknesses were obtained. The size of the capsules can be controlled by the ratio of precursor to protein in solution. Different precursors also influence the size as well as the morphology of the capsules.

Silica precursors can also be converted into silica by lysozyme, which is especially advantageous because this protein is commercially available, inexpensive and displays higher interfacial activity than other commercially available hydrolases like trypsin or papain. By varying emulsification method, different hybrid structures like nanoparticles or hollow capsules were obtained. Hybrid capsules with tunable size and surface morphology were achieved by altering the sequence of addition of silica precursor.

8 Summary

The formation of various kinds of capsules is important for potential applications. In addition to silica nanoparticles and nano-/microcapsules also inverted capsules and double emulsion capsules were prepared by changing the relative amount of the individual components. Inverted emulsion (w/o) capsules with aqueous core could be advantageous for the encapsulation of hydrophilic active agents; double emulsion (o/w/o) capsules might provide additional protection to active substances and a more precise release mechanism.

The size and shell morphology of the hybrid capsules could also be tuned without changing the preparation method but by changing the buffer type and composition with the addition of various salts or ionic surfactants. Nano-/microcapsules with smooth shell were prepared using glycine buffer, while phosphate buffer led to bigger microcapsules with a rough shell. Due to the interaction between buffer ions and lysozyme molecules or/and silicon compounds. Furthermore, the use of other additives also influenced the capsule structure. Additives like sodium salts, *e.g.* NaCl and NaF were added to the system and increased the capsule size significantly since the ion-coordination to lysozyme destabilizes the emulsion which results in a collapse of small droplets and formation of big ones. To avoid the destabilizing effect of salts, ion-pairs with additional stabilizing features, namely anionic surfactant SDS and cationic surfactant CTAB were applied instead of common sodium salts. Since SDS coordinates to the positively charged amino acids on the surface, and hydrophobic dodecyl groups shield the protein from precursor molecules, the formation of SiO₂ was prevented. With CTAB as additive, however, small nanocapsules as well as nanoparticles were obtained due to the additional stabilizing effect of CTAB.

The incorporation of functionality and reactivity in capsules would make the system more versatile for possible post-modifications. A one-step approach to introduce additional reactivity in the form of primary amine-functionalities on the capsule surface was investigated by adding a small amount of APTMS to TEOS. The activity of the primary amine groups was determined *via* reaction with dabsyl chloride and mild peptide-coupling reactions with the fluorescent molecular dye calcein. The

benefit of this approach is to avoid the use of organic solutions and high temperature, and the new reactivity on the surface also enables further addition of other kinds of interesting functionalities.

Inspired by the natural seashell structure, which is composed of alternating layers of soft proteins and hard inorganic materials and exhibits outstanding mechanical properties despite its lightweight, silica capsules with multilayer shell were prepared using a layer by layer technique. A homogenous increase of shell thickness could be achieved when using phosphate buffer solution.

The application of PNIPAAm microgels as the analogue of enzymes for the silicification was also studied, since they include many amide groups and are very interfacially active. The synthesis of silica capsules with PNIPAAm microgels was successful and a hexagonal arrangement of microgels on the shell was observed. The catalytic silicification with PNIPAAm microgels shows a great potential in the fabrication of novel silica based materials *via* interface templates because such microgels are accessible in large amount and can be designed with controlled size and new functionalities.

Lysozyme was reversibly loaded in copolymer microgels PVCL/MEA/AA, which are not catalytically active towards silicification. The change of the size, zeta potential and interfacial activity indicated a successful immobilization of lysozyme in the carrier material. For the determination of the remaining enzymatic activity of lysozyme after the immobilization, the loaded microgels were used for the synthesis of silica capsules. At pH 9, silica capsules were obtained, revealing that the lysozyme remains active after the immobilization. Since microgels do not only provide protection to enzymes but are also interfacially active and stimuli-responsive, this immobilizing approach shows a considerable potential to improve the performance in terms of stability, delivery mechanism and recyclability of enzymes/catalysts and other sensitive substances.

8 Summary

In further experiments, the enzymatic activity assay of lysozyme was performed *via* UV-Vis spectroscopy. The hydrolysis of bis(*p*-aminophenoxy)-dimethylsilane in the presence of lysozyme, which is similar to the hydrolysis of TEOS catalyzed by lysozyme, can be monitored with the absorption of the product at 300 nm. The results revealed that under the same composition, the reaction rate is determined by the overall interfacial area since the reaction processes at the interface. Furthermore it was found that different buffer types at the same pH value have no obvious influence on the enzymatic activity.

This research offers insights into the biomimetic mineralization processes using native protein functions and bio-inspired systems. The environmentally friendly straightforward synthesis approach combining the catalytic and interfacial activities of proteins (or analogues of proteins) displays high versatility for the formation of hybrid silica capsules with tunable size, morphology and functionality. This work also opens new pathways for the synthesis of novel silica materials with high efficiency.

9 Zusammenfassung

Bei der Biomineralisation hängt die Bildung mineralischer Phasen mit definierten Strukturen insbesondere von der katalytischen Aktivität, der spezifischen Größe und dem kolloidalen Verhalten der beteiligten Proteine ab. Dieser natürliche Prozess diente als Inspiration für die vorliegende Arbeit, verschiedene anorganisch-organische Hybrid-Protein-Strukturen mit ähnlicher Herangehensweise zu synthetisieren.

Im Rahmen der Doktorarbeit wurden SiO_2 Mikro-/Nanokapseln enzymatisch synthetisiert, wobei Pickering Emulsionen als Template für Kapseln verwendet wurden. Rekombinantes Silicatein (ein natürliches spezifisches Protein für die Biosilifizierung), Lysozyme (eine natürliche Hydrolase mit ähnlichem aktivem Zentrum wie Silicatein) und ein synthetisches Polymer PNIPAAm (ein Analogon zum Enzym) wurden als Enzym/Katalysator eingesetzt. Die Besonderheit dieser Synthese liegt daran, dass die Enzyme nicht nur enzymatisch aktiv sondern auch grenzflächenaktiv sind: sie ordnen sich an den Grenzflächen an und bilden Öl-in-Wasser-Emulsion (SiO_2 Vorläufer als Öl-phase und Enzymlösung als wässrige Phase) und katalysieren gleichzeitig die Kondensation der Vorläufer an den Grenzflächen.

Zuerst wurde die Anwendung des rekombinanten Silicateins für die Synthese von Protein-Siliziumdioxid-Hybrid Kapseln über Pickering-Emulsionen untersucht. Das rekombinante Silicatein an der Grenzfläche von Pickering-Emulsionen zeigte hervorragende katalytische Aktivität gegenüber der Polykondensation von TEOS oder

PEOS. Durch die Variation von Emulgiermethoden, wurden Kapseln mit verschiedenen Größen und Wanddicken erhalten. Die Größe der Kapseln konnte auch durch das Verhältnis zwischen der Menge an SiO_2 -Vorläufer und Protein-Lösung kontrolliert werden. Verschiedene Vorläufer beeinflussten darüber hinaus die Größe und die Morphologie der Kapseln.

SiO_2 kann auch durch Lysozym, eine natürliche Hydrolase, die ein ähnliches aktives Zentrum wie Silicatein besitzt, unter physiologische Bedingungen hergestellt werden. Dies ist besonders interessant, da Lysozym kommerziell erhältlich und preiswert ist und eine höhere Grenzflächenaktivität als andere Hydrolasen, wie Trypsin oder Papain aufweist. Durch die Variation von Emulgiermethoden, wurden Nanopartikel oder Mikro-/Nanokapseln erhalten. Weiterhin konnte die Größe und die Oberflächenmorphologie der Kapseln durch Variation der Zugabe an SiO_2 -Vorläufer kontrolliert werden.

Da die Strukturen verschiedener SiO_2 -Kapseln wichtig für ihre Anwendung sind, wurden neben den SiO_2 -Nanopartikel und Nano-/Mikrokapseln auch invertierte Strukturen und Doppemulsionskapseln durch die Änderung des Verhältnis der einzelnen Komponenten hergestellt. Die durch invertierte Emulsion (w/o) erhaltene Kapseln mit wässrigem Kern sind vorteilhaft für Verkapselung von hydrophilen Wirkstoffen während (o/w/o)-Kapseln aus Doppemulsionen Wirkstoffen mehr Schutz sowie präzisere kontrollierte Freisetzung bieten.

Eine Variation der Größe und Morphologie der Kapseln konnten auch durch Änderung des Puffer-Typs oder der Zusammensetzung der wässrigen Phase mit Zugabe von verschiedenen Salzen oder ionischen Tensiden erreicht werden. Während sich Mikrokapseln mit glatter Wand im Glycin-Puffer synthetisieren lassen, führte Phosphat-Puffer zu deutlich größere Mikrokapseln mit rauer Oberfläche. Dies kann durch eine Wechselwirkung zwischen den Puffer-Ionen und Lysozym-Molekülen und/oder Siliziumverbindungen erklärt werden. Weiterhin zeigten auch andere Additive Einfluss auf die Kapselstruktur. Zusatzstoffe in Form von Natriumsalzen wie

zum Beispiel NaCl und NaF wurden zur Reaktionsmischung zugegeben, wodurch die Kapselgröße deutlich erhöht wurde, da die Koordination der Ionen an Lysozyme die Emulsion destabilisiert und sich die kleinen Tröpfchen zu großen Tropfen vereinen. Um diese destabilisierte Wirkung der Salze zu vermeiden, wurden Ionenpaare mit zusätzlichen stabilisierenden Eigenschaften, nämlich ein anionisches Tensid SDS und ein kationisches Tensid CTAB statt der Natriumsalze eingesetzt. Da SDS-Moleküle mit ihrem großen hydrophoben Anteil das Protein über die Koordination an den positiv geladenen Aminosäuren abschirmt, wurde die Bildung von SiO₂ verhindert. Die Zugabe von CTAB führte dagegen zu kleinen Nanokapseln und Nanopartikeln durch die zusätzliche stabilisierende Wirkung.

Eine Funktionalisierung der SiO₂-Kapseln durch weitere Modifikation des Systems könnte zu vielseitigen potentiellen Anwendungen führen. Neue funktionelle Gruppen auf der Oberfläche würden auch die weitere Zugabe anderer Arten von interessanten Funktionalitäten ermöglichen. In dieser Arbeit ist es gelungen, eine Oberflächenfunktionalisierung in Form von primären Aminen durch Zugabe einer kleinen Menge APTMS in TEOS herbeizuführen. Die Aktivität der primären Amine wurde durch die Reaktion mit Dabsyl Chlorid und milde Peptid-Kupplungsreaktionen mit dem fluoreszierenden Farbstoff Calcein bestimmt. Diese einfache Methode kommt ohne organische Lösungen und im Gegensatz zum konventionellen Stober-Verfahren ohne hohe Reaktionstemperaturen aus.

Inspiziert von der natürlichen Muschelschalen-Struktur, die aus abwechselnden Schichten von weichen Proteinen oder Biopolymeren und harten anorganischen Materialien bestehen und hervorragende mechanischen Eigenschaften trotz leichtem Gewicht besitzen, wurden Protein-SiO₂ Hybrid-Kapseln mit mehrschichtiger Wand über die LbL-Technik hergestellt. Im Phosphatpuffer ist es gelungen, Kapseln mit mehreren Wandschichten zu synthetisieren.

Die Verwendung von PNIPAAm-Mikrogelen als Analogon von Enzymen für die SiO₂ Bildung wurde ebenfalls untersucht, da diese eine Vielzahl an Amid-Gruppen besitzen

und sehr grenzflächenaktiv sind. Die Synthese von SiO₂-Kapseln mit PNIPAAm-Mikrogelen war erfolgreich, und eine nahezu perfekte hexagonale Anordnung der Mikrogele an der Kapselwand wurde beobachtet. Die katalytische Bildung von SiO₂ mit PNIPAAm-Mikrogelen hat ein großes Potential für die Herstellung von neuen SiO₂-basierten Materialien, da die Mikrogele einfach zugänglich sind und mit einer kontrollierbaren Größe und neue Funktionen entwickelt werden können.

Lysozym wurde reversibel in Copolymer-Mikrogele PVCL / MEA / AA geladen, die selbst nicht katalytisch aktiv für die SiO₂ Bildung sind. Die Änderung der Größe, des Zeta-Potenzials und der Grenzflächenaktivität zeigte eine erfolgreiche Anlagerung von Lysozym in dem Trägermaterial. Die enzymatische Aktivität von Lysozym nach der Immobilisierung wurde durch die Anwendung der geladenen Mikrogele für die Synthese von SiO₂-Kapseln bei pH 9 bewiesen. Da Mikrogele nicht nur den Enzymen vor der Umgebung schützen sondern auch grenzflächenaktiv und stimuli-responsiv sind, zeigt dieser Immobilisierungsansatz ein großes Potenzial dafür, Eigenschaften wie die Stabilität, Freisetzung und Regenerierung von Enzymen/Katalysatoren oder anderen empfindlichen Substanzen zu verbessern.

In weiteren Experimenten wurde die enzymatische Aktivität von Lysozym mit UV-Vis Spektroskopie getestet. Die Kinetik der Hydrolyse von Bis-(*p*-aminophenoxy) dimethylsilan in Gegenwart von Lysozym, welche Ähnlichkeit zur katalysierten Hydrolyse von TEOS hat, kann anhand der Absorption des Produkts bei 300 nm gemessen werden. Die Ergebnisse zeigten, dass bei gleicher Zusammensetzung die Reaktionsgeschwindigkeit durch die Gesamtfläche der Grenzfläche bestimmt wird, da die Reaktion an der Grenzfläche stattfindet. Weiterhin wurde festgestellt, dass verschiedene Puffer-Typen mit gleichem pH Wert keinen wesentlichen Einfluss auf die Enzymaktivität haben.

Diese Arbeit bietet wichtige Einblicke in biomimetische Mineralisationsprozesse mit nativen Proteinfunktionen und bio-inspirierte Systeme. Verschiedenen SiO₂-Hybrid-Kapseln mit kontrollierbarer Größe, Morphologie und Funktionalität konnten mittels

9 Zusammenfassung

einer eleganten und umweltfreundlichen Synthesemethode hergestellt werden, wobei sowohl die katalytische Aktivität und Grenzflächenaktivität der Proteine oder anderer Katalysatoren von wesentlicher Bedeutung ist. Weiterhin zeigt diese Arbeit vielseitige Möglichkeiten der weiteren Forschung an neuartigen Materialien auf SiO₂-Basis.

10 References

- [1] H. Gao, B. Ji, I. L. Jäger, E. Arzt, P. Fratzl, *Proc. Natl. Acad. Sci. USA* **2003**, *100*, 5597-5600.
- [2] P. van Rijn, A. Böker, *Journal of Materials Chemistry* **2011**, *21*, 16735-16747.
- [3] H. Wang, T. Mirzaeigarakani, T. Krappitz, P. van Rijn, A. Böker, *J. Mater. Chem. B* **2013**, *1*, 6427-6433.
- [4] A. Schulz, H. Wang, P. van Rijn, A. Böker, *Journal of Materials Chemistry* **2011**, *21*, 18903-18918.
- [5] J. N. Cha, K. Shimizu, Y. Zhou, S. C. Christiansen, B. F. Chmelka, G. D. Stucky, D. E. Morse, *Proceedings of the National Academy of Sciences of the United States of America* **1999**, *96*, 361-365.
- [6] U. S. H. C. Schröder, A. Boreiko, F. Natalio, M. Baranowska, D. Brandt, X. Wang, W. Tremel, M. Wiens, W. E. G. Müller, *Biosilica in Evolution, Morphogenesis, and Nanobiotechnology*, Springer, **2009**.
- [7] R. L. Brutchey, D. E. Morse, *Chemical Reviews* **2008**, *108*, 4915-4934.
- [8] X. H. Wang, M. Wiens, H. C. Schroder, S. X. Hu, E. Mugnaioli, U. Kolb, W. Tremel, D. Pisignano, W. E. G. Muller, *Advanced Engineering Materials* **2010**, *12*, B422-B437.

10 References

- [9] J. C. Weaver, D. E. Morse, *Microscopy Research and Technique* **2003**, *62*, 356-367.
- [10] D. Kisailus, Q. Truong, Y. Amemiya, J. C. Weaver, D. E. Morse, *Proceedings of the National Academy of Sciences of the United States of America* **2006**, *103*, 5652-5657.
- [11] V. Abbate, A. R. Bassindale, K. F. Brandstadt, P. G. Taylor, *Journal of Inorganic Biochemistry* **2011**, *105*, 268-275.
- [12] Y. Zhou, K. Shimizu, J. N. Cha, G. D. Stucky, D. E. Morse, *Angewandte Chemie-International Edition* **1999**, *38*, 780-782.
- [13] W. E. G. Müller, U. Schlossacher, X. Wang, A. Boreiko, D. Brandt, S. E. Wolf, W. Tremel, H. C. Schroder, *Febs Journal* **2008**, *275*, 362-370.
- [14] S. E. Wolf, U. Schlossmacher, A. Pietuch, B. Mathiasch, H. C. Schroder, W. E. G. Muller, W. Tremel, *Dalton Transactions* **2010**, *39*, 9245-9249.
- [15] H. C. Schröder, O. Boreiko, A. Krasko, A. R. A, H. Schwertner, W. E. Müller, *J. Biomed. Mater. Res., Part B, Appl. Biomater.* **2005**, *75*, 387-392.
- [16] M. Wiens, X. H. Wang, F. Natalio, H. C. Schroder, U. Schlossmacher, S. F. Wang, M. Korzhev, W. Geurtsen, W. E. G. Muller, *Advanced Engineering Materials* **2010**, *12*, B438-B450.
- [17] W. E. G. Müller, A. Boreiko, X. Wang, A. Krasko, W. Geurtsen, M. R. Custodio, T. Winkler, L. Lukic-Bilela, T. Link, H. C. Schroder, *Calcified Tissue International* **2007**, *81*, 382-393.
- [18] J. L. Sumerel, W. J. Yang, D. Kisailus, J. C. Weaver, J. H. Choi, D. E. Morse, *Chemistry of Materials* **2003**, *15*, 4804-4809.

10 References

- [19] P. O'Leary, C. A. van Walree, N. C. Mehendale, J. Sumerel, D. E. Morse, W. C. Kaska, G. van Koten, R. J. M. K. Gebbink, *Dalton Transactions* **2009**, 4289-4291.
- [20] P. Curnow, P. H. Bessette, D. Kisailus, M. M. Murr, P. S. Daugherty, D. E. Morse, *Journal of the American Chemical Society* **2005**, *127*, 15749-15755.
- [21] W. E. Müller, S. Engel, X. Wang, S. E. Wolf, W. Tremel, N. L. Thakur, A. Krasko, M. Divekar, H. C. Schröder, *Biomaterials* **2008**, *29*, 771-779.
- [22] A. Rai, C. C. Perry, *Langmuir* **2010**, *26*, 4152-4159.
- [23] M. I. Shukoor, F. Natalio, H. A. Therese, M. N. Tahir, V. Ksenofontov, M. Panthofer, M. Eberhardt, P. Theato, H. C. Schroder, W. E. G. Müller, W. Tremel, *Chemistry of Materials* **2008**, *20*, 3567-3573.
- [24] A. R. Bassindale, K. F. Brandstadta, T. H. Laneb, P. G. Taylor, *J. Inorg. Biochem.* **2003**, *96*, 401-406.
- [25] M. Frampton, A. Vawda, J. Fletcher, P. M. Zelisko, *Chemical Communications* **2008**, 5544-5546.
- [26] G. P. Smith, K. J. Baustian, C. J. Ackerson, D. L. Feldheim, *Journal of Materials Chemistry* **2009**, *19*, 8299-8306.
- [27] T. Shiomi, T. Tsunoda, A. Kawai, H. Chiku, F. Mizukami, K. Sakaguchi, *Chemical Communications* **2005**, 5325-5327.
- [28] T. Shiomi, T. Tsunoda, A. Kawai, F. Mizukami, K. Sakaguchi, *Chemical Communications* **2007**, 4404-4406.
- [29] T. Shiomi, T. Tsunoda, A. Kawai, S. Matsuura, F. Mizukami, K. Sakaguchi, *Small* **2009**, *5*, 67-71.

10 References

- [30] H. R. Luckarift, M. B. Dickerson, K. H. Sandhage, J. C. Spain, *Small* **2006**, *2*, 640-643.
- [31] A. R. Bassindale, P. G. Taylor, V. Abbate, K. F. Brandstadt, *Journal of Materials Chemistry* **2009**, *19*, 7606-7609.
- [32] D. Ivnitski, K. Artyushkova, R. A. Rincon, P. Atanassov, H. R. Luckarift, G. R. Johnson, *Small* **2008**, *4*, 357-364.
- [33] J. N. Cha, G. D. Stucky, D. E. Morse, T. J. Deming, *Nature* **2000**, *403*, 289-292.
- [34] D. H. Adamson, D. M. Dabbs, I. A. Aksay, D. E. Morse, *Abstracts of Papers of the American Chemical Society* **2004**, *227*, U511-U511.
- [35] K. M. Roth, Y. Zhou, W. J. Yang, D. E. Morse, *Journal of the American Chemical Society* **2005**, *127*, 325-330.
- [36] S. D. Pogula, S. V. Patwardhan, C. C. Perry, J. W. Gillespie, S. Yarlagadda, K. L. Kiick, *Langmuir* **2007**, *23*, 6677-6683.
- [37] A. J. Goldberg, M. C. Advincula, T. Komabayashi, P. A. Patel, P. T. Mather, D. G. Goberman, R. B. Kazemi, *Journal of Dental Research* **2009**, *88*, 377-381.
- [38] A. Balaceanu, V. Mayorga, W. J. Lin, M. P. Schurings, D. E. Demco, A. Böker, M. A. Winnik, A. Pich, *Colloid and Polymer Science* **2013**, *291*, 21-31.
- [39] S. Wiese, A. C. Spiess, W. Richtering, *Angewandte Chemie-International Edition* **2013**, *52*, 576-579.
- [40] W. B. Russel, D. A. Saville, W. R. Schowalter, *Colloidal Dispersions*, Cambridge University Press, Cambridge, **1992**.

10 References

- [41] G. Lagaly, O. Schulz, R. Zimehl, *Dispersionen und Emulsionen*, Steinkopff Verlag, Darmstadt **1997**.
- [42] A. Böker, J. He, T. Emrick, T. P. Russell, *Soft Matter* **2007**, *3*, 1231-1248.
- [43] Y. Chevalier, M. A. Bolzinger, *Colloids and Surfaces a-Physicochemical and Engineering Aspects* **2013**, *439*, 23-34.
- [44] S. Tsuji, H. Kawaguchi, *Langmuir* **2008**, *24*, 3300-3305.
- [45] M. Destribats, M. Wolfs, F. Pinaud, V. Lapeyre, E. Sellier, V. Schmitt, V. Ravaine, *Langmuir* **2013**, *29*, 12367-12374.
- [46] H. L. Wang, X. M. Zhu, L. Tsarkova, A. Pich, M. Moller, *Acs Nano* **2011**, *5*, 3937-3942.
- [47] N. P. Pardhy, B. M. Budhlall, *Langmuir* **2010**, *26*, 13130-13141.
- [48] C. Kaewsaneha, P. Tangboriboonrat, D. Polpanich, M. Eissa, A. Elaissari, *Colloids and Surfaces a-Physicochemical and Engineering Aspects* **2013**, *439*, 35-42.
- [49] A. Schulz, B. M. Liebeck, D. John, A. Heiss, T. Subkowski, A. Böker, *Journal of Materials Chemistry* **2011**, *21*, 9731-9736.
- [50] H. P. Hentze, S. R. Raghavan, C. A. McKelvey, E. W. Kaler, *Langmuir* **2003**, *19*, 1069-1074.
- [51] J. J. L. M. Cornelissen, E. F. Connor, H. C. Kim, V. Y. Lee, T. Magibitang, P. M. Rice, W. Volksen, L. K. Sundberg, R. D. Miller, *Chemical Communications* **2003**, 1010-1011.
- [52] G. Fornasieri, W. Badaire, R. Backov, O. Mondain-Monval, U. Zakri, P. Poulin, *Advanced Materials* **2004**, *16*, 1094-+.

10 References

- [53] Y. Desfougeres, V. Lechevalier, S. Pezenec, F. Artzner, F. Nau, *Journal of Agricultural and Food Chemistry* **2008**, *56*, 5120-5128.
- [54] Z. Z. Liao, J. W. Lampe, P. S. Ayyaswamy, D. M. Eckmann, I. J. Dmochowski, *Langmuir* **2011**, *27*, 12775-12781.
- [55] A. Vaish, V. Silin, M. L. Walker, K. L. Steffens, S. Krueger, A. A. Yeliseev, K. Gawrisch, D. J. Vanderah, *Chemical Communications* **2013**, *49*, 2685-2687.
- [56] H. Yazici, H. Fong, B. Wilson, E. E. Oren, F. A. Amos, H. Zhang, J. S. Evans, M. L. Snead, M. Sarikaya, C. Tamerler, *Acta Biomaterialia* **2013**, *9*, 5341-5352.
- [57] G. Jutz, A. Böker, *Journal of Materials Chemistry* **2010**, *20*, 4299-4304.
- [58] S. Magdassi, *Surface Activity of Proteins: Chemical and Physicochemical Modificaitons*, Marcel Dekker, New York, **1996**.
- [59] M. B. Linder, G. R. Szilvay, T. Nakari-Setala, M. E. Penttila, *Fems Microbiology Reviews* **2005**, *29*, 877-896.
- [60] S. Schmidt, T. T. Liu, S. Rutten, K. H. Phan, M. Moller, W. Richtering, *Langmuir* **2011**, *27*, 9801-9806.
- [61] K. Geisel, L. Isa, W. Richtering, *Langmuir* **2012**, *28*, 15770-15776.
- [62] W. Richtering, *Langmuir* **2012**, *28*, 17218-17229.
- [63] H. Masoud, A. Alexeev, *Acs Nano* **2012**, *6*, 212-219.
- [64] M. Destribats, V. Lapeyre, M. Wolfs, E. Sellier, F. Leal-Calderon, V. Ravaine, V. Schmitt, *Soft Matter* **2011**, *7*, 7689-7698.
- [65] X. M. Zhu, M. Jaumann, K. Peter, M. Moller, C. Melian, A. Adams-Buda, D. E. Demco, B. Blumich, *Macromolecules* **2006**, *39*, 1701-1708.

10 References

- [66] L. Reimer, G. Pfefferkorn, *Raster-Elektronenmikroskopie*, Springer, **1977**.
- [67] L. Reimer, *Scanning Electron Microscopy. Physics of Image Formation and Microanalysis*, Springer, **1998**.
- [68] S. S. Flegler, J. W. Heckmann Jr., K. L. Klomparens, *Elektronenmikroskopie*, 1st ed., Spectrum Akademischer Verlag, Heidelberg, **1995**.
- [69] J. Goldstein, *Scanning Electron Microscopy and X-ray Microanalysis*, 3rd ed., Springer, US, **2003**.
- [70] D. A. Skoog, F. J. Holler, S. R. Crouch, *Principles of instrumental analysis*, 6th ed., Thomson Higher Education, Belmont, CA, **2007**.
- [71] P. W. Atkins, J. de Paula, *Physical chemistry*, 7th ed., Oxford, New York, **2002**.
- [72] R. Tuma, *Journal of Raman Spectroscopy* **2005**, 36, 307-319.
- [73] J. T. Pelton, L. R. McLean, *Analytical Biochemistry* **2000**, 277, 167-176.
- [74] A. W. Coats, J. P. Redfern, *Analyst* **1963**, 88, 906-&.
- [75] T. Mirzaeigarakani, H. Wang, T. Krappitz, B. M. Liebeck, P. van Rijn, A. Böker, *Chemical Communications* **2012**, 48, 10210-10212.
- [76] H. El Rassy, A. C. Pierre, *Journal of Non-Crystalline Solids* **2005**, 351, 1603-1610.
- [77] J. A. Bucaro, H. D. Dardy, *Journal of Applied Physics* **1974**, 45, 5324-5329.
- [78] G. H. Bogush, C. F. Zukoski, *Journal of Colloid and Interface Science* **1991**, 142, 19-34.
- [79] R. Vacassy, R. J. Flatt, H. Hofmann, K. S. Choi, R. K. Singh, *Journal of Colloid and Interface Science* **2000**, 227, 302-315.

10 References

- [80] A. Vanblaaderen, J. Vangeest, A. Vrij, *Journal of Colloid and Interface Science* **1992**, *154*, 481-501.
- [81] Y. X. Li, Z. Q. Wang, Z. Huang, Y. F. Pan, G. Xue, *Journal of Materials Chemistry* **2010**, *20*, 5516-5520.
- [82] H. J. Zhang, Z. Y. Li, P. P. Xu, R. F. Wu, Z. Jiao, *Chemical Communications* **2010**, *46*, 6783-6785.
- [83] N. Enomoto, T. Koyano, Z. Nakagawa, *Ultrasonics Sonochemistry* **1996**, *3*, S105-S109.
- [84] F. Leal-Calderon, J. Bibette, V. Schmitt, in *Emulsion Science*, Springer New York, **2007**, pp. 173-199.
- [85] L. R. Wetter, H. F. Deutsch, *Journal of Biological Chemistry* **1951**, *192*, 237-242.
- [86] L. Xia, Z. B. Li, *Langmuir* **2011**, *27*, 1116-1122.
- [87] S. V. Patwardhan, S. J. Clarson, C. C. Perry, *Chemical Communications* **2005**, 1113-1121.
- [88] M. D. Lad, V. M. Ledger, B. Briggs, R. J. Green, R. A. Frazier, *Langmuir* **2003**, *19*, 5098-5103.
- [89] F. Q. Tang, L. L. Li, D. Chen, *Advanced Materials* **2012**, *24*, 1504-1534.
- [90] C. Haensch, S. Hoepfner, U. S. Schubert, *Chemical Society Reviews* **2010**, *39*, 2323-2334.
- [91] I. Bohm, K. Isenbugel, H. Ritter, R. Branscheid, U. Kolb, *Angewandte Chemie-International Edition* **2011**, *50*, 7407-7409.

10 References

- [92] J. F. Zayas, *Functionality of Proteins in Food*, Springer Science & Business Media, **1997**.
- [93] R. Menig, M. H. Meyers, M. A. Meyers, K. S. Vecchio, *Acta Materialia* **2000**, 48, 2383-2398.
- [94] A. Lin, M. A. Meyers, *Materials Science and Engineering a-Structural Materials Properties Microstructure and Processing* **2005**, 390, 27-41.
- [95] J. A. A. Junior, J. B. Baldo, *New Journal of Glass and Ceramics* **2014**, 4, 29-37.
- [96] W. Tischer, F. Wedekind, in *Topics in current chemistry, Vol. 200*, Springer Verlag, Berlin Heidelberg, **1999**, pp. 95-126.
- [97] B. M. Brena, F. Bastista-Viera, in *Methods in biotechnology: immobilization of enzymes and cells*, 2nd ed. (Ed.: J. M. Guisan), Humana Press Inc., Totowa, NJ.
- [98] S. Schachschal, H. J. Adler, A. Pich, S. Wetzel, A. Matura, K. H. van Pee, *Colloid and Polymer Science* **2011**, 289, 693-698.
- [99] p. Gemeiner, in *Enzyme engineering*, Ellis Horwood, New York, **1992**, pp. 13-119.
- [100] J. M. S. Cabral, J. F. Keenedy, in *Protein immobilization. Fundamentals and Applications*, Marcel Dekker, New York, **1991**, pp. 73-138.
- [101] M. Gupta, B. Mattiasson, in *Methods of biochemical analysis, Vol. 36*, Wiley, New York, **1992**, pp. 1-34.
- [102] R. A. Messing, *Methods in enzymology, Vol. XLIV*, Academic, New York, **1976**.

10 References

- [103] J. Woodward, *Immobilized cells and enzymes: a practical approach*, Oxford, IRL, **1985**.
- [104] R. C. Davies, Neuberger, A. B. M. Wilson, *Biochimica Et Biophysica Acta* **1969**, 178, 294.
- [105] A. Armirotti, G. Damonte, M. Pozzolini, F. Mussino, C. Cerrano, A. Salis, U. Benatti, M. Giovine, *Journal of Proteome Research* **2009**, 8, 3995-4004.
- [106] F. Dong, W. Guo, S. K. Park, C. S. Ha, *Chemical Communications* **2012**, 48, 1108-1110.
- [107] F. Rafiemanzelat, S. M. Khoshfetrat, M. Kolahdoozan, *Journal of Applied Polymer Science* **2013**, 127, 2371-2379.

11 List of publications

Articles

Morphology control and surface functionalization of protein-silicon oxide hybrid capsules

H. Wang, T. Mirzaeigarakani, T. Krappitz, P. van Rijn, A. Böker

J. Mater. Chem. B, **2013**, *1*, 6427-6433

Lysozyme-silica hybrid materials: from nanoparticles to capsules and double emulsion mineral capsules

T. Mirzaeigarakani, H. Wang, T. Krappitz, B.M. Liebeck, P. van Rijn, A. Böker

Chem. Commun., **2012**, *48*, 10210-10212

Synthetic inorganic materials by mimicking biomineralization processes using native and non-native protein functions

A. Schulz, H. Wang, P. van Rijn, A. Böker

J. Mater. Chem., **2011**, *21*, 18903-18918

Ultra-sound assisted formation of biodegradable double emulsion capsules from Hen egg-white

P. van Rijn, H. Wang, A. Böker

Soft Matter, **2011**, *7*, 5274-5280

Posters

Bioinspired synthesis of protein-silica hybrid materials

H. Wang, T. Mirzaeigarakani, P. van Rijn, G. Kibar, U. Schwaneberg, A. Böker
3rd International Conference on Multifunctional, Hybrid and Nanomaterials 2013

Bioinspired synthesis of silica capsules

H. Wang, A. Balaceanu, G. Kibar, A. Pich, U. Schwaneberg, A. Böker
26th Conference of the European Colloid and Interface Society 2012

12 Acknowledgement

Foremost, I would like to express my deep gratitude to Prof. Dr. Alexander Böker, my research supervisor, thank you so much for your patient guidance, valuable suggestions and discussions about this research work.

My grateful appreciation is also extended to Prof. Dr. Andrij Pich and Prof. Dr. Ulrich Schwaneberg, together with Dr. Andreea Balaceanu, Adrea Götz, Dr. Felix Jakob and Günes Kibar, I would like to thank you for the excellent cooperation and useful advices.

Very special thanks goes to Prof. Patrick van Rijn, I thank you for your continuing motivation and constructive suggestions for my work. Without your encouragement and support this work would not have been possible.

Dr. Tayebah Mirzaeigarakani and Tim Krappitz, who also worked on this topic, I thank you so much for your great contribution to this work.

I am particularly grateful for the help given by Bernd Liebeck, who performed most of the TGA and XRD measurements for this work.

Dr. Ulrich Glebe, I would like to thank you for your great help to perform the enzyme assays.

My sincere thanks also goes to Stefan Rütten, Dr. Kom Hô Phan and Dr. Walter Tillman for the kind support during SEM, IR and Raman measurements.

Dr. Xiaoming Zhu, thank you so much for providing me PEOS.

12 Acknowledgement

Clemens Liedel, I am very grateful for your proof-reading of this thesis and your friendship, which I treasure very much.

Furthermore, I would like to thank all my office mates and other colleagues, especially Christian Lewin, Mai-Thi Nguyen-Kim, Hyunji Park and Thomas Czubak, for the great time during my PhD studies.

I also give my great appreciation to Christine Sevenich, Deborah Schnabel, Angela Huschens and Lydia Moosche for all administrative matters during the past years.

Last but not the least, I would like to thank my parents Liping Wang and Yanbin Huang for their unconditional love throughout my life.